UNIVERSITY OF SOUTHAMPTON

FACULTY OF NATURAL AND ENVIRONMENTAL SCIENCES

School of Ocean and Earth Science

Volume 1 of 1

The causes of alkalinity variations in the global surface ocean

by

Claudia Helen Fry

Thesis for the degree of Doctor of Philosophy

September 2016

UNIVERSITY OF SOUTHAMPTON

ABSTRACT

FACULTY OF NATURAL AND ENVIRONMENTAL SCIENCES

Ocean and Earth Sciences

Thesis for the degree of Doctor of Philosophy

THE CAUSES OF ALKALINITY VARIATIONS IN THE GLOBAL SURFACE OCEAN

Claudia Helen Fry

Human activities have caused the atmospheric concentration of carbon dioxide (CO_2) to increase by 120 ppmv from pre-industrial times to 2014. The ocean takes up approximately a quarter of the anthropogenic CO_2, causing ocean acidification (OA). Therefore it is necessary to study the ocean carbonate system, including alkalinity, to quantify the flux of CO_2 into the ocean and understand OA. Since the 1970s, carbonate system measurements have been undertaken which can be analyzed to quantify the causes of alkalinity variation in the surface ocean. A tracer of the oceanic calcium carbonate cycle (Alk*) was created by removing alkalinity variation caused by other processes: evaporation and precipitation, river input, and the biological production and dissolution of organic matter. The remaining variation is similar to the distribution of the major nutrients with low values in the tropical surface ocean and values 110 µmol kg^{-1} and 85 µmol kg^{-1} higher in the Southern Ocean and the North Pacific respectively. The causes of longitudinal Alk* gradients in the Pacific Ocean were then analyzed. The results indicate that outcropping of isopycnals and upwelling of water enriches Alk* in the subpolar North Pacific and along the North American margin. On the other hand, the eastern equatorial upwelling appears to be from depths too shallow to contain enhanced Alk*. Two algorithms to predict alkalinity were then created for the surface Pacific with r values between predictions and measurements of 0.970 for the entire Pacific Ocean algorithm and 0.991 for the North Pacific eastern margin. A method using in-situ Alk* and velocity measurements to estimate calcium carbonate export was developed. This method estimates a summer and autumn export in the Southern Ocean of 0.31 Pg C yr^{-1} with the majority occurring around the Polar and Subantarctic Fronts. The Alk* tracer is shown to be a useful tool which could be improved by further research into riverine alkalinity inputs and the influence of sea ice formation on alkalinity.

Table of Contents

List of Tables

List of Figures

DECLARATION OF AUTHORSHIP

I, Claudia Helen Fry

declare that this thesis and the work presented in it are my own and has been generated by me as the result of my own original research.

The causes of alkalinity variations in the global surface ocean

I confirm that:

1. This work was done wholly or mainly while in candidature for a research degree at this University;
2. Where any part of this thesis has previously been submitted for a degree or any other qualification at this University or any other institution, this has been clearly stated;
3. Where I have consulted the published work of others, this is always clearly attributed;
4. Where I have quoted from the work of others, the source is always given. With the exception of such quotations, this thesis is entirely my own work;
5. I have acknowledged all main sources of help;
6. Where the thesis is based on work done by myself jointly with others, I have made clear exactly what was done by others and what I have contributed myself;
7. Parts of this work have been published as:
   Fry, C.H., Tyrrell, T., Hain, M.P., Bates, N.R., Achterberg, E.P., 2015. Analysis of global surface ocean alkalinity to determine controlling processes. Marine Chemistry. 174, 46-57.
   Fry, C.H., Tyrrell, T., Achterberg, E.P., 2016. Analysis of longitudinal variations in North Pacific alkalinity to improve predictive algorithms. Global Biogeochemical Cycles. 30, 1493–1508.

Signed:

Date:

Acknowledgements

I would firstly like to thank all the crews, scientists, and data analysts that put together the GLODAP, CARINA, PACIFICA, and GLODAPv2 databases. Without the years of work collecting and collating alkalinity data this thesis would not have been possible.

I would also like to give a big thanks to my supervisors: Professors Toby Tyrrell and Eric Achterberg for all your feedback and patience and for spending hours trying to improve the coherence of my writing. I would also like to thank all my co-authors: Mathis Hain, Nicholas Bates, and Matthew Mazloff for the useful expertise they have provided over the last four years. I have also had useful discussions with Dieter Wolf-Gladrow, Kitack Lee, Alex Poulton, Kevin Oliver, Mark Moore, and Matt Couldrey.

I couldn't have finished this PhD without my parents and my partner. All of whom helped to check mathematical logic and didn't ask me how long until I would finish.

I am indebted to the support I have received from many friendly faces over the years. In particular, the friendship of my office mates has been especially helpful with them providing coffee breaks, lunch companions, and opinions on grammatical issues. I am also grateful to the baristas at Lion Retail Park Costa Coffee for providing a supply of tea, free cake samples, and for not telling me the Wi-Fi password.

Definitions and Abbreviations

A – ocean water body

A – magnitude of the vector in Alk*

Alk – alkalinity concentration

Alk* - alkalinity anomaly, a tracer of calcium carbonate cycling

Alk^*_{gyre} – alkalinity anomaly of the Atlantic gyre

$Alk^*_{S.Oc}$ – alkalinity anomaly of the Southern Ocean

Alk_1 - alkalinity after the removal of the effects of evaporation and precipitation

Alk_2 - alkalinity after the removal of the effects of evaporation, precipitation, and river water

Alk_3 – alkalinity after the removal of the effects of evaporation, precipitation, river water, and production and dissolution of organic matter

Alk_m – measured alkalinity

Alk_r – river alkalinity concentration

aq – aqueous

BATS – Bermuda Atlantic Time-Series

$[B(OH)_4^-]$ – concentration of tetrahydroxyborate

C – carbon

Ca^{2+} - calcium ion

$CaCO_3$ – calcium carbonate

$CaCO_3 \cdot 6H_2O$ - ikaite

CARINA – CARbon dioxide IN the Atlantic Ocean database

CDIAC – Carbon Dioxide Information Analysis Center

CFC – chlorofluorocarbon

CLIVAR – Climate and Ocean: Variability, Predictability and Change database

CO_2 – carbon dioxide

CO_3^{2-} – carbonate ion

CRM – Certified Reference Material

$CaSiO_3$ – calcium silicate

DIC – Dissolved Inorganic Carbon

Du – decrease of Alk* from mixing along the eastwards gradient

Dv – decrease of Alk* from mixing the northwards gradient

ENSO – El Niño Southern Oscillation

F – rate of decrease in Alk* along the direction of water movement

F_{ekman} – the surface Ekman flux in the Southern Ocean

F_{NADW} – the flux of North Atlantic Deep Water

GEOSECS – Geochemical Ocean Sections

GLODAP – Global Ocean Data Analysis Project

GLODAPv2 - Global Ocean Data Analysis Project version 2

GO-SHIP – Global Ocean Ship-based Hydrographic Investigations Panel

H^+ – hydrogen ion

H_2CO_3 – carbonic acid

H_2O - water

$[H_3PO_4]$ – concentration of phosphoric acid

$[H_3SiO_4^-]$ – concentration of trihydrogen silicate

H_4SiO_4 – silicic acid

HCO_3^- – bicarbonate ion

[HF] – concentration of hydrofluoric acid

$[HNO_2]$ – concentration of nitrous acid

HOT – Hawaii Ocean Times series

$[HPO_4^{2-}]$ – concentration of hydrogen phosphate

$[HS^-]$ – concentration of hydrogen sulphide

$[HSO_4^-]$ – concentration of hydrogen sulphate

IPCC – Intergovernmental Panel on Climate Change

j – current cell in a matrix

JGOFS – Joint Global Ocean Flux Study

KNOT – Kyodo western North Pacific Ocean Time-series

lat – latitude

LDEO – Lamont-Doherty Earth Observatory

ln – meters in one degree longitude (latitude dependent)

lt – meters in one degree latitude (latitude dependent)

M – magnitude of the vector of water velocity

$M_{(NO3,ATL)}$ – average spread of the data cloud

max – maximum

MATLAB – MATrix LABoratory

min – minimum

MLD – Mixed Layer Depth

MLR – multiple linear regression

MODIS – Moderate Resolution Imaging Spectroradiometer

N – nitrate concentration (Table 4-5)

N – number of data points

n – number of data points (Table 4-5)

NADW – North Atlantic Deep Water

nAlk – salinity-normalized alkalinity

NCa – salinity-normalized calcium concentration

$[NH_3]$ – concentration of ammonia

Nit – nitrate concentration

NO_3^- – nitrate concentration

$\overline{NO3_i^{ATL}}$ – mean of the nitrate values in the i'th Atlantic bin.

NOAA – National Oceanic and Atmospheric Administration

OA – Ocean Acidifcation

OACES – Ocean-Atmosphere Carbon Exchange Study

$[OH^-]$ – concentration of hydroxide ion

p – probability (*p*-value)

p – smoothing parameter

PA – Practical Alkalinity

PACIFICA – PACIFic ocean Interior Carbon database

pAlk – potential alkalinity

pCO_2 – partial pressure of carbon dioxide

PF – Polar Front

pH – the base 10 logarithm of the of the reciprocal concentration of hydrogen ion

PIC – Particulate Inorganic Carbon

$[PO_4^{3-}]$ – concentration of phosphate

ppm – parts per million

ppmv – parts per million by volume

Q_{Atl} – flux of alkalinity leaving the gyre through calcium carbonate precipitation.

r – Pearson's r correlation coefficient

R – river water

R^2 – coefficient of determination

rms – root mean square error

S - salinity

SAF – Subantarctic Front

Sal - salinity

SDC – simple dilution or concentration process

SF_6 – sulphur hexafluoride

SiO_2 – silicon dioxide

SOCAT – Surface Ocean CO_2 Atlas

SOCATv2 - Surface Ocean CO_2 Atlas version 2

SOMLO – Self-Organizing Multiple Linear Output

SOSE – Southern Ocean State Estimate

STF – Subtropical Front.

TA* - tracer of remineralized alkalinity

TrOCA – Tracer using Oxygen, inorganic Carbon, and Alkalinity

U – eastwards water velocity

V – northwards water velocity

VIF – Variance Inflation Factor

WOCE – World Ocean Circulation Experiment

ΔA – gradient in a tracer of calcium carbonate cycling along the direction of water movement

ΔAlk* – gradient in a tracer of calcium carbonate cycling

ΔAlk_m – change in measured alkalinity

ΔCa – change in calcium concentration

ΔC^* – a method to calculate anthropogenic carbon

ΔNO_3^- – change in nitrate concentration

ΔS – change in salinity

Δu – eastwards gradient in Alk*

Δv – northwards gradient in Alk*

θ – angle of the vector in Alk* from east

σ_θ – potential density

φ – angle of the vector of water velocity from east

Ω – saturation state of calcite

$\sigma\left(NO3_i^{ATL}\right)$ – standard deviation of the nitrate values in the i'th Atlantic bin

Chapter 1: Introduction

1.1 Climate change and ocean acidification

The scientific evidence is now overwhelming: climate change is a serious global threat, and it demands an urgent global response - Stern et al. [2006]

Excluding water vapor, the earth's atmosphere is made of 78% nitrogen, 21% oxygen, 0.9% argon, and about 0.04% carbon dioxide [*Sarmiento and Gruber*, 2006; *Tans and Keeling*, 2015]. Carbon dioxide is a greenhouse gas which means that it traps heat from the sun at the surface of the planet. Averaged over the whole of the Earth's surface, 340 W m^{-2} of the sun's solar radiation enters our atmosphere (Figure 1-1). Greenhouse gases reduce the amount of thermal radiation released back to space, trapping it near the surface so the surface temperature builds up and the planet warms. The amount of thermal radiation released back to space is in proportion to the temperature of the planet; once the planet warms sufficiently, the incoming radiation equals the outgoing radiation and a new equilibrium is formed. The higher the concentration of greenhouse gases, the higher the surface temperature [*Wild et al.*, 2013]. This is called the greenhouse effect because the layer of greenhouse gases keeps the surface of the planet warm in a similar, although not identical, way to how glass in a greenhouse traps the sun's heat causing the air inside to warm.

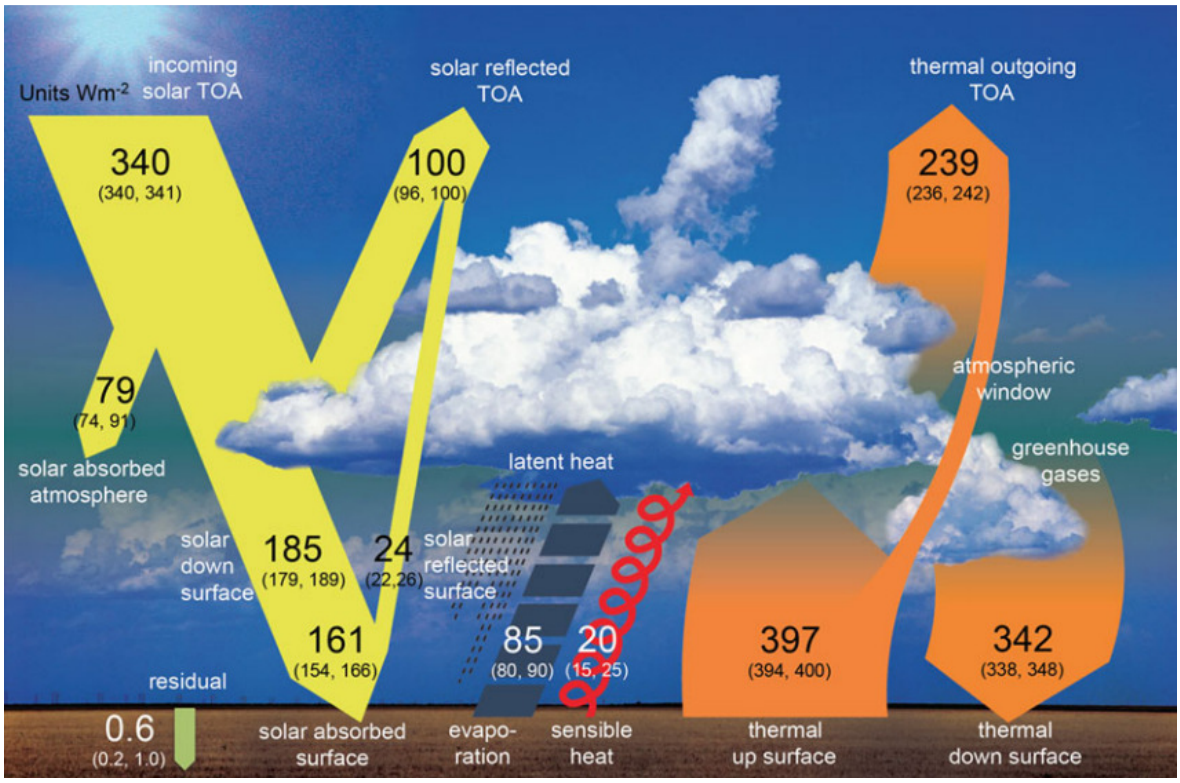

Figure 1-1. Schematic of the global mean energy balance of the Earth. The large numbers are the estimates of the globally averaged energy balance and the brackets contain the uncertainty estimates. All units are in W m^{-2} [*Wild et al.*, 2013]

Carbon dioxide is not the only greenhouse gas. Other greenhouse gases include: water vapor, methane, nitrous oxide, and halocarbons. Most greenhouse gases are increasing in the atmosphere due to human activities [*Hartmann et al.*, 2013]; for example, the concentration of carbon dioxide in the atmosphere has risen from about 280 ppmv in pre-industrial times to 316 ppmv in 1959 and to 399 ppmv in 2014 [*Tans and Keeling*, 2015] (Figure 1-2). Human activities that release carbon dioxide into the atmosphere include the burning of fossil fuels such as oil and natural gas, as well as deforestation and the production of cement. Human activities have also caused the concentration of methane in the atmosphere to increase. Methane is released from agricultural practices: digestion by cows and sheep and anaerobic decomposition of organic matter in rice paddies. Just like in rice paddies, the anaerobic decomposition of organic matter in landfill sites also causes methane to be released [*Hartmann et al.*, 2013]. Nitrous oxide is another agricultural greenhouse gas, and has increased by 20% since 1750 [*Prather et al.*, 2012]. Emissions of nitrous oxide are dominated by soils treated with synthetic and organic fertilizer [*Ishijima et al.*, 2007]. International effort has reduced the use of chlorofluorocarbons (CFCs) which are greenhouse gases and also cause the atmospheric ozone layer to thin. Instead chlorofluorocarbons have been replaced by other halocarbons. Unfortunately, these man-

made gases, which are used in fridges, air-conditioning units, and trainers, are some of the strongest greenhouse gases with one molecule of sulphur hexafluoride (SF_6) warming the atmosphere 23,900 times more than a molecule of carbon dioxide over 100 years [*Hartmann et al.*, 2013]. Interestingly, because these gases are man-made, their concentrations in the atmosphere have only been increasing since we started making them. This makes them useful for studying the ocean because the concentration of halocarbons indicates when a body of water was last in contact with the atmosphere [*Hall et al.*, 2002; *McNeil et al.*, 2003; *Waugh et al.*, 2004].

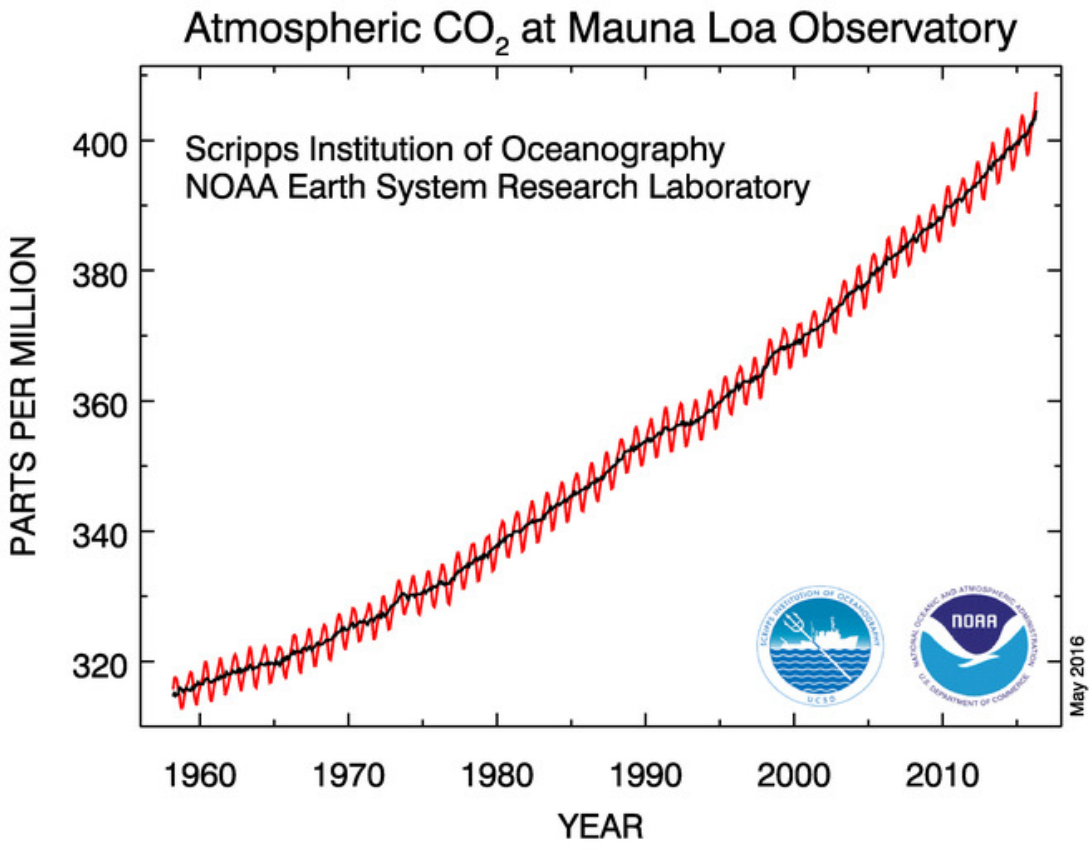

Figure 1-2. Atmospheric CO_2 from the Mauna Loa Observatory obtained from NOAA Earth System Research Laboratory.

The global warming caused by the increase in greenhouse gases has many implications. For example, the warmth will cause the sea ice to melt which will change the habitat and circulation of the Arctic Sea [*Aagard and Carmack*, 1989; *Shimada et al.*, 2006; *Serreze et al.*, 2007] affecting ice dwelling animals such as walrus and polar bear [*Kovacs et al.*, 2011]. Also, warmer earth surface temperatures will cause the ice caps to melt and therefore the sea level to rise, but sea level also rises as the ocean warms because warmer water has a greater volume than colder water [*Wigley and Raper*, 1987; *Rahmstorf*, 2007;

Meehl et al., 2009]. The higher temperature will also allow the atmosphere to hold more moisture, which causes an increase in the frequency of rainfall and severe flooding events; however, the changing rainfall patterns will also mean that some areas, such as in the centers of large continents, may have an increase in droughts [*Trenberth*, 1998; *Allen and Ingram*, 2002; *Min et al.*, 2011]

There are also positive and negative feedbacks that increase or decrease the effect of greenhouse gases [*Lin et al.*, 2002a; *Soden and Held*, 2006; *Cornelissen et al.*, 2007]. A positive feedback is when a change in a system is enhanced or exacerbated by the change happening in the first place. For example, higher atmospheric temperatures cause the ice caps and glaciers to melt. However, both ice caps and sea ice have a high albedo, meaning that they reflect a large proportion of the sun's radiation out to the atmosphere instead of absorbing the energy and increasing the temperature of the earth's surface. With fewer ice caps and less sea ice, less energy is reflected and more is absorbed which causes the temperature of the earth's surface to rise further [*Serreze et al.*, 2007]. A negative feedback is the opposite of a positive feedback; when a change occurs in a system it causes another effect which reduces the original change in the system. An example of this is when concentrations of carbon dioxide in the atmosphere increase, which causes plants to produce more organic matter, and this uses more carbon dioxide from the atmosphere and decreases the atmospheric concentration of carbon dioxide [*Lamarche et al.*, 1984]. The positive and negative feedbacks in the climate system make it difficult to predict the future state of the climate with increasing greenhouse gases.

In the 2014 Intergovernmental Panel on Climate Change (IPCC) report, the authors predict that by the mid-21st century the average atmospheric temperature will very likely be 1.5ºC to 2ºC greater than the pre-industrial temperature. However, these predictions vary substantially depending on much humans emit in the future. The increase in atmospheric temperature will cause the mean surface temperature of the earth to increase leading to fewer cold events and more heatwaves. There will also be more precipitation at high latitudes and in mid-latitude regions that are currently wet. Dry mid-latitude regions will probably experience a decrease in precipitation [*IPCC*, 2014].

Not only will these changes affect other species on this planet, they will also affect our species. For example, increasing temperatures will allow greater transfer of diseases such as malaria because the mosquitoes that carry the disease cannot survive in cold temperatures [*Martens et al.*, 1999; *Tanser et al.*, 2003; *Caminade et al.*, 2014]. Sea level rise from the melting ice caps and the warmer oceans will cause flooding of many areas

including low-lying countries such as Bangladesh and the Maldives [*Castro Ortiz*, 1994; *Khan et al.*, 2002; *Church et al.*, 2006; *Karim and Mimura*, 2008]. Also, the changing rainfall patterns will cause droughts and floods that will affect the success of crops and could lead to famine and the migration of people [*Patz et al.*, 2005]. Studies also suggest that famine and the movement of people will cause increased war and conflict [*Barnett and Adger*, 2007; *Hendrix and Salehyan*, 2012]. In conclusion, climate change means that our everyday choices have the ability to kill others through disease, famine, and war.

However, climate change is not the only problem caused by the increasing concentration of carbon dioxide in the atmosphere; there is also ocean acidification. Carbon dioxide from the atmosphere dissolves in the ocean releasing hydrogen ions. The definition of pH is approximately the base ten logarithm of the reciprocal of the hydrogen ion concentration, which means that the more hydrogen ions, the lower the pH, and the more acidic the water [*Zeebe and Wolf-Gladrow*, 2001]. So the anthropogenic carbon dioxide dissolves in sea water and causes the ocean to acidify. According to the 2014 IPCC report, the higher carbon dioxide in the atmosphere will increase the surface acidity (hydrogen ion concentration) by 15% to 17% by the mid-21st century for the lowest emission scenario and 100% to 109% for the highest emission scenario [*IPCC*, 2014]

The changing chemistry also potentially affects many species that create shells out of calcium carbonate. A lower pH (more acidic), lowers the saturation state of calcium carbonate [*Feely et al.*, 2004, 2012; *Chierici and Fransson*, 2009]. The saturation state describes how easily calcium carbonate dissolves and the further the saturation state is below 1, the easier calcium carbonate dissolves. There are two main types of calcium carbonate: calcite and aragonite. Due to its structure, calcite is more stable than aragonite; therefore, the saturation state of calcite is higher than the saturation state of aragonite for a sample of water [*Zeebe and Wolf-Gladrow*, 2001]. Lower pH oceans with lower saturation states could negatively impact some species that produce these shells to protect themselves, like corals; however, it is not yet certain why many other species produce calcium carbonate and so further research needs to take place in this area [*Riebesell et al.*, 2000; *Doney et al.*, 2009; *Yara et al.*, 2012].

Ocean acidification will also affect cetaceans because a lower pH will reduce the sound absorption of the ocean. The sound absorption of low frequencies is controlled by the relaxation of the borate and magnesium carbonate which changes with pH. Therefore lowering the pH may allow low-frequency sound (below 1kHz) to travel further [*Brewer et al.*, 1995]. For example, a decrease of pH by 0.3 units, projected to occur by the mid-21st

century, may result in a 40% decrease in sound absorption [*Hester et al.*, 2008]. This will affect the communication of marine mammals [*Ilyina et al.*, 2010] and could have an impact on the early survival of fishes [*Simpson et al.*, 2011].

Changes to species caused by ocean acidification could also impact the human food chain and our activities. For example, *Orr et al.* [2005] found that pteropods contribute to the diet of many zooplankton and through them the diet of North Pacific salmon, mackerel, herring, and cod all of which are widely eaten by humans. Human activities will also be affected by the pH-dependent changes in ocean sound adsorption. The world's navies and industries use the low-frequencies that will be affected by ocean acidification and therefore these activities could be disrupted [*Hester et al.*, 2008].

1.2 How does studying the ocean carbonate system help us understand climate change and ocean acidification?

Knowledge of the carbonate system enables us to understand how carbon dioxide dissolves in the ocean. Studies of the ocean carbonate system are important as they improve the understanding of climate change and ocean acidification through quantifying air-sea fluxes, predicting the magnitude of ocean acidification, and understanding the relationship between inorganic and organic carbon fluxes.

The current concentration of carbon dioxide in the atmosphere is higher than for the past 650,000 years and this is causing the planet to warm [*Feely et al.*, 2008]. The ocean presently absorbs about 2.2 Pg of carbon every year and this long term removal of carbon dioxide reduces the extent of global warming because the carbon dioxide is no longer in the atmosphere causing warming [*Le Quéré et al.*, 2009]. But once in the ocean the carbon dioxide reacts, releasing hydrogen ions (see Section 1.3), which causes ocean acidification [*Orr et al.*, 2005].

To produce accurate climate predictions, further research is needed to understand future changes in the ocean carbon sink, because the magnitude of the sink affects how much carbon dioxide is available to warm the atmosphere. One area needing to be understood in more detail is the Southern Ocean, as data in this region are sparse [*McNeil et al.*, 2007; *Carter et al.*, 2016]. Another topic needing research is how changes in the circulation affect the air-sea flux. For example, in the Southern Ocean a strengthening of the polar vortex could cause more upwelling, bringing water with enhanced dissolved inorganic carbon to the surface, and reducing the air-sea gradient and the amount of carbon dioxide

the ocean could absorb [*Le Quéré et al.*, 2007; *Lovenduski et al.*, 2008; *Lenton et al.*, 2012]. However, there is evidence to suggest that the opposite may be occurring and that in the Southern Ocean the sink of carbon dioxide is increasing in strength [*de Lavergne et al.*, 2014; *Landschützer et al.*, 2015]. Research is also needed to understand biological changes that may affect the air-sea flux. For example, phytoplankton use carbon to produce organic matter that eventually sinks out of the surface mixed layer thereby moving the carbon into the deep ocean. If warmer temperatures or ocean acidification kill phytoplankton and production decreases [*Sommer and Lengfellner*, 2008; *Lewandowska and Sommer*, 2010; *Sommer and Lewandowska*, 2011], then climate change could decrease the rate of carbon dioxide entering the ocean and increase the magnitude of global warming.

Another change that could affect the rate carbon dioxide is absorbed into the ocean is warming. Increasing temperature reduces the amount of gas the ocean can hold at equilibrium with the atmosphere [*Sarmiento and Le Quéré*, 1996]. This is a positive feedback on atmospheric carbon dioxide [*Cubasch et al.*, 2013]; the warming ocean temperature will reduce the amount of carbon dioxide dissolving in the ocean so more will stay in the atmosphere to cause further warming.

The carbonate system of the ocean also needs to be researched to predict ocean acidification. For example, the Southern Ocean is susceptible to ocean acidification because the upwelling water is already enriched in dissolved carbon so only a small amount of additional carbon dioxide could have implications [*Orr et al.*, 2005]. *Bednaršek et al.* [2012] found that aragonite pteropods in the Southern Ocean are dissolving due to the already low carbonate concentrations being pushed even lower by the invasion of anthropogenic carbon dioxide. Understanding the carbonate system can help us predict the future changes in carbonate chemistry and impacts of these changes.

Studying the ocean carbonate system is also important because it enables understanding of the earth's climate and rates of calcification. During calcification, bicarbonate and carbonate ions are used to create calcium carbonate. The more carbonate ions and the higher the saturation state of calcium carbonate, the more difficult it is for calcium carbonate to dissolve. For many species, the rate of calcification is positively correlated with the calcium carbonate saturation state of the water [*Langdon et al.*, 2000; *Riebesell et al.*, 2000; *Barker et al.*, 2003].

Calcification affects ingassing and outgassing of carbon dioxide from the ocean. Calcification locally lowers the alkalinity, a measure of the charge balance of the water,

and releases carbon dioxide; however, the synthesis of one mole of calcium carbonate does not actually raise the concentration of carbon dioxide by one mole because the carbonate system buffers the changes slightly [*Ware et al.*, 1992; *Barker et al.*, 2003]. The increase in the seawater partial pressure of carbon dioxide caused by calcification usually reduces the air-sea gradient and the amount of carbon dioxide entering the ocean [*Falkowski et al.*, 2000; *Barker et al.*, 2003; *Chung,* 2003].

Although the partial pressure of carbon dioxide is increased by calcification, organisms producing calcium carbonate also produce organic matter and therefore take up carbon dioxide. In general the quantity of carbon dioxide produced through calcification is less than that produced through organic matter production, so calcifiers usually still induce a net flux of carbon dioxide into the ocean. However, some environments, such as coral communities, are a net source of carbon dioxide to the atmosphere [*Barker et al.*, 2003]. It is therefore important to understand the ratio between the rate of export of inorganic to organic carbon known as the rain ratio. The rain ratio can be used predict the impact of biological production on the partial pressure of the surface ocean [*Lee,* 2001].

The synthesis and export of calcium carbonate is part of the carbonate "counter" pump, so named as it has the opposite effect on atmospheric carbon dioxide to that of the organic carbon pump (where production of organic carbon increases the air-sea flux of carbon dioxide) [*Salter et al.*, 2014]. The carbonate pump also reduces alkalinity in the surface ocean, exports calcium carbonate to the deep ocean, and increases alkalinity in the deep ocean when the calcium carbonate dissolves [*Lee et al.*, 2006].

The processes affecting the production of calcium carbonate also affect the organic carbon cycle [*Barker et al.*, 2003]. The organic carbon cycle pumps carbon dioxide from the atmosphere into the ocean by taking up carbon and producing organic matter [*Sarmiento and Gruber,* 2006]. Organic matter can then be exported to the deep ocean, which removes the carbon from the atmosphere. However, a lot the organic matter is regenerated (transferred back to dissolved species through dissolution and bacterial respiration) in the upper water column [*Armstrong et al.*, 2002]. Particles of organic matter can sink faster if other materials are incorporated and this is called ballasting. The ballast materials can also protect the organic matter from remineralizing during transportation and burial in sediments [*Armstrong et al.*, 2002; *Francois et al.*, 2002; *Barker et al.*, 2003]. Studies show that calcium carbonate is a good ballast material [*Armstrong et al.*, 2002; *Klaas and Archer,* 2002]. This means that, although the calcification processes by itself reduces the

air-sea flux, the production of calcium carbonate can increase the overall organic sink of carbon dioxide from the atmosphere.

In the future, the ocean may have lower calcification rates due to ocean acidification [*Caldeira and Wickett,* 2005; *Orr et al.*, 2005; *Doney et al.*, 2009]. The reduced calcification would increase the surface alkalinity, potentially increasing the flux of carbon dioxide to the ocean [*Barker et al.*, 2003; *Hofmann and Schellnhuber,* 2009]. However, reducing the calcification would also reduce the ballast effect of calcium carbonate on the organic carbon cycle [*Feely et al.*, 2004; *Hofmann and Schellnhuber,* 2009]. *Barker et al.* [2003] estimated that the combined feedback on the atmosphere is less than 1 ppmv because the reduction in the ballast effect reduces the amount of carbon in organic matter leaving the surface ocean. The reduced ballast effect may also change the oxygenation of the water at mid-depths as the increased remineralization at this depth uses up oxygen and expands the hypoxic zones of the ocean [*Hofmann and Schellnhuber,* 2009].

Knowledge of the ocean carbonate system can also help us predict the long term impacts of climate change and ocean acidification. In a few thousand years, the ocean carbonate system will absorb the excess atmospheric carbon dioxide and help to stabilize the global climate [*Montenegro et al.*, 2007]. The long term impact, after carbonate compensation, is controlled by the behavior of the ocean carbonate system [*Tyrrell et al.*, 2007].

1.3 What is the ocean carbonate system?

The carbonate system describes how carbon dioxide reacts in the ocean, the largest reservoir of carbon [*Sarmiento and Gruber*, 2006]. Unlike oxygen, which has only one dissolved form, carbon dioxide exists in the ocean in mainly three different chemical species. These are aqueous carbon dioxide (CO_2aq), bicarbonate ion (HCO_3^-), and carbonate ion (CO_3^{2-}) [*Zeebe and Wolf-Gladrow*, 2001].

The carbonate species are related by Equation 1-1. Atmospheric carbon dioxide dissolves in the ocean to produce aqueous carbon dioxide. The aqueous carbon dioxide then reacts with water to produce carbonic acid (H_2CO_3). Almost all the carbonic acid then dissociates to bicarbonate ions and protons (H^+) and some of the bicarbonate further dissociates to carbonate ions and more protons. The equilibrium constants between the reactions are affected by temperature and pressure, and salinity [*Zeebe and Wolf-Gladrow*, 2001].

$$CO_2(aq) + H_2O \leftrightarrow H_2CO_3 \leftrightarrow HCO_3^- + H^+ \leftrightarrow CO_3^{2-} + 2H^+ \quad (1\text{-}1)$$

Most of the species in Equation 1-1 are not measurable, so we measure the carbonate variables instead. The species in Equation 1-1 that is measurable, and therefore called a carbonate variable, is the partial pressure of the aqueous carbon dioxide (pCO_2). The second carbonate variable, Dissolved Inorganic Carbon (DIC), is the total of all dissolved carbon species (CO_2, HCO_3^-, CO_3^{2-}, and the small concentration of H_2CO_3). pH can also be used to measure the protons released when carbon dioxide dissolves. The final carbonate variable is alkalinity (Equation 1-2) which is a carbonate variable because the majority of alkalinity is made up of bicarbonate and carbonate ions [*Zeebe and Wolf-Gladrow*, 2001].

To calculate the concentrations of individual species or other carbonate system variables you need measurements of at least two seawater carbonate variables. Because the equilibrium constants are affected by temperature, pressure, and salinity, these values also need to be measured. Silicate and phosphate are also needed as they affect alkalinity (Equation 1-2) [*Zeebe and Wolf-Gladrow*, 2001].

1.4 What is alkalinity?

Alkalinity is a concept that has been progressively developed and can be defined simply as the acid neutralization capacity of a liquid [*Dickson*, 1992]. The understanding of alkalinity has developed over time since the 1700s when seawater was first found to be alkaline (pH > 7) [*Marsili*, 1725].

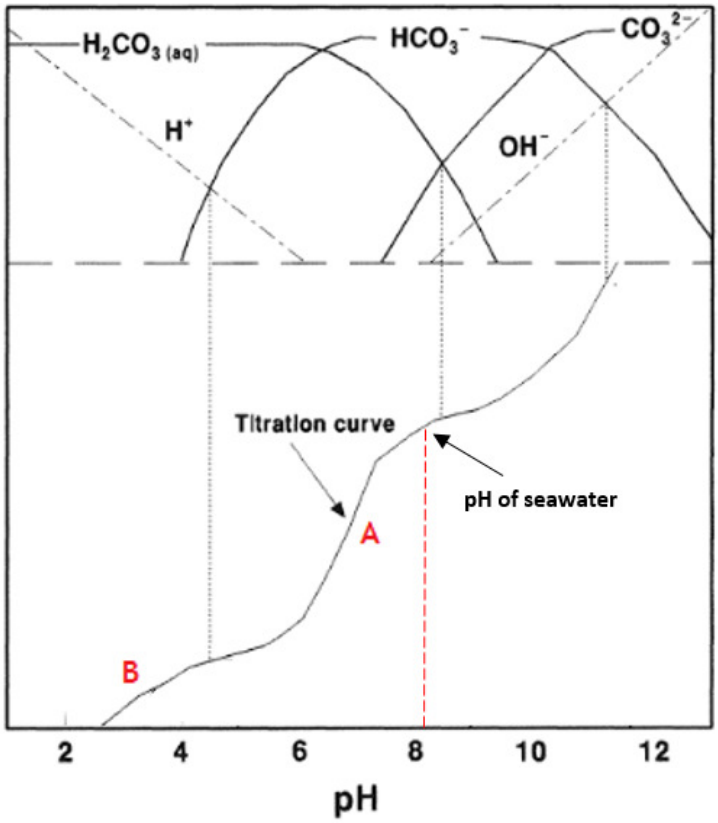

Figure 1-3. Titration of a carbonate based system showing the change in pH along with the relative proportions of each species (adapted from *Eby* [2016]). The points A and B are the inflection points of the titration curve.

Seawater was observed to be alkaline in the 1700s due to its reaction with color indicator [*Marsili*, 1725]. In the 1880s the term alkalinity was first used [*Dittmar*, 1884 in *Dickson*, 1992], and described the concentration of carbonate bases in a solution. Alkalinity was analyzed during that period by neutralizing sea water with sulphuric acid [*Schloesing*, 1880 in *Dickson*, 1992]. In 1916 alkalinity was calculated from the inflection points, which are where the titration curve changes concavity (Figure 1-3) [*Dickson*, 1992]. In 1939 the International Association of Physical Oceanography defined alkalinity as the number of mille-equivalents of hydrogen ion neutralized by one liter of water at 20ºC [*Anderson and Robinson*, 1946]. Rakestraw introduced the idea of proton donors and acceptors to describe what was measured in an alkalinity titration [*Dickson*, 1992; *Wolf-Gladrow et al.*, 2007]. With the use of mathematical methods to calculate the equivalence points of titrations (when the amount of acid is of the exact proportional concentration as the alkalinity) [*Gran et al.*, 1950; *Gran*, 1952], the calculation of alkalinity was improved [*Dyrssen*, 1965; *Dyrssen and Sillén*, 1967]. This led to the development of closed cell titration [*Edmond*, 1974] and large databases of measurements [*Dickson*, 1992]. *Dickson* [1992] reports a more detailed history of alkalinity and provided the first specific definition of alkalinity.

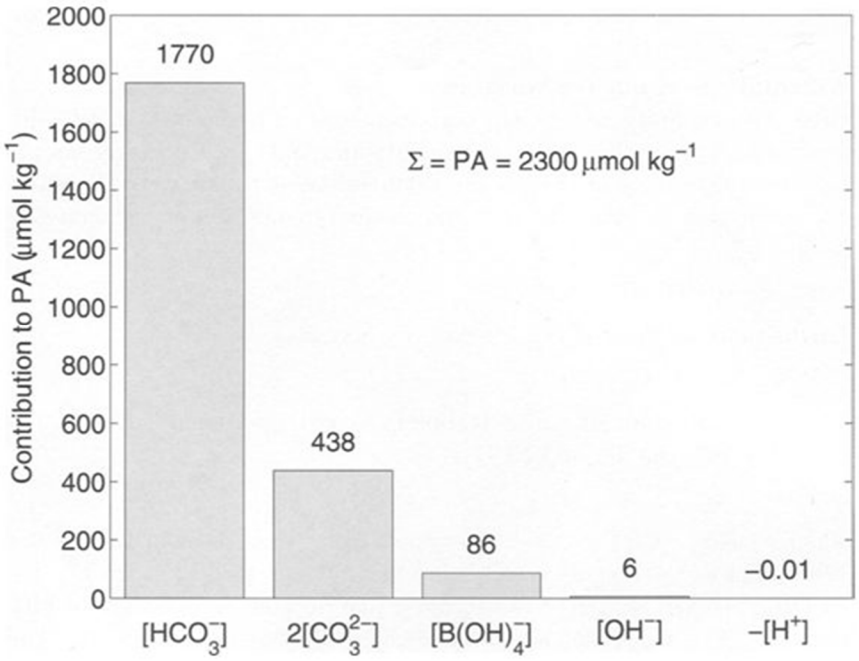

Figure 1-4. The contribution of different ions to Practical Alkalinity (PA), which is a simplified alkalinity for which is accurate for most practical purposes. When PA = 2300 μmol kg $^{-1}$, DIC = 2000 μmol kg $^{-1}$, temperature = 25ºC, and salinity = 35. From [*Zeebe and Wolf-Gladrow*, 2001].

Total alkalinity, hereafter referred to as alkalinity, is the excess of proton acceptors over proton donors made up by weak ions (Figure 1-4, Equation 1-2). It is measured by the stepwise addition of hydrochloric acid to determine the equivalence points of the titration curve [*Gran et al.*, 1950; *Dickson*, 1981, 2010]. Alkalinity is usually reported as the number of moles per kilogram of acid needed to replace the minor ions; however, it is not a true concentration of the species in Equation 1-2. The weight of each species in Equation 1-2 is the number of protons each species has accepted when the pH is reduced to 4.3.

$$\begin{aligned} Alk = {} & [HCO_3^-] + 2[CO_3^{2-}] + [B(ON)_4^-] + [OH^-] + [HPO_4^{2-}] + 2[PO_4^{3-}] \\ & + [H_3SiO_4^-] + [NH_3] + [HS^-] - [H^+] - [HSO_4^-] - [HF] \\ & - [H_3PO_4] - [HNO_2] \end{aligned} \qquad (1\text{-}2)$$

The concept of alkalinity can be simplified for theoretical purposes by only accounting for the most common species in Equation 1-2. For example, carbonate alkalinity only includes the bicarbonate and carbonate ions ($[HCO_3^-] + 2[CO_3^{2+}]$). There is also practical alkalinity (Figure 1-4), which is the total of the carbonate alkalinity plus the borate alkalinity ($[B(ON)_4^-]$) and water alkalinity ($[OH^-] - [H^+]$) [*Zeebe and Wolf-Gladrow,* 2001].

Carbonate alkalinity makes up 96% of practical alkalinity and practical alkalinity makes up 99% of total alkalinity [*Zeebe and Wolf-Gladrow,* 2001; *Emerson and Hedges,* 2008].

Alkalinity is conservative with respect to mixing and independent of changes in temperature and pressure, unlike pCO_2, pH, and concentrations of individual species in the seawater carbonate system [*Dyrssen and Sillén*, 1967; *Wolf-Gladrow et al.*, 2007]. This means that when two water masses of different alkalinity are mixed the resulting concentration of alkalinity is in proportion to the volume of water from each water mass. Also, when a water mass is heated or cooled or changes depth, the alkalinity is not affected.

1.5 What causes variations in the surface ocean alkalinity?

The global surface distribution of alkalinity is similar to the variation in surface ocean salinity. Alkalinity is high in the ocean gyres and low at the equator and poles. Figure 1-5 shows the surface distribution of alkalinity.

The sea surface distribution of alkalinity is affected by several processes. These include: (1) changes in seawater concentration caused by evaporation and precipitation [*Millero et al.*, 1998b]; (2) ventilation and upwelling of subsurface waters with high alkalinity from dissolution of calcium carbonate ($CaCO_3$) increasing the surface alkalinity [*Lee et al.*, 2006]; (3) production and export of $CaCO_3$; (4) consumption or regeneration of nutrients from primary production or respiration, respectively [*Brewer and Goldman*, 1976; *Millero et al.*, 1998a; *Wolf-Gladrow et al.*, 2007], and; (5) riverine input of alkalinity [*Friis et al.*, 2003; *Cai et al.*, 2010]. Recently it has been shown that ikaite formation in sea ice can change alkalinity [*Rysgaard et al.*, 2012b, 2013] and sulphate reduction in the deep sea and hydrothermal vents also affects alkalinity [*Deutsch et al.*, 2001; *Wolf-Gladrow et al.*, 2007].

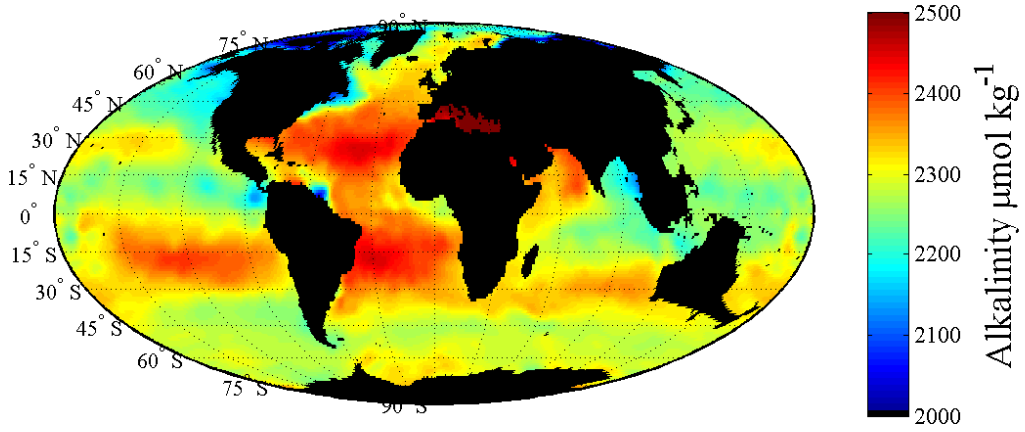

Figure 1-5. Gridded alkalinity (µmol kg^{-1}) at 10 dbars from GLODAPv2.

Evaporation and precipitation affect alkalinity through direct dilution through the addition of pure water, and concentration by removal of pure water [*Millero et al.*, 1998b]. Alkalinity is conservative with mixing. Conservative mixing is when waters with different properties mix, the resulting water has properties which are the linear weighted average of the input properties. Conservative mixing results in a change in alkalinity that is directly proportional to the amount of water added or removed and the alkalinity in the water [*Wolf-Gladrow et al.*, 2007].

River water also affects alkalinity in a conservative way. Unlike evaporation and precipitation, river water often contains dissolved ions that contribute to alkalinity [*Amiotte Suchet et al.*, 2003; *Friis et al.*, 2003; *Cai et al.*, 2010]. The effect of river water on a body of sea water can be predicted through conservative mixing; however, because it typically does not mix with an origin of zero salinity and zero alkalinity, there are implications for the common salinity normalization of alkalinity and so a correction is needed [*Friis et al.*, 2003; *Cai et al.*, 2010], see section 1.6.2.

The biological production and dissolution of calcium carbonate affects alkalinity [*Horibe et al.*, 1974; *Cross et al.*, 2013]. Production of calcium carbonate removes calcium and

bicarbonate from the water which decreases alkalinity [*Wolf-Gladrow et al.*, 2007]. The dissolution of calcium carbonate produces an equivalent increase in alkalinity.

Biological uptake of ions also affects alkalinity [*Brewer and Goldman*, 1976; *Millero et al.*, 1998b; *Wolf-Gladrow et al.*, 2007]. Phytoplankton take in charged nutrient ions and, to keep the charge balance of the cell neutral, they take up other oppositely charged species. Or, alternatively they exchange ions by pumping protons or a species of the same charge as the nutrient out of the cell. Examples of ions taken up in this way are nitrate, sulphate, and phosphate [*Wolf-Gladrow et al.*, 2007]. Remineralization of organic matter, from organic to inorganic compounds, releases the ions back into the ocean which causes the opposite change in alkalinity. Table 1-1 shows how alkalinity changes when different biological processes occur.

Table 1-1. The change in alkalinity (μmol kg^{-1}) caused by different biological processes.

Species	Change in alkalinity for every mole (μmol kg^{-1})
Uptake of nitrate, nitrite, or ammonia	+1
Nitrification	-2
Nitrogen fixation followed by remineralization and nitrification	-1
Denitrification	+1
Uptake of phosphate	+1
Uptake of silicic acid	No change
Uptake of sulphate	+2
Methane oxidation	+2

The formation and destruction of sea-ice changes the alkalinity of seawater. Ikaite ($CaCO_3 \cdot 6H_2O$) is a mineral that forms from carbonate in sea-ice in the Polar Regions. The formation of ikaite is similar to the formation of normal anhydrous calcium carbonate;

therefore, the change in alkalinity in the seawater is twice the change of DIC [*Rysgaard et al.*, 2012b, 2013]. Ikaite is produced when sea ice forms, and alkalinity is released when the sea ice melts. The process causes a deviation from the expected relationship of salinity and alkalinity, because when sea ice forms it reduces alkalinity and increases salinity. When sea ice melts alkalinity relatively increases whilst salinity decreases.

The ocean circulation affects the distribution of alkalinity because it moves and mixes water with different concentrations. It does not directly affect alkalinity but must be taken into account when analyzing local variations in alkalinity (Chapter 3). For example, upwelling water often increases the surface alkalinity because it contains alkalinity from dissolved calcium carbonate [*Lee et al.*, 2006], much in the same way as nitrate concentrations are higher in the surface waters where upwelling takes place.

1.5.1 The alkalinity in the past and future

Figure 1-66 shows the long term sources and sinks of alkalinity in the ocean which, through the buffer system, affect the concentration of carbon dioxide in the atmosphere and ocean. The major input is from rivers [*Amiotte Suchet et al.*, 2003] with minor additions from glaciers and groundwater. Hydrothermal vents are also a small sources of alkalinity [*Milliman and Droxler,* 1996]. Alkalinity is removed from the water through calcification by organisms producing calcium carbonate. The resulting calcium carbonate sinks and more than 80% of it is redissolved in the water column increasing the deep alkalinity concentration. The major long term sink of alkalinity is the burial of calcium carbonate [*Ridgwell and Zeebe,* 2005]. There may also be some authigenic production of calcium carbonate in sediments precipitated by dissolution of calcified shells [*Sun and Turchyn,* 2014]. Section 1.2 shows that the production of calcium carbonate is related to the alkalinity concentration and it can affect the climate.

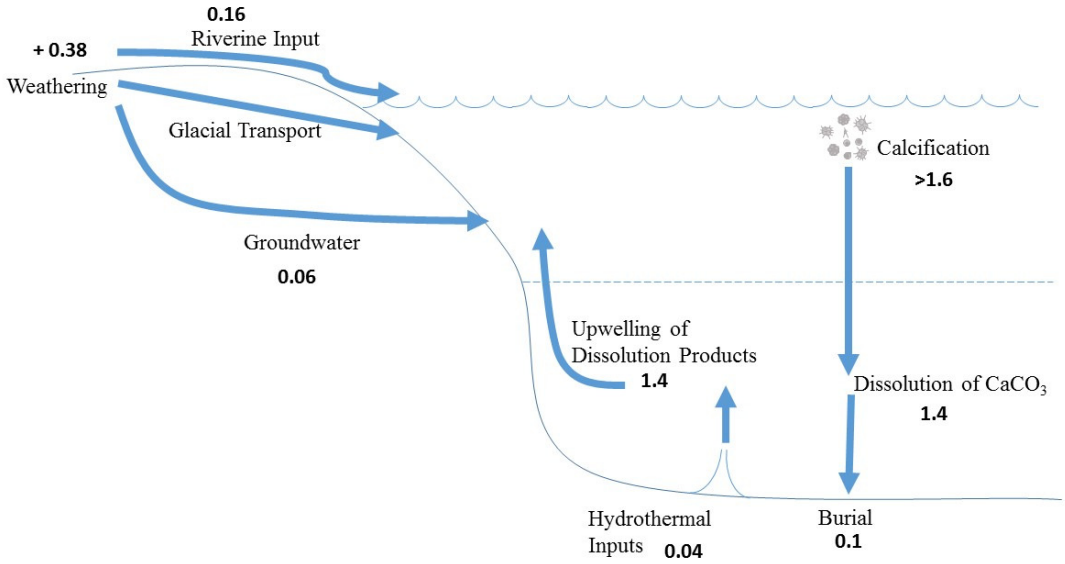

Figure 1-6. Schematic of the long term alkalinity cycle with sources and sinks of carbonate alkalinity. Numbers in bold indicate fluxes of alkalinity in of Pg C yr^{-1} and may not add up as they are from different sources [*Milliman and Droxler,* 1996; *Amiotte Suchet et al.*, 2003; *Berelson et al.*, 2007]. Fluxes from glacial transport have not been quantified.

The precipitation of calcium carbonate reduces the air-sea flux of carbon dioxide (section 1.2); however, the production calcium carbonate is actually a sink on a geologic timescale. This occurs when the precipitated calcium carbonate is buried in sediments in the ocean [*Falkowski et al.*, 2000; *Ridgwell and Zeebe,* 2005]. However, the source of the alkalinity to the surface ocean is important. Equation 1-3 shows what happens when calcium carbonate from rock is dissolved to provide the ocean bicarbonate which then produces new calcium carbonate.

$$CO_2 + H_2O + CaCO_3 = Ca^{2+} + 2HCO_3^- = CaCO_3 + CO_2 + H_2O \quad (1\text{-}3)$$

Equation 1-4 shows the reactions when silicate weathering is used to provide the ocean with bicarbonate before being used to produce calcium carbonate.

$$2CO_2 + 3H_2O + CaSiO_3 = Ca^{2+} + 2HCO_3^- + H_4SiO_4 = CaCO_3 + CO_2 + SiO_2 + 3H_2O \quad (1\text{-}4)$$

The reactions in Equation 1-3 produce one mole of carbon dioxide for every one mole used to dissolve the rock. However, Equation 1-4 shows that only one mole of carbon dioxide is

released but two moles of carbon dioxide are used to dissolve the rock [*Amiotte Suchet et al.*, 2003; *Ridgwell and Zeebe,* 2005].

Long term changes in the weathering rates of silicate rock and burial rates of ocean calcium carbonate can therefore control the global temperature [*Amiotte Suchet et al.*, 2003; *Ridgwell et al.*, 2003; *Ridgwell and Zeebe,* 2005]. Changes in weathering have been used to explain icehouse/greenhouse swings in climate. If more silicate rock is weathered, then the carbon dioxide concentration goes down and the temperature of the surface of the planet cools. However, the concentration of carbon dioxide and the temperature of the atmosphere affect the rate of weathering; therefore, eventually the weathering rate decreases and the temperature will stabilize [*Brady and Carroll,* 1994; *Kump et al.,* 2000].

On a shorter timescale the ocean and the carbonate system buffer the atmospheric carbon dioxide concentration [*Ridgwell and Zeebe,* 2005]. When the concentration of carbon dioxide in the atmosphere increases, the quantity of carbon entering the ocean also increases. This increase in the DIC of the ocean reduces the pH; however, the dissolution of carbon dioxide does not directly increase the alkalinity [*Feely et al.*, 2004, 2012; *Orr et al.*, 2005]. The reduced alkalinity to DIC ratio indicates a reduction in the saturation state of calcium carbonate in the ocean which shoals the carbonate compensation depth (the depth at which calcium carbonate in sediments completely dissolves), and causes more calcium carbonate sediments to dissolve [*Barker et al.*, 2003; *Ridgwell and Zeebe,* 2005]. The dissolution of calcium carbonate increases the alkalinity and the saturation state of calcium carbonate. The increased alkalinity causes more carbon dioxide to enter the ocean until equilibrium is reached. These processes take between 5 and 8 thousand years to react and will be the eventual fate of up to 20% of the anthropogenic carbon dioxide with silicate weathering ultimately consuming the rest [*Ridgwell and Zeebe,* 2005; *Tyrrell et al.*, 2007]

It is possible to increase the absorption of anthropogenic carbon dioxide into the ocean by increasing surface ocean alkalinity and this is called ocean liming or alkalization. Increasing the surface alkalinity would entail adding large amounts of chalk and limestone [*Kheshgi,* 1995; *Harvey,* 2008; *Williamson and Turley,* 2012]. The calcium carbonate from these rocks would dissolve and increase ocean alkalinity which would enable larger amounts of carbon dioxide to enter [*Harvey,* 2008]. This scheme would stabilized ocean acidification and absorb up to 5000 Pg C, but would cost between 0.5 to 2.8 $US trillion per year depending on the scale of the operation and carbon capture and storage would be necessary to reduce the impact of processing the rock [*Paquay and Zeebe,* 2013].

1.6 How is alkalinity used in studies?

1.6.1 Approximating alkalinity

Alkalinity in the surface ocean has often been predicted because it is conservative with mixing [*Millero et al.*, 1998b] and therefore correlates strongly with salinity (Pearson's r correlation coefficient = 0.94, Chapter 3) as shown in Figure 1-7. Alkalinity needs to be predicted because there are limited carbonate measurements (alkalinity, DIC, pCO_2, pH) compared with nutrients and physical measurements. For example, the global database for carbonate measurements, GLODAPv2, contains about 42 thousand casts whereas the World Ocean Database of nutrients, salinity, and temperature contains over 3 million casts.

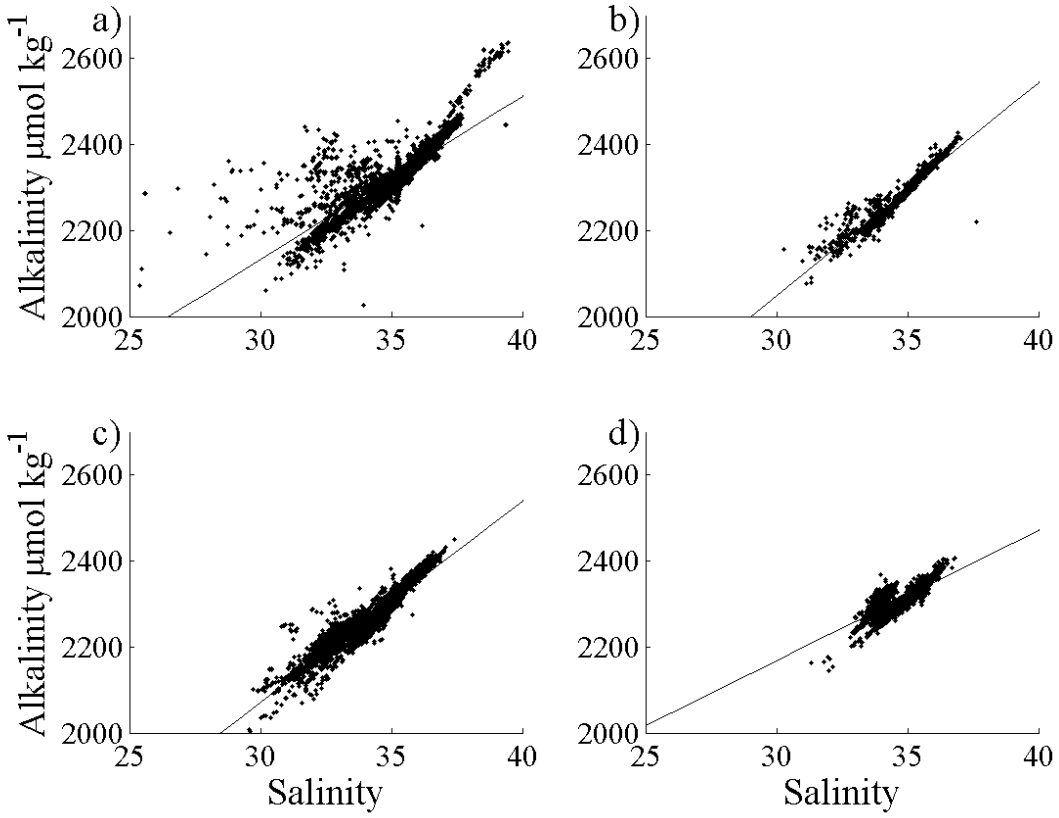

Figure 1-7. Alkalinity (µmol kg^{-1}) as a function of salinity in surface ocean (<30 m) of (a) the Atlantic Ocean, (b) the Indian Ocean, (c) the Pacific Ocean, and (d) the Southern Ocean (south of 30ºS) using the GLODAPv2 database. The fitted line is the relationship between salinity and alkalinity in the given basin.

The first paper to predict alkalinity in the surface ocean was *Millero et al.* [1998b]. The authors analyzed the variations in alkalinity and compared the patterns with salinity and

sea surface temperature. They then produced equations to predict alkalinity in the global surface ocean from sea surface temperature and salinity.

Lee et al. [2006] updated the *Millero et al.* [1998b] equations with the help of greater data (n = 5692 for *Lee et al.* [2006] and n = 1740 for *Millero et al.* [1998b]). Again, the authors used sea surface temperature and salinity to predict alkalinity; however, they used polynomial equations which further improved the predictive ability of their equations. The *Lee et al.* [2006] equations for predicting alkalinity cover all the ocean except the Arctic and Mediterranean Seas. The equations are especially useful in that salinity and temperature are frequently measured, and when combined with pCO_2, the most commonly measured carbonate parameter (10.1 million data points in SOCATv2 [*Bakker et al.*, 2014]), they can predict the carbonate system over large areas of the global surface ocean. For this reason, the equations by *Lee et al.* [2006] are widely used [*Gledhill et al.*, 2008; *Körtzinger et al.*, 2008; *Wootton et al.*, 2008; *Clark et al.*, 2009].

Further algorithms have been created for alkalinity; however, these are local rather than global and focus on areas where the *Lee et al.* [2006] algorithm has issues. For example, *McNeil et al.* [2007] found a seasonal bias in the prediction error when using the *Lee et al.* [2006] algorithm in the Southern Ocean. *McNeil et al.* [2007] made a new equation for the area using salinity, nitrate, and silicate. Temperature was avoided as a variable because it was the cause of the seasonal bias. *Takatani et al.* [2014] used sea surface height to predict alkalinity in the surface of the North Pacific. In this region, *Lee et al.* [2006] used longitude as an extra parameter to increase the fit. *Takatani et al.* [2014] improved on the *Lee et al.* [2006] algorithm; however, they also split the North Pacific into more regions. The *Lee et al.* [2006] algorithm does not cover the Mediterranean Sea so *Touratier and Goyet* [2011] used potential temperature and salinity to form an algorithm that predicts alkalinity at all depths in this area, not just the surface.

1.6.2 Alkalinity as a tracer

Alkalinity can be included in different equations to produce tracers of different processes. The most common is salinity-normalized alkalinity [*Postma*, 1964; *Millero et al.*, 1998b]. Salinity normalization proportionally changes the alkalinity to a standard salinity, normally 35 (Equation 1-5). This is often used as it removes the majority of the variation which is caused by evaporation and precipitation. This allows samples with different salinities to be compared [*Friis et al.*, 2003]. Examples of where it has been used include in the North Pacific to identify formation of calcium carbonate (calcification) and, when compared to

temperature, to identify physical processes [*Wong et al.*, 2002]. Salinity-normalized alkalinity has also been used in the northern South China Sea, where it has been compared against salinity-normalized DIC to show organic carbon production [*Cao et al.*, 2011].

$nAlk = 35\frac{Alk_m}{S}$ where nAlk is salinity normalized alkalinity, Alk_m is measured alkalinity, and S is salinity. (1-5)

The problem with the standard salinity normalization is that it works in the open ocean where the only freshwater removal and addition is evaporation and precipitation respectively. Around river plumes there is a deviation as the river water has negligible salinity but often measurable alkalinity. This leads to significant over correction of the alkalinity value [*Friis et al.*, 2003]. *Jiang et al.* [2014] took the idea forward by dividing variations in alkalinity into simple dilution or concentration processes (SDC) and non-SDC processes. They also noted that, although the intercept of the alkalinity-salinity relationship can be the river concentration of alkalinity [*Cai et al.*, 2010], in certain areas the value is negative (the Mediterranean Sea), see section 1.6.3.

Potential alkalinity is usually the same salinity-normalization in Equation 1-5, but the nitrate concentration is added to the measured alkalinity first. There are slight variations, for example, *Brewer et al.* [1975] used "potential alkalinity" which was alkalinity plus nitrate and phosphate. In potential alkalinity the nitrate, or phosphate, is added because uptake or release of charged ions is balanced by changes in alkalinity to keep the charge of the ocean neutral [*Wolf-Gladrow et al.*, 2007]. Potential alkalinity is useful because it correlates with bomb-produced radiocarbon so is an estimate of water mixing [*Rubin and Key*, 2002; *Sabine et al.*, 2002]. *Sabine et al.* [2002] used potential alkalinity to analyze deep ocean circulation in the Indian Ocean. Potential alkalinity improves on salinity-normalized alkalinity by accounting for the changes in alkalinity caused by biological activities [*Wolf-Gladrow et al.*, 2007]. The concept of potential alkalinity could be improved by standardizing its use, for example, always using a salinity normalization and a standard multiplier of nitrate.

Preformed alkalinity is an estimate of the alkalinity the water had when it left the surface [*Sabine et al.*, 1999, 2002; *Feely et al.*, 2004]. There are various ways to estimate the preformed alkalinity. For example, *Gruber et al.* [1996] produced a generic preformed alkalinity from a multiple linear regression using salinity, phosphate, and oxygen. *Sabine et al.* [1999] used a best fit for pressures less than 60 dbars with the variables of salinity, phosphate, oxygen, and potential temperature. *Chung et al.* [2004] used a relationship with

nitrate rather than phosphate due to lack of phosphate data in the Atlantic Ocean. Preformed alkalinity has the same problem as potential alkalinity, in that its definition/equation varies between uses. However, this has not stopped it being a useful measure, especially for estimating the accumulation of anthropogenic carbon in the water (see below).

TA* is a tracer of remineralized alkalinity which is the alkalinity that has been released into the water body through dissolution of sinking calcium carbonate particles [*Feely et al.*, 2002a; *Sabine et al.*, 2002; *Chung et al.*, 2004]. TA* is calculated along each isopycnal layer from the preformed alkalinity and the apparent oxygen utilization [*Feely et al.*, 2002a]. TA* is used along with water mass estimates from chlorofluorocarbons and carbon-14 to estimate dissolution of $CaCO_3$. Estimations of $CaCO_3$ dissolution in water bodies are useful for approximating the global magnitude of the export of calcium carbonate; however, because this tracer is used in deep water bodies it cannot be used to estimate exactly where the production of calcium carbonate took place and therefore is not useful for estimating calcification rates.

Measured alkalinity and preformed alkalinity are used in several tracers to calculate the quantity of anthropogenic carbon in the ocean [*Sabine et al.*, 1999, 2002; *Matsumoto and Gruber,* 2005; *Touratier et al.*, 2007; *Khatiwala et al.*, 2013]. Measured alkalinity is used to account for calcification and preformed alkalinity is used to calculate the DIC concentration of the water if the ocean was in equilibrium with the pre-industrial ocean (usually pCO_2 = 280 ppm) [*Gruber et al.*, 1996; *Matsumoto and Gruber*, 2005]. There are several methods for estimating anthropgenic carbon from in situ data [*Khatiwala et al.*, 2013]. The oldest common method is ΔC^*; however it assumes nutrients are used in the Redfield ratio and it over estimates anthropogenic carbon in the surface ocean and underestimates in the deep ocean [*Gruber et al.*, 1996; *Khatiwala et al.*, 2013]. Another method is the Tracer using Oxygen, inorganic Carbon, and Alkalinity (TrOCA) which is useful as it only uses one equation for all regions; however, it also overestimates anthropogenic carbon in some areas of the ocean [*Touratier et al.*, 2007; *Khatiwala et al.*, 2013].

1.6.3 How is alkalinity used in studies?

Alkalinity is widely predicted because its conservative nature means that the algorithm can be quite accurate (section 1.6.1). Therefore, it is often used as a second carbonate variable when only one variable has been measured. The *Lee et al.* [2006] algorithm has been used

in many studies, such as analyzing long-term trends in ocean acidification and measuring carbonate conditions experienced by echinoid larvae. *Gledhill et al.* [2008] studied the long-term trends in the saturation state of aragonite in the Caribbean region between 1996 and 2006. They used voluntary ships, which analyzed pCO_2, along with alkalinity estimated from *Lee et al.* [2006], to fully reconstruct the carbonate system. Their results showed the area is highly variable, but overall there was a decrease in the aragonite saturation, the aragonite form of $CaCO_3$ dissolved more easily, over the 10-year period of study. *Körtzinger et al.* [2008] used a surface alkalinity product produced from mean monthly temperature and salinity fields and the *Lee et al.* [2006] algorithm. This data was used to understand the wider picture of biological production around a specific site. They believe the site has one of the most significant spring blooms and that the seasonal drawdown of pCO_2 causes an average undersaturation of carbon dioxide in the surface waters causing the area to be a sink of atmospheric carbon dioxide.

The *Lee et al.* [2006] algorithm has also been used in biological studies. *Wootton et al.* [2008] used measured pH and the *Lee et al.* [2006] algorithm to constrain the entire carbonate system around Tatoosh Island off the coast of Washington State. Their analysis shows that the coastal ocean has fluctuating pH that may have an impact on the local ecology, with species such as California mussel *Mytilus californianus*, the goose barnacle *Pollicipes polymerus*, and filamentous red algae being affected. *Clark et al.* [2009] used alkalinity to back up pH measurements at remote locations where a second parameter measurement would not have been feasible. In this study they collected samples of four echinoid species along with the ambient sea water and lowered the pH to understand the effects of ocean acidification. They showed that decreasing the pH decreased the survival and the size of the species and calcification was reduced.

The mainly conservative nature of alkalinity means that it is a useful marker of different water bodies. It has been used in coastal areas and marginal seas to analyze different sources of water. One of the first studies to analyze alkalinity was in the Fraser River estuary [*Mora*, 1983]. They found apparent non-conservative behavior at low salinities that could be caused by error or from the mixing of different sources. A third alternative could be removal of alkalinity at low-salinities. Greater research in recent years has enhanced scientific understanding of marginal seas. *Cai et al.* [2010] analyzed the alkalinity around the western North Atlantic margin to find the sources of the different waterbodies. They identified two types of margin, alongshore current-dominated and river-dominated. Current dominated water carried the salinity-alkalinity ratio of the water upstream compared with

river-dominated waters which carried the salinity-alkalinity ratio of the local water inputs. The authors thereby showed that the intercept of the salinity-alkalinity relationship is not always a reliable indicator of the alkalinity of local rivers. *Jiang et al.* [2014] studied alkalinity from ships of opportunity and used alkalinity and salinity to identify sources of water and formation of calcium carbonate. They found river inputs along the western North Atlantic margin similar to *Cai et al.* [2010] and they also identified similar mixing occurring in the eastern North Pacific and the Mediterranean Sea. Like *Cai et al.* [2010] they also found areas influenced by shelf currents, but they also found upwelling and calcification can confuse the salinity-alkalinity relationship. They even found negative intercepts for the salinity-alkalinity relationship in the Mediterranean where the areas with higher salinities are closer to the sources of river alkalinity.

Coastal alkalinity is studied as anaerobic processes, such as sulphate reduction in the sediments, often increase alkalinity (Table 1-1). An increased alkalinity can enhance the uptake of atmospheric carbon dioxide in coastal regions. *Chen* [2002] calculated using data from the North Pacific that anaerobic production of alkalinity produces $16 – 31 \times 10^{12}$ mol yr^{-1} above the lysocline (the depth where calcium carbonate starts to dissolve). *Thomas et al.* [2008] analyzed the sources and sinks of alkalinity in the North Sea. They calculate that anaerobic alkalinity causes 20-25% of the North Seas total CO_2 uptake. They postulate that in the future, higher production in the ocean margins will increase the scale and therefore impact of anaerobic alkalinity. *Hu and Cai* [2011] calculated that net alkalinity production from anaerobic processes releases only $4\text{-}5 \times 10^{12}$ mol yr^{-1} of alkalinity which is smaller than past estimates [*Chen*, 2002; *Thomas et al.*, 2008]. This is because only processes that result in permanent loss of anaerobic remineralization products, such as gas escaping after nitrogen production or sulphur loss by pyrite burial, will result in permanent changes in the alkalinity.

Areas with high organic matter, for example around estuaries and fjords, can also contain a significant amount of organic alkalinity that can interfere with the interpretation of the carbonate system [*Kim and Lee*, 2009]. *Kim et al.* [2006] demonstrated that organic alkalinity in unfiltered seawater samples could cause errors when calculating the carbonate system. They determined that the alkalinity was from negatively charged areas of the surface of phytoplankton and bacterial cells and that this would have a similar magnitude impact on alkalinity as the borate ion. *Kim and Lee* [2009] showed that dissolved organic matter produced by marine phytoplankton during photosynthesis has buffering capacities and *Yang et al.* [2015] found organic alkalinities up to 26.4 µmol kg^{-1} along the coast of

North America both from direct titrations and from the difference between calculated and measured alkalinity. This is a similar content of measured alkalinity to that from fjord water near Bergen, Norway which has 2-22.3 μmol L^{-1} [*Muller and Bleie*, 2008].

Alkalinity can also be used in studies about the general carbonate system; therefore, alkalinity measurements are important in climate change studies. For example, alkalinity is often used to calculate the state of the ocean and therefore the magnitude of the flux of carbon dioxide into the ocean. This is important because carbon dioxide entering the ocean decreases the amount left to warm the atmosphere; however, once in the ocean it causes ocean acidification. *Rysgaard et al.* [2012a] used alkalinity along with DIC, temperature, salinity, and phosphate and silicate concentrations to calculate the partial pressure of carbon dioxide around Southern Greenland. They used the knowledge of the local carbonate system to analyze how the air-sea carbon dioxide fluxes changed with time on continental shelves. They found that, although air-sea fluxes varied throughout the year, the continental shelves around Greenland are a sink for carbon dioxide. A longer time series around Bermuda was analyzed for changes over many years [*Bates et al.*, 1996]. *Bates et al.* [1996] used alkalinity and DIC, like *Rysgaard et al.* [2012a], to calculate the partial pressure of carbon dioxide from October 1988 to December 1993 at the Bermuda Atlantic Time Series site. They found that most of the changes in the partial pressure of carbon dioxide correlate to temperature.

Many studies used estimated alkalinity as a second parameter, as mentioned above in section 1.6.1. One example is *Barbero et al.* [2011], who used estimated alkalinity, from *Lee et al.* [2006], to compliment pCO_2 measured from drifters. They estimated the changes in DIC and air-sea CO_2 fluxes in the Subantarctic Zone of the Pacific Ocean. Being able to use estimated alkalinity is useful as this area is remote and therefore has few measurements. They find that the area is a weaker sink of carbon dioxide than previous studies have suggested.

Ocean acidification and the influx of anthropogenic carbon are often measured using alkalinity as one of the carbonate properties (section 1.3). Alkalinity is also used in other methods to measure ocean acidification and anthropogenic carbon. One of these methods is TrOCA which estimates anthropogenic carbon [*Touratier et al.*, 2007]. This was then used to analyze how much anthropogenic carbon has entered the Mediterranean Sea [*Touratier and Goyet*, 2011]. *Touratier and Goyet* [2011] used interpolated alkalinity to calculate that all the water bodies in the Mediterranean Sea contain at least 37.5 μmol kg^{-1} of anthropogenic carbon with the Western basin having more than the Eastern basin. *Byrne et*

al. [2010] analyzed the extent of ocean acidification from 1991 to 2006 in the North Pacific on a transect from Hawaii to Alaska. They measured pH and used either measured or calculated alkalinity to produce estimates of acidification and anthropogenic carbon uptake. They found anthropogenic carbon in the top 800 m and basin wide acidification at 500 m which could be partially attributed to changes in ventilation. Alkalinity from the Global Ocean Data Analysis Project has also been used to calculate future ocean acidification and the effectiveness of ocean liming [*Harvey*, 2008]. *Harvey* [2008] used column calculations and simple low resolution models based on in situ measurements of alkalinity and DIC to calculate the effect of spreading limestone (calcium carbonate) in the surface ocean of upwelling regions. The hypothesis is that the calcium carbonate will fall to below saturation horizon, which is shallower in upwelling regions, and dissolve. The dissolution products will then rise to the surface and reduce the acidification of the water and cause a flux of carbon dioxide to enter the mixed layer which would offset anthropogenic global warming. *Harvey* [2008] showed that this method could potentially absorb an average of 0.48 Gt of carbon every year; however, this would take hundreds of years and is therefore a long term commitment.

1.7 Summary

The ocean carbonate system is important to study to understand how anthropogenic carbon will affect the climate and the chemistry of the Earth. Alkalinity is part of the ocean carbonate system and it can be used with another carbonate chemistry variable to calculate the entire inorganic carbon system in sea water because alkalinity is mainly made of bicarbonate and carbonate ions. First measured in the 1700s and understood since the 1930s, alkalinity is the difference between the major anions and cations made up by minor ions. It is measured in a titration with a stepwise addition of hydrochloric acid. Alkalinity is affected by evaporation, precipitation, input of river water, biological uptake of ions, remineralization of organic matter, calcification, sea ice formation and melt, and ocean circulation. Alkalinity is often used as a tracer and its value is often estimated in order to calculate the whole carbonate system. It is easier to estimate than other parameters because it is conservative and is highly correlated to salinity.

1.8 Aims and objectives

Millero et al. [1998b] and *Lee et al.* [2006] previously analyzed alkalinity in the global surface ocean. However, these studies created empirical algorithms and described the

variation in alkalinity rather than exploring the causes of variation. The following questions on the causes of variation are therefore addressed in this thesis:

1. What are the major factors causing variation in the surface ocean alkalinity?
2. How much of the variation do the major processes affecting alkalinity cause?
3. Where in the surface ocean is alkalinity most affected by each of the major processes which cause its variation?
4. What processes cause the longitudinal variations in salinity-normalized alkalinity in the North Pacific that *Lee et al.* [2006] found difficult to predict?
5. Can the prediction of alkalinity in the surface of the North Pacific be improved?
6. Can an in-situ alkalinity tracer improve the estimation of the export of calcium carbonate in the Southern Ocean?

The main aims of this thesis are to further scientific knowledge of alkalinity by understanding the controlling process on alkalinity in the surface ocean and understanding the causes of large-scale regional variations. To achieve these aims, the objectives were to:

1. Identify the magnitude of variations in surface ocean alkalinity caused by different major processes, such as evaporation and precipitation, river inputs, organic matter production, upwelling, and production of calcium carbonate.
2. Identify in which areas surface alkalinity is most affected by each of the major processes in objective 1.
3. Explain the causes of longitudinal variations in alkalinity and salinity-normalized alkalinity in the North Pacific which have previously proven difficult to ascertain [*Lee et al.,* 2006].
4. Produce an algorithm to predict alkalinity in the surface ocean of the North Pacific that is an improvement upon the algorithm by *Lee et al.* [2006].
5. Produce a new method to map and quantify the production of calcium carbonate in the subpolar frontal region of the Southern Ocean using a tracer of calcium carbonate cycling.

1.9 Structure of thesis

Chapter one has summarized the current knowledge of alkalinity. Chapter two summarizes the data used in this study, both how the data was collected and how it was quality controlled. In Chapter three, the main causes of surface alkalinity variation in the ocean are removed, leaving a tracer for the calcium carbonate cycle. Chapter four uses the tracer

from Chapter three to identify local variations of alkalinity in the surface North Pacific and produces simple predictive algorithms for alkalinity in the area. In Chapter five, a method is produced to quantify the amount of calcium carbonate production in the Southern Ocean. In Chapter six, all the results are discussed along with the future implications of the work.

Chapter 2: Databases used in this thesis

2.1 History of carbon datasets

To enhance scientific understanding of the carbonate system (Chapter 1), international collaborations made an effort to collate and organize carbon related measurements in the ocean. The first attempts to create largescale datasets of inorganic carbon variables took place in the 1970s. The first project, the Geochemical Ocean Sections (GEOSECS) Program, measured carbonate chemistry variables in the Atlantic, Indian, and Pacific oceans and provided the foundation on which much of the current understanding of ocean carbonate chemistry is based [*Bradshaw et al.*, 1981; *Key et al.*, 2004]. Then, in 1981, the Transient Tracers in the Ocean study obtained carbonate chemistry measurement along with radiochemical tracers. The study's aim was to investigate ocean mixing and was restricted to the North Atlantic Ocean [*Brewer et al.*, 1986b]. However, despite these two different attempts to create largescale datasets, there was still very little data until the 1990s.

During the 1990s, three major projects expanded the range of measurements and together sampled most of the global ocean. These studies were: the World Ocean Circulation Experiment (WOCE), the Joint Global Ocean Flux Study (JGOFS), and the Ocean-Atmosphere Carbon Exchange Study (OACES). These were all planned, organized, and funded in different ways and covered separate areas [*Sabine et al.*, 2005]. However, they all had the one aim in common: to understand the flux of CO_2 into the ocean to quantify how the ocean mitigates the increasing atmospheric concentration of anthropogenic CO_2 [*Brewer et al.*, 1986a; *Millero et al.*, 1998a; *Sabine et al.*, 2005]. The existence of these data products allowed large scale studies which are important when studying the carbon cycle [*Olsen et al.*, 2016]. About this time Certified Reference Materials and quality control also started to be developed (see section 2.2).

In 2004, the Global Ocean Data Analysis Project (GLODAP) combined GEOSECS and the three 1990s studies with other historical data to produce a global quality-controlled database of carbon, nutrients, and other measurements, such as CFCs and carbon isotope data [*Sabine et al.*, 2005]. GLODAP was made available (open access) on the internet and contained mapped fields of the carbon parameters, DIC and alkalinity. GLODAP has been widely used, for instance, for producing estimates of pre-formed alkalinity [*Pardo et al.*,

2011], analyzing ocean trends in pCO_2 [*Lenton et al.*, 2012], and designing biogeochemical models [*Le Quéré et al.*, 2005].

The release of GLODAP was followed by CARINA (CARbon dioxide IN the Atlantic Ocean) and PACIFICA (PACIFic ocean Interior Carbon database). These newer datasets had additional new data and filled in some of the gaps. For example, they had greater coverage of high latitude winters, marginal seas, and the Arctic Sea [*Key et al.*, 2010]. CARINA and PACIFICA have been used in various studies, for example, they have been used to predict carbon parameters in the ocean [*Sasse et al.*, 2013; *Carter et al.*, 2016], to compare local data with global patterns [*Jiang et al.*, 2014], and to calculate the depth at which calcite currently dissolves in the South Pacific [*Bostock et al.*, 2011].

The 2000s also saw the start of the CLIVAR (Climate and Ocean: Variability, Predictability and Change) repeat surveys which repeated measurements along the same lines as of some of the 1990s WOCE cruises. CLIVAR then evolved into the Global Ocean Ship-based Hydrographic Investigations Panel (GO-SHIP) which started in 2012 and aims to repeat the same cruises as WOCE and CLIVAR as well as new routes in the Arctic Sea [*Hood*, 2009]. GO-SHIP measurements are designed to be of the highest possible quality [*Feely et al.*, 2014; *Olsen et al.*, 2016]. Repeat cruises enable the study of long-term trends and can also be used for sensor calibration. As an example of the use of repeat surveys, *Álvarez et al.* [2011] used repeat cruises in the Indian Ocean between Africa and Australia to detect changes in salinity, nutrients, and oxygen in the subtropical Indian gyre. They showed that the changes they found were related to changes in the area of formation of the Subantarctic Mode Water in that region of the Indian Ocean.

Datasets of the partial pressure of carbon dioxide were also released near the end of the 2000s. The pCO_2 datasets are often separate from other in situ datasets as they are from autonomous instruments that do not necessarily have concurrent measurements of nutrients. The autonomous instruments also sample at high frequency resulting in large datasets from surface waters. These datasets started with the Lamont-Doherty Earth Observatory (LDEO) dataset which was made public in 2007 [*Takahashi and Sutherland*, 2009; *Pfeil et al.*, 2013]. Further data were then complied into a global and accessible, quality controlled database of pCO_2 measurements called the Surface Ocean CO_2 Atlas (SOCAT). The first version was released in 2011 and contained 6.3 million samples covering from 1968 to 2007 [*Pfeil et al.*, 2013]. An updated version of SOCAT was then released in 2013 and contained 10.1 million samples covering up to 2011 [*Bakker et al.*, 2014]. SOCATv2 has been used in many studies; one example is assessing the

improvement after data assimilation of modelled carbon parameters in a coupled ocean biogeochemical model [*Visinelli et al.*, 2016].

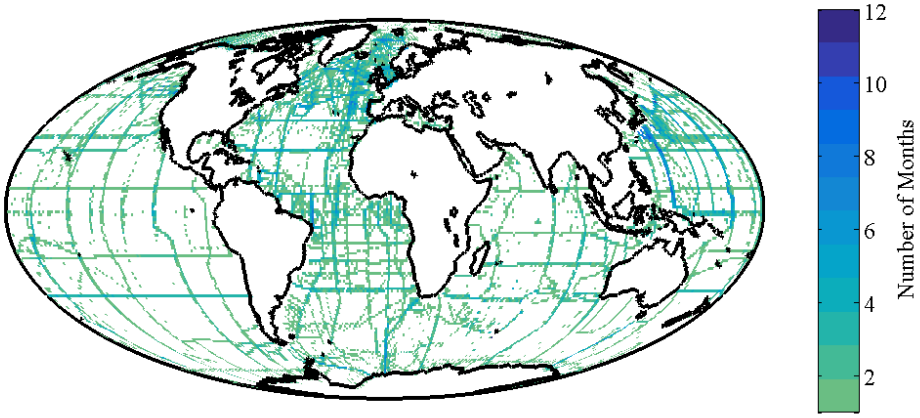

Figure 2-1. Distribution of data in GLODAPv2 in the top 30 m gridded to a one-degree grid. The color represents the number of months with data in each one-degree area.

In 2016 the second version of GLODAP was released [*Olsen et al.*, 2016]. GLODAPv2 combines the original GLODAP database with CARINA and PACIFICA as well as 168 other cruises that were not included in the original GLODAP product [*Olsen et al.*, 2016]. GLODAPv2 has 42 thousand casts and 32.3% of those casts contain alkalinity measurements. GLODAPv2 provides greater spatial coverage, including in the Arctic Sea (Figure 2-1), and has more winter coverage in both hemispheres, although there is still poor seasonal coverage of the South Pacific.

2.2 Quality control

Quality control ensures that the database is internally consistent. Internally consistent means that there are no biases between cruises. For example, measurements of the same water by different institutes yield the same alkalinity value. Because databases of ocean carbonate measurements are a collection of cruises at different times by different institutes, errors and biases are likely to occur. Figure 2-2 shows the steps of quality control used to reduce and remove these errors and biases and make the database more internally consistent. These procedures were originally created for the WOCE database and have been adapted for GLODAP, CARINA, PACIFICA and GLODAPv2 [*Johnson et al.*, 2001; *King et al.*, 2001; *Key et al.*, 2004; *Tanhua et al.*, 2010; *Suzuki et al.*, 2013; *Olsen et al.*, 2016].

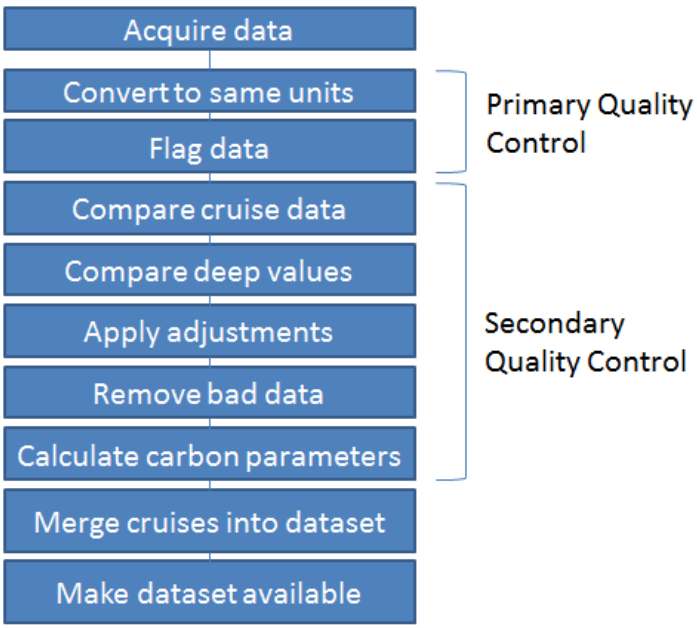

Figure 2-2. The steps taken to create and quality control large, internally consistent carbon datasets.

Quality control is used to produce a consistent data product. Methods were developed to detect and account for variations between measurements in different cruises because the first carbon measurements did not have standards or a Certified Reference Material (CRM) [*Sabine et al.*, 2005; *Tanhua et al.*, 2010]. Carbonate system CRMs are made by collecting seawater which is then measured to high level of accuracy. Other laboratories can then analyze the CRM and compare their measurement with the certified value. Any difference between the certified value of the CRM and the lab measurement can be used to correct other data measured at the same time [*Dickson et al.*, 2003]. The CRM widely used for alkalinity and dissolved inorganic carbon is produced by the laboratory of Andrew Dickson at Scripps Institution of Oceanography. There are limitations with the current CRM; for example, it is less useful for correcting measurements with values that are far from those of the CRMs value, such as in the Mediterranean where the alkalinity concentration is relatively high [*Lauvset and Tanhua*, 2015]. A recent intercomparison between different laboratories showed that most laboratories cannot measured alkalinity to within of 2 µmol kg^{-1}, with inaccuracies coming from using simple titration techniques or using small sample sizes (less than 20 mL) [*Bockmon and Dickson*, 2015].

2.2.1 Primary quality control

Primary quality control is used to identify outliers and obvious errors in the data. Each data point for each transect undergoes primary quality control where the measurements are flagged manually for reliability. Table 2-1 shows the flags used for GLODAPv2.

Table 2-1. Flags used in GLODAPv2.[a]

Flag	Use in GLODAPv2
0	Approximated
2	Good
3	Questionable (not included in product)
4	Clearly bad (not included in product)
5	Value not reported
6	Average of replicate
9	Not measured

[a] Based on WOCE flags; flags 1, 7, and 8 were not used.

A flag represents the reliability of the datum and they are either created at the time of measurement or later by identifying the datum as an outlier [*Velo et al.*, 2009; *Tanhua et al.*, 2010]. The flagging procedure is variable. As an example, in CARINA, if data were submitted with flags, the flags were checked for obvious errors. However, when data were submitted without flags, outliers were identified by property-property plots and bottles were flagged as questionable if they were outliers in more than one plot. As there is no true cut-off between good (flag 2) and questionable (flag 3) data, the final flag a data point receives is subjective. Flags are also likely to be biased with depth because seawater is much more variable at the surface; therefore, surface samples are less likely to be flagged as questionable unless they are seriously anomalous or the measurement was known to be faulty [*Tanhua et al.*, 2010].

The flagging system was first used by WOCE [*Tanhua et al.*, 2010], but was changed for GLODAP with the addition of flag 0 to represent data that could have been measured but

was calculated [*Key et al.*, 2004]. A carbonate system example of a data point calculated rather than measured could be alkalinity from two other variables rather than a direct measurement, or nutrients and oxygen interpolated through the depth of a cast to allow focus on the carbon data [*Olsen et al.*, 2016].

2.2.2 Secondary quality control

After the cruises are flagged, the data from the cruises are compared through secondary quality control. This is a process in which the data are objectively studied in order to quantify systematic biases in the measurements – the accuracy [*Velo et al.*, 2009; *Tanhua et al.*, 2010]. Techniques used in secondary quality control include crossover analysis, multiple linear regression (MLR), and inversion analysis [*Sabine et al.*, 2005; *Velo et al.*, 2009]. Secondary quality control is only performed on data flagged as good during primary quality control [*Velo et al.*, 2009], but the secondary quality control provides a check on the primary quality control, because large adjustments can highlight outliers missed with the flagging system [*Tanhua et al.*, 2010].

Crossover analysis is the main technique used to identify offsets between cruises [*Tanhua et al.*, 2010]. Crossover analysis compares deep data of nearby stations from different cruises and quantifies any difference (offset) between cruises which could be caused by systematic bias [*Sabine et al.*, 2005; *Velo et al.*, 2009]. The theory behind secondary quality control is that deep values change very slowly with time and space; therefore, if you have two cruises in the same area, then the deep values should be the same for each which allows you to calculate the difference between the cruises if there are systematic biases [*Tanhua et al.*, 2010]. Usually, water is defined as deep if it is deeper than 1500 m in the Atlantic Ocean, 2000 m in Pacific Ocean, and 2500 m in the Indian Ocean [*Sabine et al.*, 2005; *Velo et al.*, 2009]. Although called crossover analysis, the cruises do not have to cross over; the cruise tracks can be parallel as long as they are close enough in space, usually within 2 degrees of each other. Crossover analysis is less reliable in some areas, such as the North Atlantic, which are known to have changed over time [*Tanhua et al.*, 2010].

The first step of crossover analysis is to interpolate the variables with depth or some proxy for depth. A variable other than depth is usually used to account for internal waves and different water masses. The most common vertical variables are pressure, potential density, and potential temperature rather than depth [*Tanhua et al.*, 2010]. Potential temperature is useful because it is independent of salinity which itself can be corrected using crossover

analysis. However, all vertical variables were used and compared in CARINA and GLODAPv2 and they often showed little difference in the resulting offsets [*Tanhua et al.*, 2010; *Olsen et al.*, 2016].

In the second step of crossover analysis, two cruises are compared by either (a) using the average vertical profile of both cruises in the regions where the profiles are in proximity, or by (b) comparing the profile of one cruise with the average of all the profiles in proximity to that profile from the other cruise. Cluster analysis, a sub-routine of crossover analysis, is used where cruises fall into more than one region or when there are repeat cruises (the entirety of the two cruises are in proximity) that could provide a great number of crossovers and so bias the offset estimate. During cluster analysis the cruise is broken into sections, clusters, before the crossover analysis takes place [*Tanhua et al.*, 2010].

The final step of crossover analysis is to calculate the offset and standard deviation of each crossover [*Tanhua et al.*, 2010]. The quantifications for each crossover in a cruise are then used to calculate the correction or correction factor.

Crossover analysis was first used during the creation of the WOCE and JGOFS databases [*Johnson et al.*, 2001; *Tanhua et al.*, 2010]. In WOCE and the original GLODAP database, crossover analysis was manually applied; however, crossover analysis is now semi-automated [*Velo et al.*, 2009] and can be undertaken collaboratively over the internet. The semi-automated crossover analysis is performed by a computer; however, the results are visually inspected to check the quality of the offsets and whether the analysis has run correctly. Standard deviations of cruises and difference profiles can be used to assess the quality of the offsets [*Velo et al.*, 2009]. Manually analyzing the results of automated procedures can be used to check if the results are reliable; however, the more manual intervention, the slower and less repeatable the process [*Tanhua et al.*, 2010].

Multiple linear regression (MLR) can also be used to calculate offsets. A MLR equation is created using variables from one cruise to calculate the predictive coefficients. The resulting equation is then applied to the data from a second cruise and the difference between the predicted and measured variable in the second cruise is used to quantify the offset [*Sabine et al.*, 2005]. MLR was not used for GLODAPv2, but was used extensively for the original GLODAP where MLR was combined with crossover analysis to analyze individual cruises [*Sabine et al.*, 2005; *Olsen et al.*, 2016]. In the original GLODAP, MLR was also used on a basin-wide scale in the North Pacific (north of 20ºN) as there were few crossovers in that region [*Sabine et al.*, 2005]. In this situation, where cruises are far apart,

MLR is better than crossover analysis because it accounts for the mixing of water bodies through the variations of the other variables; however, with more cruises, using only one technique is more consistent and so less likely to be biased.

Both crossover analysis and MLR produce offsets. An offset is the difference between two cruises and/or cruise sections and one cruise may have several offsets describing its relation to other cruises. Therefore the next stage in secondary quality control is to combine the offsets to produce a single correction parameter for each cruise using inversion analysis. The most common method used to calculate the corrections is the Weighted Least Squares model which is an intermediate complexity model [*Tanhua et al.*, 2010]. This model uses the standard deviations of the offsets to indicate the confidence of each offset and makes no assumptions as to which cruises are more accurate [*Johnson et al.*, 2001]. However, in CARINA and GLODAPv2, certain cruises were assumed to be better quality (GO-SHIP) and so Weighted Damped Least Squares was used to calculate the correction parameters that correct other cruises to the better quality cruises [*Tanhua et al.*, 2010; *Olsen et al.*, 2016]. This produces smaller, conservative corrections but is useful when some cruises are known to be of a higher quality [*Johnson et al.*, 2001].

The inversion analysis produces a correction factor (multiplicative) or a correction (additive). The final stage of creating the correction factor or correction is to manually check if they have a temporal trend; a time versus correction plot can indicate if the stated correction may include a time-trend [*Tanhua et al.*, 2010].

Time factors can be added to correction parameters to account for temporal trends in specified areas. These work by weighting the variation allowed (calculated using the standard deviation of the offset) by the time passed between the cruises: the more time passed the greater the variation deemed acceptable and so the less likely the future cruise is to be outside those bounds. Time factors were added to the CARINA data in regions where it was thought necessary [*Tanhua et al.*, 2010].

If the correction or correction factor for the cruise is applied, it is called an adjustment. The data for entire cruises, where there is a significant difference in the deep measurements, are adjusted to produce similar deep values [*Tanhua et al.*, 2010]. For carbonate chemistry variables the correction value is additive; however, additive corrections in GLODAP produced negative surface nutrient concentrations. Therefore, CARINA, PACIFICA, and GLODAPv2 used multiplicative corrections for nutrients [*Key et al.*, 2010; *Suzuki et al.*, 2013]. This makes sense theoretically because errors in nutrient measurements are often

caused by standardization, and so suit a multiplicative adjustment, whereas DIC, alkalinity, and salinity often have a bias with the reference material, therefore work better with an additive adjustment. pH is logarithmic therefore only additive adjustments work correctly [*Tanhua et al.*, 2010].

Not every correction is used as there is often a minimum allowable adjustment. The reason for the minimum adjustment is to avoid removing real variability [*Olsen et al.*, 2016] and applying small adjustments gives relatively small gains in internal consistency, so it is always better to err on the side of caution [*Tanhua et al.*, 2010]. Minimum adjustments started to be used with the creation of CARINA [*Tanhua et al.*, 2010], but were then also used for PACIFICA and GLODAPv2. However, not all quality control operations are as rigorous at applying the minimum adjustment. In GLODAPv2 the collaborators decided to adjust cruises of high quality in regions where the deep values are not likely to have changed. In the alkalinity data, 10% of the final adjustments were below the "minimum adjustment" of 6 µmol kg^{-1}. In total, 150 of 465 cruises or partial cruises with alkalinity were adjusted [*Olsen et al.*, 2016].

Multiple linear regression, as well as being used to calculate offsets, can be used to check that the cruises have been fully adjusted. In the same way as calculating offsets, one cruise is used to create an equation that can be used on a second cruise. The residual, the difference between the predicted and measured values of a variable, can then be calculated. The calculated residuals should be lower after than before the adjustments are applied. The residuals should also be lower than the minimum adjustment threshold [*Velo et al.*, 2009].

After secondary quality control, and the cruise data adjustment, the data from the cruises are combined into large data files. These files are made available to researchers along with the original data, metadata and documentation of the quality control process.

2.2.3 Sources of error

Possible sources of error in the quality control can be caused by: (1) temporal trends, (2) drift in the accuracy or precision of measurements over the duration of a cruise, (3) errors in the depth interpolation, or (4) differing routines between analysts [*Tanhua et al.*, 2010].

Temporal trends, such as increasing DIC from invasion of anthropogenic carbon, can cause the deep values to change over time [*Tanhua et al.*, 2010]. Adjustments that don't account for trends can cause biases to be added to the data rather than removed. The North Atlantic is particularly susceptible to temporal trends and the deep water formation means that deep

water can be influenced by anthropogenic inputs over periods of decades. As shown above, this bias can be minimized by scrutinizing each correction compared to time. A trend between the correction and time suggests there is an underlying trend in the variable which is caused by a process rather than an error [*Olsen et al.*, 2016]. The adjustments can then be changed to account for trends or the standard deviation could be weighted to allow greater variation to occur before a correction is applied [*Tanhua et al.*, 2010]. However, to correctly identify temporal variation requires enough cruises over time for trends to be detected.

Drifting of measurement accuracy over the course of a cruise can cause an error in some parts of the cruise after the adjustments have been made [*Tanhua et al.*, 2010]. For example, if the crossover at one end of the cruise shows a large offset but the accuracy drifts towards less offset, the adjustment needed at the other end of the cruise would be less. Therefore some data in cruises may be over- or under-adjusted. To minimize this error, several cruises can be used to produce several offsets or cluster analysis can be used to split the cruise into multiple sections. Unfortunately, it may not be obvious if there is a drift in the measurement accuracy of a single cruise's data and there is not always sufficient data to produce multiple robust crossovers.

An error in the vertical interpolation would affect the offsets by causing the cruise data in different water masses to be compared [*Tanhua et al.*, 2010]. By comparing different water masses, with different variable concentrations, offsets could be overestimated. Using multiple depth variables could reduce this bias.

Flagging is subjective and so can vary between different analysts (see section 2.2.1). Also, before crossover analysis was automated (such as for GLODAP), the offsets and adjustments could be different depending on the analyst [*Tanhua et al.*, 2010]. This would result in a bias between cruises analyzed by different analysts in slightly different ways. With the development of automated routines, this bias is reduced [*Velo et al.*, 2009]; however, the amount of manual interaction in crossover analysis, the choice of a time factor, and the choice of whether to apply an adjustment can all still cause bias due to subjective aspects [*Tanhua et al.*, 2010]. Further automation, such as detection and quantification of temporal trends, could reduce bias between cruises; however, they could also cause more errors than they solve by accounting for trends without any mechanistic understanding of whether they are possible.

There is also a problem quantifying the accuracy of the databases. A large number of data points have a greater uncertainty than the predicted measurement accuracy (e.g. alkalinity measurement predicted accuracy of 3 µmol kg^{-1} [*Dickson et al.*, 2003]) because of systematic biases between the cruises. Although the process of quality control should remove these errors, this process is not perfect and so there will still be inaccuracies. The minimum adjustment could be used to quantify the database accuracy (e.g. alkalinity minimum adjustment in GLODAPv2 of 6 µmol kg^{-1} [*Olsen et al.*, 2016]). However, 10% of the adjustments of alkalinity in the GLODAPv2 database were in fact of a magnitude below the nominal minimum adjustment. The error assessment could be improved by using MLR routinely to check the adjusment of the cruises (see section 2.2.2). The difference between a predicted and measured variable should be lower after the adjustments have been applied and should be lower than the minimum adjustment threshold [*Velo et al.*, 2009]. This difference and the accuracy of the MLR equation could then be reported with the database.

2.3 Use of data in this thesis

In this thesis, large carbon datasets containing alkalinity are used. Those that are currently available are CARINA, PACIFICA, GLODAP, and GLODAPv2. They were downloaded from: http://cdiac.ornl.gov/oceans/. All the analysis was performed in MATrix LABoratory (MATLAB, The MathWorks Inc., Natick, MA) and all figures were produced in MATLAB with the exception of Figure 3-5 which is a depth plot of GLODAP data and was produced using Ocean Data View.

In Chapter 3, salinity, alkalinity, and nitrate data from GLODAP, CARINA, and PACIFICA were used. Only bottle data were analyzed rather than interpolated gridded products. The surface ocean was defined as shallower than 30 m at latitudes greater than 30º, and shallower than 20 m at latitudes less than 30º, to be consistent with the most recent paper on the distribution of alkalinity in the surface ocean [*Lee et al.*, 2006]. Shelf and marginal sea data were removed by excluding data in the Arctic or Mediterranean seas or with a seafloor depth of less than 200 m.

In Chapter 4, discrete bottle data from GLODAPv2 were used [*Olsen et al.*, 2016] and surface data were defined in this analysis as sampled from shallower than 30 m. The GLODAPv2 data were compared with other datasets to test hypotheses. The other datasets were gridded dissolved oxygen and nitrate products, mixed layer depth data, and the

strength of the El Nino Southern Oscillation (ENSO). The gridded annual mean dissolved oxygen and nitrate at 1° resolution were obtained from the World Ocean Atlas 2013 [*Garcia et al.*, 2014a, 2014b]. Mixed layer depth data using a variable potential density criterion were obtained from the National Oceanic and Atmospheric Administration (NOAA) [*Monterey and Levitus,* 1997]. The maximum mixed layer depth was defined as the largest of the monthly values for each gridpoint with February the most common month for the deepest mixed layer. The effect and strength of the ENSO was taken from a Multivariate ENSO Index also from NOAA [http://www.esrl.noaa.gov/psd/enso/mei/].

In Chapter 5, bottle data of alkalinity and other variables from the summer and autumn were obtained from the GLODAPv2 database [*Olsen et al.*, 2016]. The southern hemisphere summer and autumn was defined as being from the start of 1st November to the end of 30th April. Gridded water velocity and mixed layer depth values in summer and autumn were obtained from the Southern Ocean State Estimate (SOSE) model [*Mazloff et al.*, 2010]. The mean positions of the fronts in the Southern Ocean (Polar Front, the Subantarctic Front, and the Subtropical Front) were obtained from the Australian Antarctic Data Centre [*Orsi et al.*, 1995; *Orsi and Harris*, 2015]. The rate of calcification was estimated using the equation by *Balch et al.* [2007], along with monthly, satellite climatologies at 9 km resolution of particulate inorganic carbon (PIC), chlorophyll concentrations, and sea surface temperature from MODIS (satellite) datasets (http://oceancolor.gsfc.nasa.gov).

2.4 Summary

There have been wide scale efforts to collect alkalinity and dissolved inorganic carbon data since the 1970s. The first worldwide dataset, GLODAP, was released in 2004 and the next generation, GLODAPv2, has recently been released [*Olsen et al.*, 2016]. Data added to the datasets must go through quality control to ensure that the resulting database is internally consistent. Quality control was especially important before CRMs were available. During the first stage of the quality control procedure, data are manually flagged to show the quality of data. Then deep data of good quality are compared between cruises under the assumption that cruises near to each other should have similar deep values. Offsets between different cruises are then combined, using inversion techniques, and the original cruise data maybe adjusted. MLR can be used to assess the quality of the adjustments or calculate offsets. Errors in primary quality control may come from the subjective nature of manual flagging. Errors in secondary quality control can be caused by temporal trends,

drifting accuracy, errors in the depth interpolation, or different people or groups using different methods to calculate the offsets. After quality control, data from all the cruises are combined and the corrected dataset is made available to researchers. In this thesis, in situ carbon datasets (GLODAP, CARINA, PACIFICA, and GLODAPv2) are analyzed and compared with other freely available ocean data. All analysis was performed on MATLAB and all figures were also created using MATLAB with the exception of Figure 3-5.

Chapter 3: Analysis of global surface ocean alkalinity to determine controlling processes

This chapter is published as Fry, C.H., T. Tyrrell, M.P. Hain, N.R Bates, and E.P. Achterberg (2015), Analysis of global surface ocean alkalinity to determine controlling processes. Mar. Chem., 174, 46-57. T. Tyrrell provided feedback on the methods and detailed feedback on the manuscript. M.P. Hain assisted with the calculation of export in section 3.5.8. N.R. Bates and E.P. Achterberg provided feedback on the manuscript. The writing of the chapter and all analysis and production of figures was performed by C.H. Fry.

3.1 Abstract

The export of calcium carbonate ($CaCO_3$) from the surface ocean is poorly constrained. A better understanding of the magnitude and spatial distribution of this flux would improve our knowledge of the ocean carbon cycle and marine biogeochemistry. Here, we investigate controls over the spatial distribution of total alkalinity in the surface global ocean and produce a tracer for $CaCO_3$ cycling. We took surface ocean bottle data for total alkalinity from global databases (GLODAP, CARINA, PACIFICA) and subtracted the effects of several processes: evaporation and precipitation, river discharge, and nutrient uptake and remineralization. The remaining variation in alkalinity exhibits a robust and coherent pattern including features of large amplitude and spatial extent. Most notably, the residual variation in alkalinity is more or less constant across low latitudes of the global ocean but shows a strong polewards increase. There are differences of ~110 µmol kg^{-1} and ~85 µmol kg^{-1} between low latitudes and the Southern Ocean and the subarctic North Pacific, respectively, but, in contrast, little increase in the high-latitude North Atlantic. This global pattern is most likely due to production and export of $CaCO_3$ and to physical resupply of alkalinity from deep waters. The use of river corrections highlights the large errors that are produced, particularly in the Bay of Bengal and the North Atlantic, if alkalinity normalization assumes all low salinities to be caused by rainfall. The residual alkalinity data can be used as a tracer to indicate where in the world's ocean most $CaCO_3$

export from the surface layer takes place, and of future changes in calcification, for instance due to ocean acidification.

3.2 Introduction

Total alkalinity, afterwards referred to as alkalinity (Alk), is a measure of the acid neutralization capacity of seawater, or, more technically, the excess of proton acceptors over proton donors compared to a zero level of protons at a pH of approximately 4.3. It is measured by the stepwise addition of hydrochloric acid to determine the equivalence points of the titration curve [*Gran*, 1952; *Dickson*, 1981, 2010]. Total alkalinity can be written as:

$$\begin{aligned} Alk = {} & [HCO_3^-] + 2[CO_3^{2-}] + [B(ON)_4^-] + [OH^-] + [HPO_4^{2-}] + 2[PO_4^{3-}] \\ & + [H_3SiO_4^-] + [NH_3] + [HS^-] - [H^+] - [HSO_4^-] - [HF] \\ & - [H_3PO_4] - [HNO_2] \end{aligned} \quad (3\text{-}1)$$

Measurements of two of the seawater carbonate system variables (i.e., dissolved inorganic carbon (DIC), alkalinity, pH or the partial pressure of carbon dioxide (pCO_2)), in combination with observations of temperature, salinity, silicate and phosphate concentrations, are sufficient to determine the entirety of the carbonate system. The measurement of alkalinity is particularly useful because it is conservative with respect to water mass mixing. Alkalinity is also independent of changes in temperature and pressure, unlike pCO_2, pH, and concentrations of individual chemical species (e.g. carbonate and bicarbonate) of the seawater carbonate system [*Dyrssen and Sillén*, 1967; *Wolf-Gladrow et al.*, 2007].

The sea surface distribution of alkalinity is affected by several processes. These include: (1) changes in seawater dilution caused by evaporation and precipitation [*Lee et al.*, 2006]; (2) riverine inputs of alkalinity [*Friis et al.*, 2003; *Cai et al.*, 2010]; (3) production and export of $CaCO_3$; (4) consumption or regeneration of nutrients from primary production or respiration, respectively [*Brewer and Goldman*, 1976; *Millero et al.*, 1998b; *Wolf-Gladrow et al.*, 2007], and; (5) ventilation and upwelling of subsurface waters with high alkalinity as a result of dissolution of calcium carbonate ($CaCO_3$) [*Lee et al.*, 2006]. The inorganic carbon pump is a fundamental component of the marine carbon cycle (e.g., [*Holligan and Roberstson*, 1996; *Kwon et al.*, 2009; *Hain et al.*, 2010]), and may be important for

sequestering organic carbon through ballasting organic matter to the deep ocean [*Armstrong et al.*, 2002; *Klaas and Archer*, 2002; *Barker et al.*, 2003]. However, the magnitude of the ocean particulate $CaCO_3$ export flux is poorly known; it is currently estimated only within a large range (0.4-1.8 Pg PIC yr^{-1}; [*Berelson et al.*, 2007] and its spatial distribution is also poorly constrained. For instance, whereas satellite-based determinations of surface $CaCO_3$ concentration lead to predictions of higher calcification rates at high latitudes than at low latitudes [*Balch et al.*, 2005], fluxes of $CaCO_3$ into sediment traps [*Berelson et al.*, 2007] and geochemical calculations [*Sarmiento et al.*, 2002] point to most $CaCO_3$ export occurring at low latitudes.

In this study we combined potential alkalinity [*Brewer et al.*, 1975; *Sarmiento et al.*, 2002] with procedures for appropriately cancelling river impacts; we subtracted all of the major processes affecting alkalinity except for (a) alkalinity removal due to formation and export of $CaCO_3$, and (b) alkalinity resupply through the upwards transport of $CaCO_3$ dissolution products from the ocean interior, hereafter jointly referred to as $CaCO_3$ cycling. Our analyses showed the large impacts of rivers on alkalinity in specific ocean regions, particularly the Bay of Bengal and the North Atlantic Ocean. The surface alkalinity data, when adjusted to take this into account, reveal greatly elevated values in the Southern Ocean and North Pacific, with well-defined gradients separating these polar regions from the rest of the ocean, which is characterized by near constant values across low latitudes. We argue that this distinct spatial pattern is consistent with its being caused by the ocean's internal $CaCO_3$ cycle, and hence that the adjusted alkalinity can be used as a tracer of $CaCO_3$ cycling.

3.3 Methods

3.3.1 Seawater CO_2-Carbonate Chemistry Data

Salinity, alkalinity, and nitrate data were downloaded from the GLODAP, CARINA and PACIFICA databases (http://cdiac.ornl.gov/oceans/glodap/, http://cdiac.ornl.gov/oceans/CARINA/, http://cdiac.ornl.gov/oceans/PACIFICA/). These databases were synthesized from data collected during various scientific programs since the 1980s including: (1) the Geochemical Ocean Sections Study (GEOSECS); (2) the World Ocean Circulation Experiment (WOCE); (3) the Joint Global Ocean Flux Study

(JGOFS), and; (4) the Ocean and Atmosphere Carbon Exchange Study (OACES). During synthesis of each database, the data were subjected to rigorous quality control procedures. First, data flags were used to indicate the quality of the individual measurements in the cruise. Then, the data from different cruises were compared using the assumption that deep values have low spatial and temporal variability, and therefore that adjacent data points from different cruises should have similar values. Data with a lower than acceptable quality were removed and small biases in cruises adjusted [*Millero et al.*, 1998a; *Key et al.*, 2004, 2010]; http://cdiac.ornl.gov/oceans/PACIFICA/). For this study, we used only bottle data rather than any gridded products. The surface ocean was defined as shallower than 30 m at latitudes greater than 30º, and shallower than 20 m at latitudes less than 30º, as in previous studies [*Lee et al.*, 2006]. We included only open ocean data (seafloor depth > 200 m) in our analysis. Data from the Arctic and Mediterranean seas were excluded. Thus this study excluded shelf seas, shallow coastal seas, and enclosed seas.

3.3.2 Analysis of Process Contributions

Controls on surface alkalinity were analyzed using in-situ alkalinity data together with associated hydrographic properties. The impacts of various processes on the spatial distribution of alkalinity in the surface ocean were calculated from related variables. The effects of freshwater fluxes (evaporation, precipitation, river discharge) were quantified based on salinity, and biological fluxes of nutrients calculated using nitrate data.

Following the subtraction of each major process that affects alkalinity, the overall distribution of alkalinity was recalculated and reanalyzed to assess whether it had become more coherent (i.e., less scatter among nearby observations). For each basin, the data were binned by 5º latitude, and the mean and standard deviation of each bin was calculated. To create a dimensionless statistical variable, the value of which could be compared to other hydrographic variables, the mean standard deviation for each basin was divided by the range of the bin means for that basin. The same statistical approach was undertaken for nitrate, phosphate, and silicate. As an example, for nitrate in the Atlantic, the metric for the average spread of the data cloud is calculated as:

$$M_{NO3,ATL} = \frac{\left(\frac{1}{36}\sum_{i=1}^{i=36}\sigma\left(NO3_i^{ATL}\right)\right)}{\left(max\left(\overline{NO3_i^{ATL}}\right) - min\left(\overline{NO3_i^{ATL}}\right)\right)} \quad (3\text{-}2)$$

where $\overline{NO3_i^{ATL}}$ and $\sigma\left(NO3_i^{ATL}\right)$ are the mean and standard deviation of the nitrate values in the i'th Atlantic bin.

After subtraction of all processes except the $CaCO_3$ cycle, the final surface distribution of alkalinity was assessed as a tracer of $CaCO_3$ cycling.

3.4 Results

3.4.1 Evaporation and Precipitation

Table 3-1. Variability in alkalinity and nutrients[a]

	Alkalinity				Nutrients		
	Initial	After correction					
		Evaporation Precipitation	Riverine Input	Biological Growth and remineralization	Nitrate	Phosphate	Silicate
Atlantic	0.17	0.14	0.13	0.095	0.064	0.077	0.067
Indian	0.11	0.095	0.080	0.071	0.066	0.086	0.060
Pacific	0.17	0.14	0.14	0.11	0.097	0.10	0.065

[a]Calculated as the average of the standard deviations in the 5° latitude bins, divided by the range in the mean values of the 5° latitude bins. Calculations are made for each ocean basin after each cumulative stage has been taken into account, and for each macronutrient.

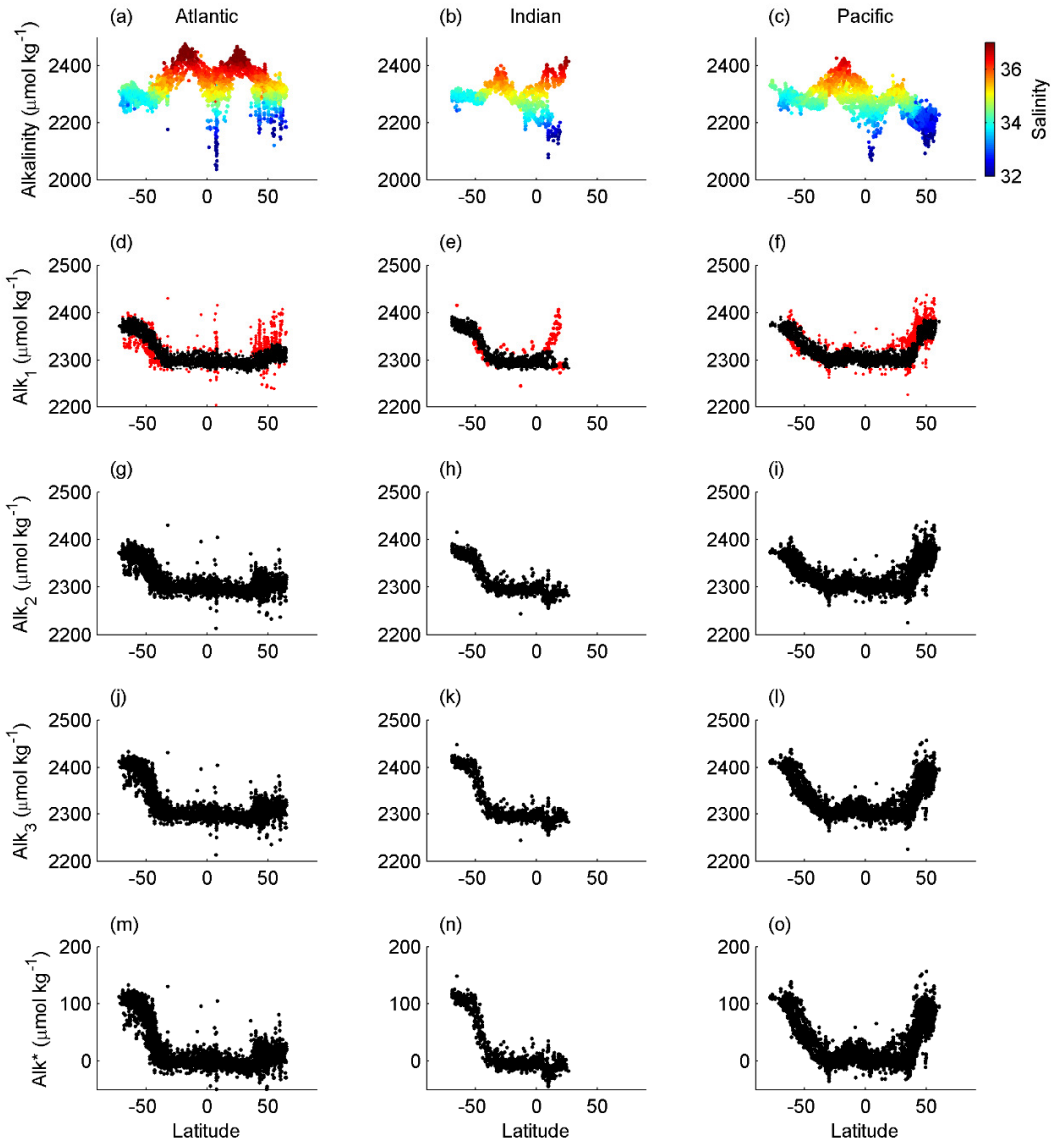

Figure 3-1. The distribution of alkalinity (µmol kg^{-1}) and normalized alkalinity (µmol kg^{-1}) in each ocean basin. a,b, and c show the observed alkalinity with the colors indicating the salinity from 32 to 37. d,e, and f show salinity normalized alkalinity (Alk_1) with red points indicating values more than 20 µmol kg^{-1} from the 5º of latitude running mean. g,h and i are Alk_2, where rivers are included for each basin. j,k, and l show Alk_3, where the biological uptake of nutrients is also included, for each basin. m,n and o show Alk^*. Note the different y-axis scale on the first row of plots.

Figure 3-1a, b and c show the measured surface ocean alkalinity distributions in the Atlantic, Indian and Pacific basins as a function of latitude, with colors indicating salinity. The relative mean standard deviations of the 5º bins are shown in Table 3-1. For all three basins, the most obvious features of the datasets are the local maxima of alkalinity around 30ºN and 20ºS, which correspond to the centers of the subtropical gyres. These peaks contrast with much lower values (up to 400 µmol kg^{-1} lower) near the equator and in the polar ocean regions.

The consistent elevation of alkalinity in the subtropical gyres is caused principally by the hydrological cycle driving substantial excess evaporation over precipitation in these regions. Net evaporation concentrates substances dissolved in seawater, as freshwater is lost to the atmosphere and solutes are left behind. Conversely, net precipitation dilutes seawater, as relatively pure water is added. Because alkalinity is a weighted sum of different dissolved constituents (Equation 3-1), its concentration rises and falls proportionally with salinity.

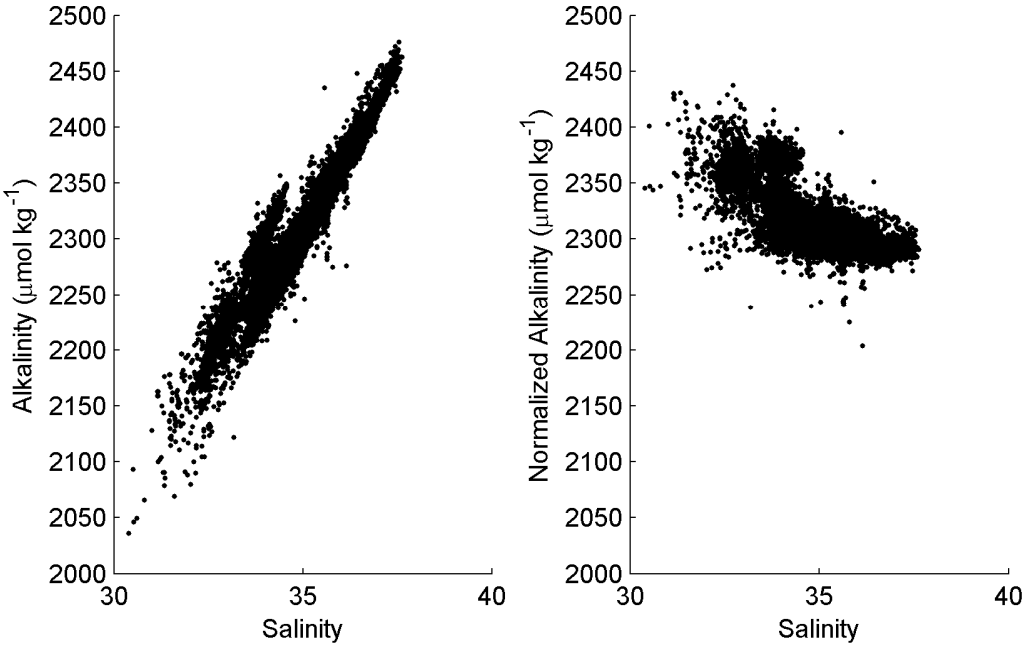

Figure 3-2. Salinity versus (a) alkalinity (µmol kg^{-1}) and (b) normalized alkalinity (Alk_I, µmol kg^{-1}) in the global surface ocean.

Variations in salinity are used to calculate the balance between the effects of evaporation and those of precipitation. Figure 3-2a shows alkalinity plotted against salinity in the

global surface ocean. Pearson's correlation coefficients (r) were 0.94 in the Atlantic Ocean, 0.87 in the Indian Ocean, 0.92 in the Pacific Ocean, and 0.94 when data from all the oceans were combined. These strong correlations are consistent with evaporation and precipitation being responsible for most of the variation in alkalinity.

The effects of evaporation and precipitation can be removed from alkalinity by converting each alkalinity measurement, Alk_m, to its expected value at a salinity (S) of 35, i.e. by normalizing each value to a salinity of 35 [*Postma*, 1964; *Millero et al.*, 1998b]:

$$Alk_1 = \frac{Alk_m}{S} \times 35 \tag{3-3}$$

Figure 3-2b shows that the major correlation between salinity and alkalinity, especially at high salinities, is removed using Equation 3-3. Equation 3-3 successfully negates the effect of the hydrological cycle, eliminating the elevated alkalinity of the subtropical gyres and the local minima of alkalinity along the equator, thereby resulting in fairly constant low-latitude surface Alk_1 (Figure 3-2d, e and f). As can be seen in Table 3-1, the variability of alkalinity relative to its overall range is reduced in all three basins following removal of evaporation and precipitation effects.

3.4.2 Riverine Input

Although salinity normalization reduces the spatial variability in alkalinity in the subtropics, many features still remain (Figure 3-1d, e and f). For instance, in the north Indian Ocean there are two different regimes of alkalinity at a similar latitude: the Bay of Bengal is characterized by lower observed alkalinity and salinity, but by a higher normalized alkalinity than the Arabian Sea. There is also a significant high anomaly in normalized alkalinity at 8ºN in the Atlantic Ocean, and several high anomalous groups between 40ºN and 60ºN in the North Atlantic. In both oceans these areas also correspond to low observed salinity (compare Figure 3-1a and Figure 3-1d, and Figure 3-1b and Figure 3-1e; salinity-normalized alkalinity values that are more than 20 μmol kg^{-1} from the 5º latitude running mean are indicated in red).

Low salinity is not always produced by rainfall, but can also be produced by sea-ice melt or by inputs of river water. In non-polar waters, the obvious likely cause of the overcorrection from the salinity-normalization is therefore river input. Based on a global

analysis of volume of river water received, the ocean areas most likely to be affected are the Arctic Ocean, the Bay of Bengal, the Labrador Sea, the Amazon River and Congo River plumes in the Atlantic, and the South China Sea [*Kang et al.*, 2013].

Friis et al. [2003] found that misleading results are produced if Equation 3-3 is used to normalize alkalinity to salinity in ocean regions receiving river outflows. Equation 3-3 assumes that freshwater discharged by rivers (i.e., zero salinity) also has zero alkalinity, which is not the case since many rivers have substantial concentrations of alkalinity, in particular those draining limestone catchments [*Cai et al.*, 2010]. In marginal seas, the y-intercept of the relationship between alkalinity and salinity usually (although not always, see *Jiang et al.* [2014]) corresponds to the alkalinity of the river end member, Alk_r, because, assuming conservative mixing, this is the value of alkalinity when the salinity is negligible (river water). Following *Friis et al.* [2003], we used Equation 3-4 to account for river input:

$$Alk_2 = \frac{Alk_m - Alk_r}{S} \times 35 + Alk_r \tag{3-4}$$

The peak at 8ºN in the Atlantic basin is close to the South American continent; therefore, it is likely that these data have been influenced by the Amazon River, and examination of the geographical locations of the anomalous points confirms that they lie in the general area of the Amazon outflow plume. The water from the mouth of the Amazon River has an Alk_r value of around 300 µmol kg^{-1} [*Cooley and Yager*, 2006; *Cooley et al.*, 2007]. When the salinity normalization by *Friis et al.* [2003] (Equation 3-4, with Alk_r = 300 µmol kg^{-1}) is applied for the region between the latitudes of 5 and 10ºN and west of 45ºW in the Atlantic basin, the anomalous peak at 8ºN is eliminated (Figure 3-1g versus Figure 3-1d).

Figure 3-3 shows that the anomalously high normalized alkalinity values in the region between 40ºN and 60ºN in Figure 3-1a are geographically situated close to the Labrador coast. *Millero et al.* [1998b] also found an anomalous area in salinity-normalized alkalinity in the vicinity of the Labrador Sea. *Cai et al.* [2010] suggested that the Labrador Current is the source of the anomalous alkalinity rather than local runoff. This implies that the intercept of the salinity-alkalinity relationship will not agree with the alkalinity for local continental runoff. The y-intercept of the Labrador Current, Alk_r, equals 1124 µmol kg^{-1}, which is close to the composite of the runoff from the six largest Arctic rivers of

approximately 1100 µmol kg^{-1} [*Cooper et al.*, 2008]. A revised alkalinity was calculated for the Atlantic Ocean (Figure 3-1g) where an Alk_r = 300 µmol kg^{-1} was used for the region between 5ºN and 10ºN and west of 45ºW to correct for the Amazon River plume, and Alk_r = 1100 µmol kg^{-1} in the Labrador Sea inflow area (defined as north of 40ºN and west of 30ºW). Comparing Figure 3-1g to 1d, the Atlantic Ocean has fewer anomalously high points and a lower standard deviation (Table 3-1). However, some of the points in the Labrador Current are now lower than the mean and appear to have been overcorrected; this is most likely due to the presence of anomalous surface water in the area, of unknown origin, which has previously been found to have a much lower Alk_r of 273 µmol kg^{-1} [*Cai et al.*, 2010].

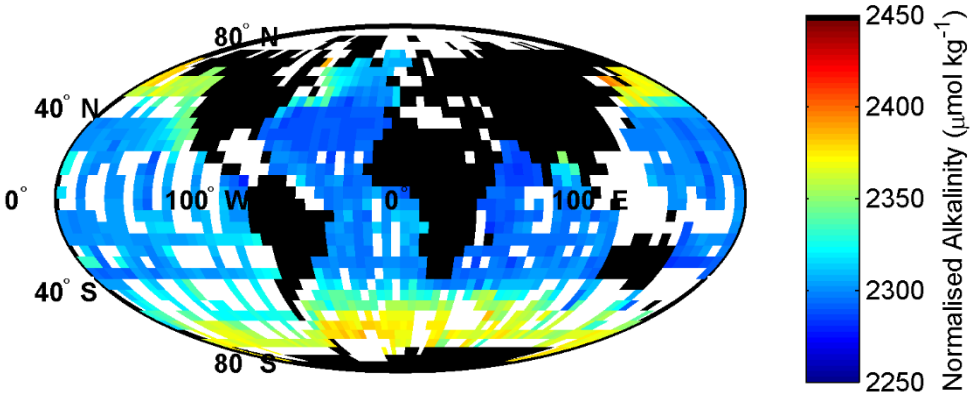

Figure 3-3. Salinity-normalized alkalinity (Alk_I, µmol kg^{-1}) gridded to 5º latitude and longitude in the surface ocean.

Figure 3-3 also shows that the high salinity normalized alkalinity values in Figure 3-1e come from the Bay of Bengal. The mean measured alkalinity in the outflow of the Ganges-Brahmaputra is 1106 µmol kg^{-1} [*Galy and France-Lanord*, 1999]. Using this as the value of Alk_r in the Bay of Bengal area (defined as the part of the Indian Ocean north of 5ºN and between 80ºE and 94ºE) led to an overcorrection of the higher branch in the north Indian Ocean (Figure 3-4). When river alkalinity based on modeling of annual river runoff and basin lithology and weathering (Alk_r = 840 µmol kg^{-1}; [*Amiotte Suchet et al.*, 2003]) was used instead of direct measurements, the anomaly in the north Indian Ocean was successfully corrected (Figure 3-1h). The Ganges-Brahmaputra alkalinity [*Bates et al.*, 2006] and water [*Kang et al.*, 2013] fluxes vary seasonally; the differences between modeled and observed Alk_r may therefore be down to seasonal differences.

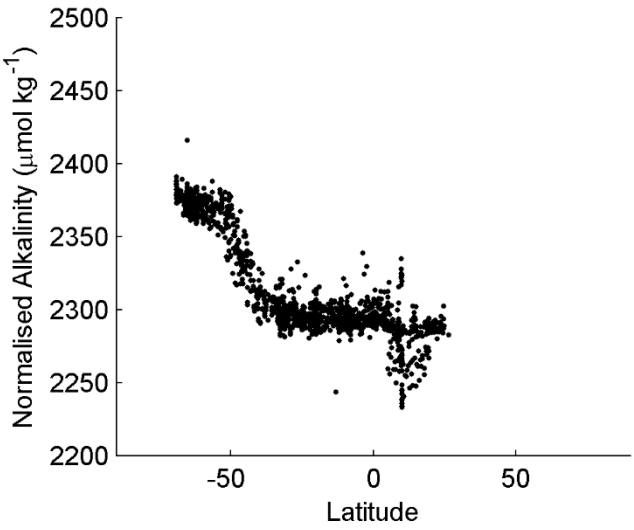

Figure 3-4. Indian Ocean alkalinity (µmol kg^{-1}) as a function of latitude following salinity-normalization using Equation 3-4 with Alk_r = 1107 µmol kg^{-1} in the Bay of Bengal area (north of 5ºN and between 80ºE and 94ºE).

After removing the salinity normalization error caused by large river inputs (summarized in Table 3-2), the remaining alkalinity distribution is as shown in Figure 3-1g, h, i. The standard deviations of those basins where changes were made are improved (lower), as shown in Table 3-1.

Table 3-2. River Alkalinity (Alk_r) Corrections

Area Name	Ocean Basin	Area boundaries	Alk_r (µmol kg^{-1})
Amazon plume	Atlantic	5ºN<Latitude<10ºN, Longitude<-45ºE	300
Labrador Sea	Atlantic	Latitude>40ºN, Longitude<-30ºE	1100
Bay of Bengal	Indian	Latitude>5ºN, 80ºE<Longitude<94ºE	840

3.4.3 Nutrient Uptake and Remineralization

Biological consumption and production of nitrate cause an equivalent change in alkalinity [*Brewer and Goldman*, 1976; *Goldman and Brewer*, 1980] despite the fact that nitrate does not appear in the formal definition of alkalinity (Equation 3-1). This is because nitrate consumption/production is stoichiometrically tied to the removal/addition of nitric acid, and the H^+ removed/added does affect alkalinity. A reduction in nitrate concentration has to be matched with an increase in alkalinity of the same magnitude in order to maintain the balance of charge in the water. Therefore, nitrate consumption and denitrification increase alkalinity, and nitrate generation (nitrification) following remineralization decreases alkalinity. Other species such as sulphate and phosphate have similar effects on alkalinity [*Wolf-Gladrow et al.*, 2007].

The alkalinity changes arising from the biological cycling of nitrate are often accounted for in the concept of potential alkalinity, *pAlk* (e.g. [*Brewer et al.*, 1975; *Sarmiento et al.*, 2002]), where the sum of the nitrate and alkalinity concentrations is normalized to a salinity of 35. *Wolf-Gladrow et al.* [2007] calculated changes in alkalinity from primary productivity, taking into account the proportional uptake of other ions such as phosphate and sulphate. They suggested that the impact of phytoplankton growth on alkalinity should be calculated by multiplying changes in the nitrate ion concentration, NO_3^-, by a factor of 1.36. Hence:

$$pAlk = \frac{Alk_m + 1.36 \times NO_3^-}{S} \times 35 \tag{3-5}$$

Figure 3-1j, k, l show the resulting patterns in alkalinity, after variations in nutrient concentration have also been taken into account, using:

$$Alk_3 = \frac{Alk_m - Alk_r + 1.36 \times NO_3^-}{S} \times 35 + Alk_r \tag{3-6}$$

Incorporation of the effects of creation and remineralization of biological matter increases the average offset between low latitudes and high latitudes from ~75 µmol kg^{-1} to ~100 µmol kg^{-1}. This is because the Southern Ocean and subarctic North Pacific are both regions of the global ocean with high surface nitrate concentrations.

3.4.4 Pattern in the Residual Alkalinity

After excluding the effects of nutrients on alkalinity, there is a fairly uniform alkalinity of ~2300 µmol kg^{-1} in the low-latitude surface oceans (30ºN-30ºS). Table 3-1 shows that with every additional step the width of the data cloud relative to the overall range of the data has decreased. This suggests that the effects of processes causing variation have been successfully removed. The remaining variation is comparable to that of the major nutrients (Table 3-1). This would be expected if Alk_3 and the nutrients are mainly controlled by uptake to form new phytoplankton, and returned through exchange with deep water following export and remineralization.

To examine the remaining large-scale spatial pattern in the distribution of surface alkalinity. We define the new tracer Alk* to have a low latitude concentration of ~ 0 µmol kg^{-1} (i.e. Alk* = Alk_3 – 2300 µmol kg^{-1}). Thus, the value of Alk* corresponds to the "excess alkalinity" compared to the tropical and subtropical surface ocean. It can be seen (Figure 3-1m, n and o) that Alk* values in the high-latitude regions of the North Pacific and Southern Ocean are strongly elevated by ~85 µmol kg^{-1} (north of 55ºN) and ~110 µmol kg^{-1} (south of 75ºS), respectively. Interestingly, there is no correspondingly large elevation of Alk* in the high-latitude North Atlantic: the average Alk* value at 55ºN in the Atlantic is only 24 µmol kg^{-1}. Notably, the low-latitude to polar ocean increases in alkalinity are somewhat weaker when nutrient cycling effects are not included; the same overall geographic distribution is obtained but with smaller magnitude differences (e.g., compare Alk_2 in Figure 3-1g, h, and i to Alk_3 in Figure 3-1j, k, and l).

3.5 Discussion

3.5.1 Comparison to Other Approaches

In this paper we have derived a tracer for $CaCO_3$ cycling in the surface ocean based on observed alkalinity and removal of other influences, including: (1) freshwater evaporation and precipitation; (2) inputs of river water containing alkalinity at negligible salinity; and (3) biological cycling of nutrients.

The procedure we employed is an extension of the potential alkalinity concept [*Brewer et al.*, 1975; *Rubin and Key*, 2002; *Sarmiento et al.*, 2002; *Wolf-Gladrow et al.*, 2007];

however, it also includes a correction for the influence of high-alkalinity rivers [*Friis et al.*, 2003; *Cai et al.*, 2010]. Our analysis shows that high-alkalinity rivers can influence large ocean areas (e.g. Figure 3-1g versus Figure 3-1d). We show that the North Atlantic Ocean and the Bay of Bengal are strongly influenced by river derived alkalinity inputs. We expect that with incorporation of more marginal regions [*Key et al.*, 2010], such as the South China Sea [*Kang et al.*, 2013], and more seasonal data, river alkalinity will become an increasingly important part of alkalinity process analysis. Our Alk* tracer for surface waters also bears some resemblance to that of 'excess' alkalinity [*Feely et al.*, 2002b, 2004; *Sabine et al.*, 2002], which was developed to quantify $CaCO_3$ dissolution rates along isopyncal surfaces. We use Alk* to constrain surface $CaCO_3$ cycling (as defined here) as a whole, as opposed to specifically targeting the dissolution of $CaCO_3$ at depth. This gives a tracer that is similar to nutrient tracers and can be used to investigate biological production in a similar way to that of nutrients.

In this paper we revisit some of the same issues as those of an earlier study [*Millero et al.*, 1998b], which used salinity-normalized alkalinity. Some of the large-scale patterns we find were also noted previously by *Millero et al.* [1998b], but are now more clearly defined and can be accepted with greater confidence, based on the improved analysis techniques and larger quantity of data used in this study.

3.5.2 Accounting for the Patterns in Alk*

The surface field of Alk* is distinct from the actual alkalinity observations (first and last rows of Figure 3-1). Eliminating the effects of the hydrological cycle, rivers and nutrient cycling reveals coherent basin-scale patterns in Alk* that are not apparent in Alk_m. We argue that these patterns directly reflect the imprint of the ocean's $CaCO_3$ cycle, or in other words that the patterns in Alk* are maintained by the inorganic carbon pump acting against ocean overturning and mixing. As with dissolved nutrients, Alk* is reduced when and where biological precipitation of $CaCO_3$ occurs. The $CaCO_3$ sinks from the mixed layer into the deep ocean, where $CaCO_3$ undersaturation causes it to dissolve and increase the deep Alk* concentration. Large-scale ocean circulation brings the deep water back to the surface, producing higher Alk* concentrations in the polar ocean surface of the Southern Ocean and the North Pacific.

3.5.3 High Alk* in High-latitude Oceans

In line with previous interpretations [*Millero et al.*, 1998b; *Sabine et al.*, 2002; *Key et al.*, 2004; *Lee et al.*, 2006], we identify the source of increased salinity-normalized alkalinity at high latitudes as supply of excess alkalinity from deep waters. High alkalinity at depth can be transferred to high-latitude surface waters either through upwelling, transfer along isopycnals outcropping at high latitudes, and/or entrainment of deep waters into the mixed layer during deep winter mixing. The individual contribution of these physical processes to high Alk* in surface waters may vary among distinct regions, and subsurface waters are also expected to contain variable concentrations of excess alkalinity to be brought to the surface in different parts of the world's ocean (see explanation for low North Atlantic Alk* below). In addition, the strength of these sources may vary seasonally; for example, deep winter mixing may cause higher Alk* in an area during winter with subsequent lower levels in summer.

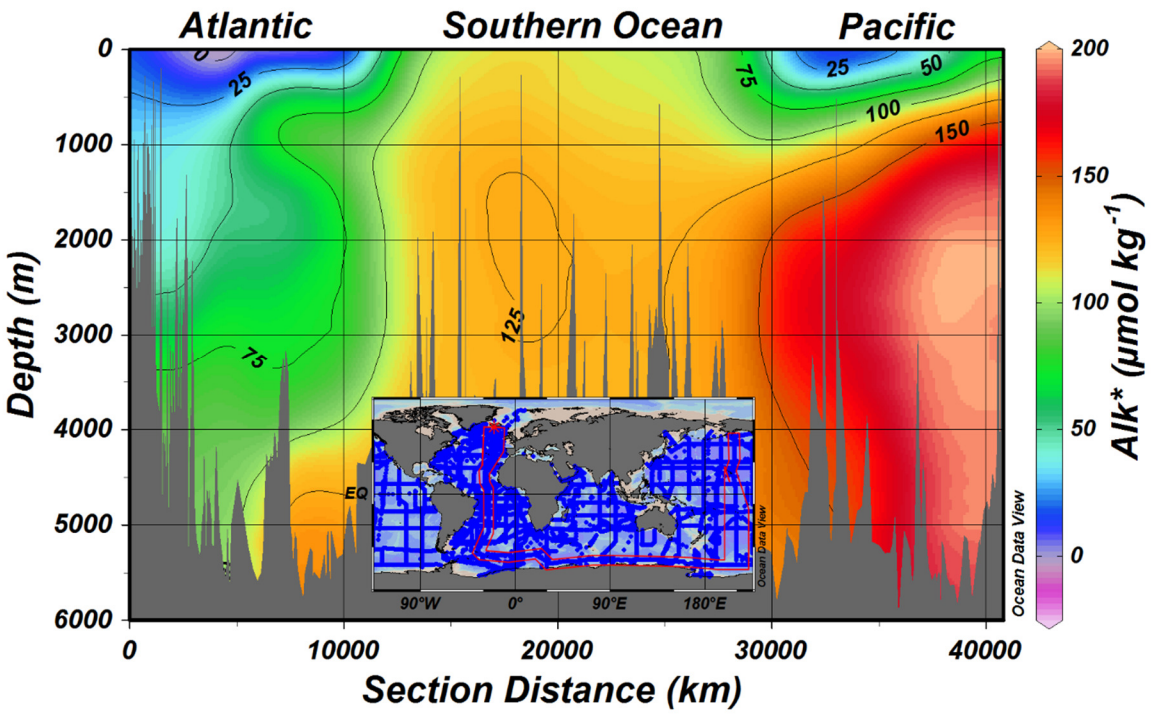

Figure 3-5. Normalized alkalinity anomaly ($Alk^* = Alk_3$ - 2300, µmol kg^{-1}) along the GLODAP section illustrated in the insert.

We attribute the relatively low Alk* values in the subarctic North Atlantic to the low Alk* values at depth in this region. To illustrate the reason for this exception, we calculated

Alk* along a vertical ocean section from the North Atlantic, through the Southern Ocean and into the North Pacific (Figure 3-5). From this interior ocean view of the alkalinity anomaly, it is clear that the high surface Alk* values of the Southern Ocean and subarctic North Pacific directly correspond to elevated Alk* in subsurface waters, whereas the low surface Alk* values of the subarctic North Atlantic are above low Alk* of the North Atlantic Deep Water (NADW). The difference between the regions can be attributed in part to differences in the ages of the deep waters underlying the various regions. The main source of NADW is surface water that was recently subducted following poleward transport from lower latitudes (e.g., [*Lozier*, 2012]).Therefore, the subpolar North Atlantic surface and NADW both inherit a low Alk* from the Atlantic meridional overturning circulation passing through the low-latitude surface Atlantic, where Alk* is also low. Because of the small vertical gradient, winter mixing in the high-latitude North Atlantic, although penetrating to considerable depths (hundreds of meters; [*de Boyer Montégut*, 2004]), produces little increase in surface Alk*. Alkalinity distributions along similar sections to Figure 3-5 have been explained [*Pardo et al.*, 2011; *Vázquez-Rodríguez et al.*, 2012] using the concept of pre-formed alkalinity, which is the alkalinity at the point subducting water loses contact with the atmosphere. As the high-latitude North Atlantic is a deep-water formation region, the low Alk* determines the pre-formed value, with $CaCO_3$ dissolution increasing Alk* as NADW travels southward through the Atlantic Ocean.

The subarctic North Atlantic contrasts with the subarctic North Pacific, where winter mixing, although not reaching to such great depths (up to about 150 m on the eastern side and 250 m on the western side; [*Ohno et al.*, 2008], does reach high Alk* subsurface waters (50-200 µmol kg^{-1}) because of the strong vertical gradients (Figure 3-5). In the Southern Ocean the situation is more complicated but there is no formation of deep water from low-latitude surface water, and deep water consequently has high Alk* (Figure 3-5). Furthermore, wind-driven upwelling introduces high Alk* water to the surface from greater depths than in other parts of the world's ocean [*Toggweiler and Samuels*, 1995].

3.5.4 Low Alk* in Low-latitude Oceans

To the degree that the global $CaCO_3$ cycle is near internal balance, the net upwards transport of dissolved Alk* across the main thermocline must equal the global downwards $CaCO_3$ rain across the thermocline. Low Alk* values in the tropical and subtropical surface

oceans are therefore understood as resulting from $CaCO_3$ formation and export leading to removal of Alk* from surface waters, together with an absence of significant replenishment from deep water. The data show surprisingly similar values in all basins at low latitudes (averages of 2297, 2294 and 2305 µmol kg^{-1} between 30ºS and 30ºN in the Atlantic, Indian and Pacific Oceans, respectively).

3.5.5 Similarity of Residual Alkalinity Distribution to Nutrients

Attributing the Alk* patterns to $CaCO_3$ cycling is further supported by the partial resemblance between the latitudinal distributions of Alk* and those of the nutrients: nitrate, phosphate and silicate (Figure 3-6). Concentrations of all are depleted in the subtropical surface ocean due to biological use. All four exhibit maxima in concentrations at high latitudes in the Southern Ocean and North Pacific, but a more modest increase in the high-latitude North Atlantic.

There are however some differences. For example, in contrast to nitrate and phosphate, neither silicate nor alkalinity exhibit large increases in concentration in the north Indian Ocean or in the eastern Equatorial Pacific. This may reflect different remineralization depths (nitrate and phosphate are both returned to solution at much shallower depths than silicate from opal rain or alkalinity from $CaCO_3$ rain; [*Schlitzer*, 2000]) and the source of the water. Alternatively, it may be co-occurrence of upwelling and intensive $CaCO_3$ production, which would not be identified in our tracer. A previous study has found salinity-normalized alkalinity to be ~40 µmol kg^{-1} higher in upwelled water in the eastern Equatorial Pacific [*Millero et al.*, 1998b].

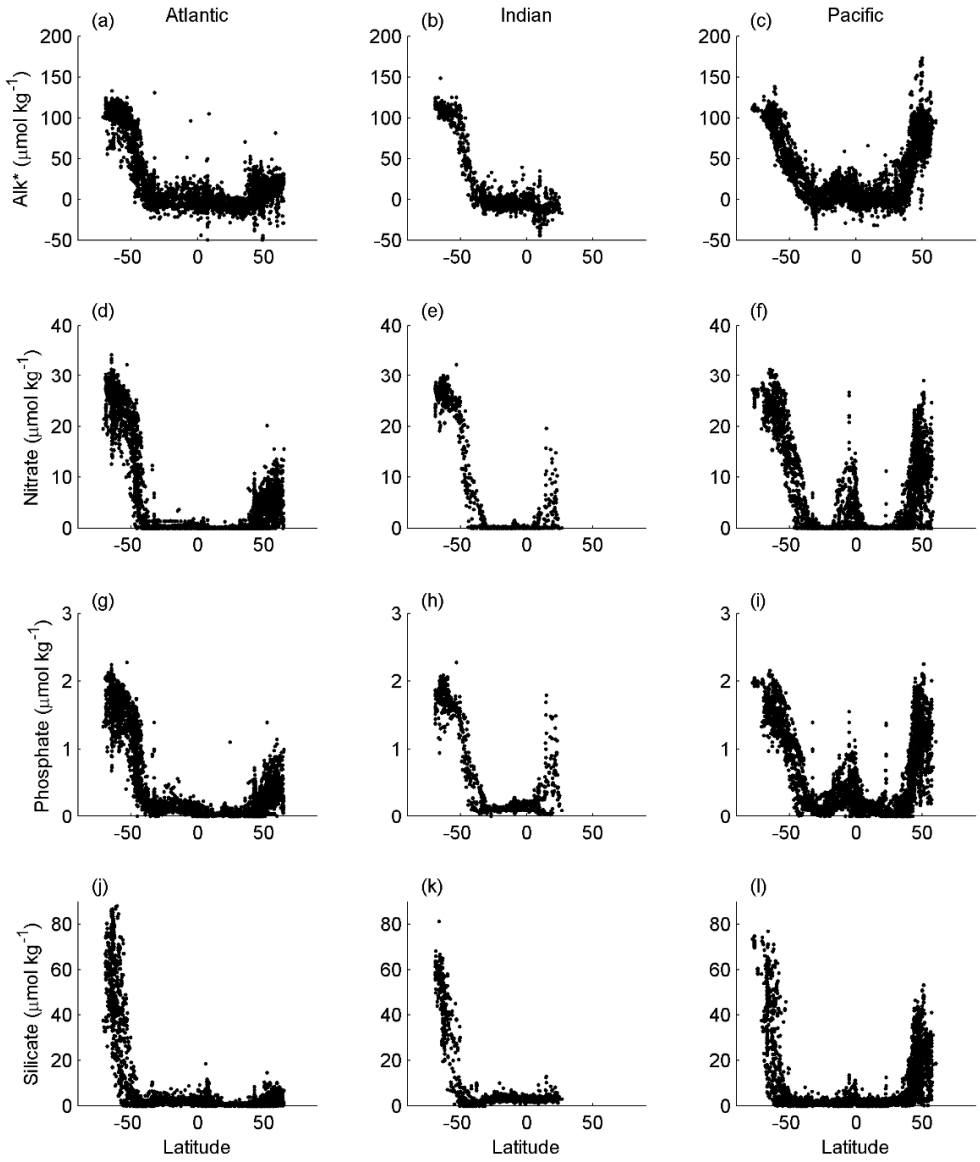

Figure 3-6. Surface distribution of *Alk** µmol kg^{-1} (a,b,c), nitrate µmol kg^{-1} (d,e,f), phosphate µmol kg^{-1} (g,h,i), silicate µmol kg^{-1} (j,k,l) in each ocean basin from the GLODAP, CARINA and PACIFICA databases.

A second difference is apparent when comparing the latitude at which all four variables decrease to negligible levels when moving northwards away from Antarctica. Concentrations of silicate have declined almost to zero by about 50ºS, whereas Alk*, nitrate and phosphate are all still significantly elevated at this latitude and it is not until about 40ºS that all three decline to near zero (Figure 3-6). One explanation of this feature

could be the greater competitive success of silicifiers in the Southern Ocean, with diatoms blooming and depleting silicate concentrations further south than other phytoplankton. Therefore, silicate is used up further south than nitrate, phosphate, and Alk* [*Sarmiento et al.*, 2004]. Pronounced yearly blooms of coccolithophores are seen in satellite observations in the region of the subantarctic zone (about 50ºS to 40ºS) of the Southern Ocean [*Iglesias-Rodríguez et al.*, 2002]. This feature has been termed the "Great Calcite Belt" [*Balch et al.*, 2011] and may be responsible for one third of global export of $CaCO_3$ [*Jin et al.*, 2006]. However, in order to identify more confidently where $CaCO_3$ production and export take place, the tracer should ideally be used in conjunction with an ocean circulation model.

Overall, the nutrient-like distribution of Alk* is consistent with the expected behavior of a tracer of $CaCO_3$ production and dissolution.

3.5.6 Similarity of Residual Alkalinity to Residual Calcium

Results from a second and independent method of constraining $CaCO_3$ cycling can be compared to those from the Alk* method. The concentration of calcium ions (measurable to a precision of about ± 3 µmol kg^{-1}; [*Olson and Chen*, 1982] is also directly affected by dilution and concentration, production and dissolution of $CaCO_3$, and river input of $CaCO_3$, but not biological cycling processes affecting alkalinity. After salinity normalization, the surface ocean has a slightly lower concentration of calcium than at depth, due to the $CaCO_3$ pump [*Milliman et al.*, 1999]. The ratio of Ca^{2+} to salinity has previously been demonstrated as a tracer of $CaCO_3$ cycling in the South China Sea [*Cao and Dai*, 2011], and salinity-normalized calcium concentration (NCa) agrees well with salinity-normalized alkalinity as a tracer of $CaCO_3$ cycling in deep waters of the Sea of Okhotsk [*Pavlova et al.*, 2008]. Both Ca-based and Alk-based tracers of $CaCO_3$ cycling are made less effective in the deep ocean because low-temperature hydrothermal vents are an alternative source of calcium [*de Villiers*, 1998; *de Villiers and Nelson*, 1999; *Chen*, 2002].

If $CaCO_3$ cycling is the dominant influence over both Alk* and NCa then we predict the following NCa patterns in surface waters: (1) it should be relatively invariant across low-latitude oceans; (2) it should differ by about 40 µmol kg^{-1} (ΔCa from $CaCO_3$ formation/ dissolution = 0.5 * ΔAlk*) between low and high latitudes in the North Pacific; (3) it should be about 55 µmol kg^{-1} higher in the high-latitude Southern Ocean than in low-

latitude regions; and (4) it should not vary greatly between low and high latitudes in the North Atlantic.

Relatively few calcium data currently exist with which to test these predictions, and what does exist is only partly compatible with them. *Chen* [2002] reported calcium concentrations along 150ºW in the North Pacific from 8 to 55ºN: highest NCa values along the transect were observed at the highest latitudes (north of 45ºN); however, an unexpectedly high degree of low-latitude variability (> 20 µmol kg^{-1}) is also apparent in the data. NCa values from the Weddell Sea are approximately 70 µmol kg^{-1} higher than values from the low-latitude Pacific Ocean [*Chen*, 2002]. *Tsunogai et al.* [1973] found a poleward increase of the calcium to chlorinity ratio along 170^0W.

3.5.7 Some Uncertainties and How They Might be Reduced in Future Work

Here, we consider sources of uncertainty in Alk* and, where applicable, how they might be minimized in future work. The geographical differences in Alk* are large compared to the accuracy of alkalinity measurements (~3 µmol kg^{-1}, [*Dickson et al.*, 2003]), which can thus be ruled out as a cause. There is some bias in the collection of data, with surveys in high latitude regions occurring more frequently during summer months because of weather considerations [*Key et al.*, 2004]. Because alkalinity resupply to the surface by vertical mixing changes with season including more wintertime data could increase high-latitude Alk* values, thereby further increasing the contrast to the low-latitude surface that has no seasonal bias.

Some local river flows need to be considered when using open ocean data [*Cai et al.*, 2010], as demonstrated here by the wide-scale influences of river derived alkalinity inputs to the Bay of Bengal and Atlantic Ocean. *Kang et al.* [2013] identified the South China Sea as another area affected by river inputs of alkalinity; however, we made no adjustment because of a lack of seawater data for the region. When using river alkalinity data to correct for river influences in offshore regions, it should be kept in mind that differences in riverine input alkalinity can be caused by non-conservative estuarine changes to fluxes such as from anaerobic processes occurring in the river delta [*Hu and Cai*, 2011], as has been recorded in river systems [*Wong*, 1979; *Cai and Wang*, 1998]. Also, simply fitting a line to alkalinity-salinity data is not always a reliable method of determining the river end-

member alkalinity [*Jiang et al.*, 2014]. Further research is required on alkalinity in the outflows of major rivers and the penetration of their effects into the open ocean.

$CaCO_3$ cycling is the dominant influence on the residual alkalinity, but other processes will also have smaller effects. Some second-order or locally important processes for alkalinity have not been calculated and removed from Alk*. These include anaerobic remineralization processes (denitrification and sulphate reduction could affect the surface waters in coastal regions), formation and destruction of sea-ice and ikaite [*Rysgaard et al.*, 2012b, 2013], organic alkalinity [*Bradshaw and Brewer*, 1988], and nitrogen-fixation [*Wolf-Gladrow et al.*, 2007]. Development of techniques for the removal of these influences would further improve Alk*. Many of these processes, such as the impact of organic alkalinity, the formation and destruction of sea-ice, and anaerobic remineralization are of greater importance in areas that are not included in this study, such as in coastal regions and the Arctic Ocean.

There is a limit to the accuracy with which the magnitude of calcification can be determined in river affected ocean from an alkalinity-based tracer. This is because the order in which calcification and mixing take place (which is not usually known) affects the resulting change in alkalinity [*Jiang et al.*, 2014]. This can be important when two bodies of water mix, for example when seawater mixes with river water. If calcification occurs (A to b in Figure 3-7) before the mixing with river water (b towards R in Figure 3-7), then the final alkalinity value (c in Figure 3-7) differs from that when mixing occurs before calcification (A to d to e in Figure 3-7). Equation 3-6 for Alk* assumes calcification occurs before mixing and so if they occur in the opposite order then the inferred amount of calcification would be inaccurate. But, from calculations on our dataset when we assumed a reversed order, the difference is within the current measurement error of alkalinity (<3 $\mu mol\ kg^{-1}$). In addition, Alk* is not completely conservative because of salinity-normalization. When two water bodies mix, the calculated Alk* of the mixture is not exactly equal to the weighted average of the source Alk* values, although the difference is usually small (<5%).

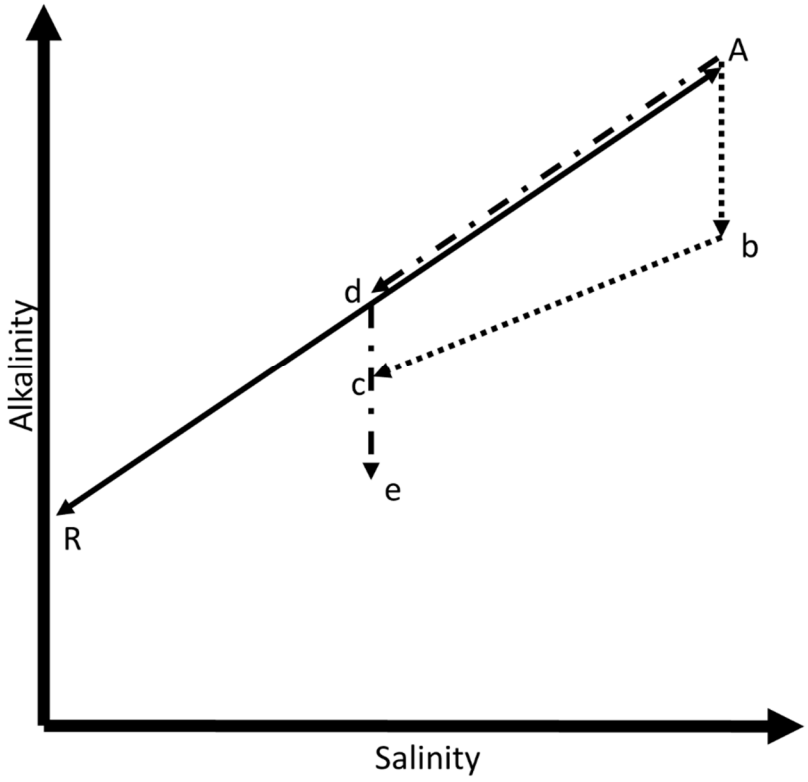

Figure 3-7. The mixing relationship between salinity and alkalinity when calcification also takes place. When an ocean body (A) mixes with river water (R) and calcification occurs, the final alkalinity-salinity relationship will depend on whether the calcification occurred before (A to b to c) or after (A to d to e) mixing.

We can quantify the propagated measurement uncertainty in Alk* from the definition of Alk_3 (Equation 3-6), which in absolute terms has the same uncertainty as Alk*, and from rules for propagating uncertainties through calculations [*Taylor*, 1982]. The uncertainty in Alk* values is calculated using Equation 3-7 and measurement uncertainties of: alkalinity, ΔAlk_m, 3 µmol kg^{-1} [*Dickson et al.*, 2003]; salinity, ΔS, 0.0015 [*Perkin and Lewis*, 1980], and nitrate, ΔNO_3^-, 0.2 µmol kg^{-1} [*Aminot and Kirkwood*, 1995]. Errors in river input measurements were not considered as most of the dataset is not affected by the adjustment. The estimated overall uncertainty of Alk*, ΔAlk*is 3.02 µmol kg^{-1}. The uncertainties are thus small compared to the large latitudinal differences in Alk*.

$$\Delta Alk^* = \frac{35 \times (Alk_m + 1.36 \times NO_3^-)}{S} \times \sqrt{\left(\frac{\Delta S}{S}\right)^2 + \frac{(\Delta Alk_m)^2 + (1.36 \times \Delta NO_3^-)^2}{(Alk_m + 1.36 \times NO_3^-)^2}} \quad (3\text{-}7)$$

3.5.8 Potential Uses of Alk*

This new tracer of surface $CaCO_3$ cycling is likely to be useful in a number of ways. The first example is in the calculation of $CaCO_3$ export fluxes.

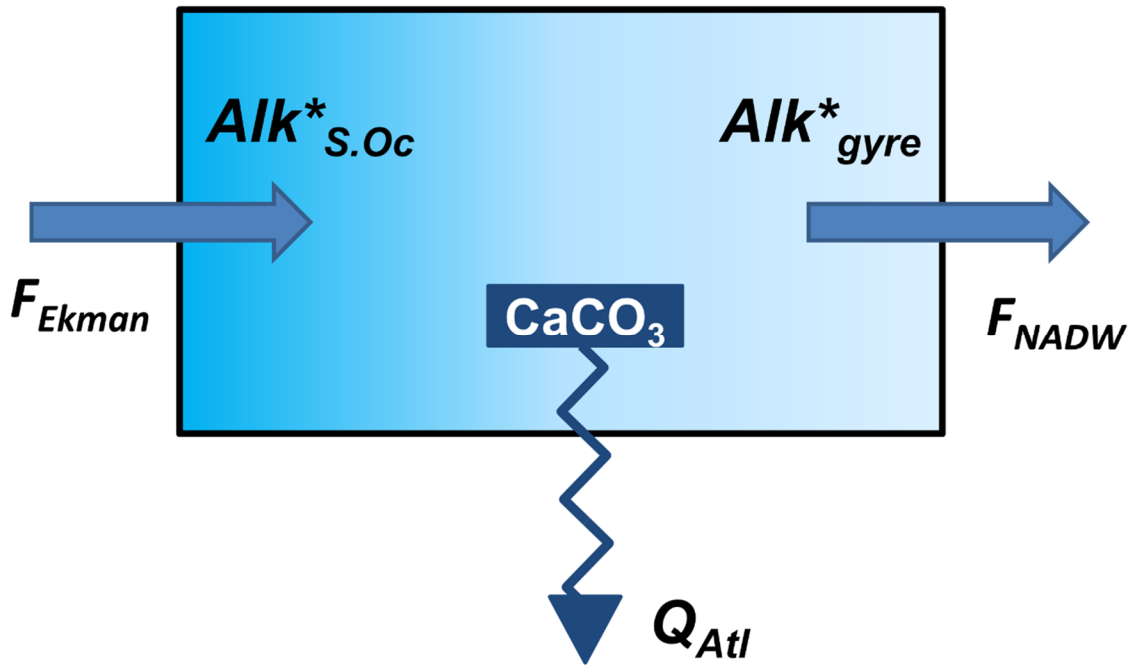

Figure 3-8. Representation of Atlantic Basin circulation and fluxes. $Alk^*_{S.Oc}$ and Alk^*_{gyre} are the alkalinity anomalies of the Southern Ocean and Atlantic gyre respectively. F_{ekman} is the surface Ekman flux in the Southern Ocean, F_{NADW} the NADW flux and Q_{Atl} is the flux of alkalinity leaving the gyre through $CaCO_3$ precipitation. Equatorial upwelling and mixing across the thermocline are omitted as they do not contribute to the first order Alk* pattern.

Where horizontal and vertical water fluxes are known, they can be combined with Alk* gradients to estimate the rate of loss of calcium carbonate (export flux) from the mixed layer. Figure 3-8 shows the fluxes that affect Alk* of the low-latitude surface water in the

Atlantic. Supply of Alk* through mixing across the thermocline and equatorial upwelling is assumed negligible as this process does not contribute to the observed surface ocean pattern. Average Alk_3 is 2299 µmol kg^{-1} at 30ºS ($Alk^*_{S.Atl.}$ = -1) and 2289 µmol kg^{-1} at 30ºN ($Alk^*_{N.Atl.}$ = -11) (Figure 3-1j). If NADW formation (F_{NADW}) and the surface Ekman water flux from the Southern Ocean (F_{Ekman}) are equal at 18±3 Sverdrups [*Talley et al.*, 2003], then the rate of Alk* vertical export, Q_{Atl}, from the Atlantic Ocean can be calculated as a function of the water flux and the decline in alkalinity in transit:

$$Q_{Atl} = F_{Ekman} \times Alk^*_{S.Atl} - F_{NADW} \times Alk^*_{N.Atl} = F_{Ekman} \times (Alk^*_{S.Atl} - Alk^*_{N.Atl}) \quad (3\text{-}8)$$

This produces an estimated $CaCO_3$ export of ~0.03 Pg PIC yr^{-1} with an uncertainty of ±0.01 based on the uncertainty in the Ekman flux. This value is significantly lower than previous estimates of Atlantic $CaCO_3$ production (0.11-0.69 Pg PIC yr^{-1}; see Table 3-3) and an Atlantic-wide estimate of $CaCO_3$ dissolution in deep water (0.13 Pg PIC yr^{-1}; [*Chung*, 2003]). Our value suggests that rather little calcification takes place in the upper mixed layer of the Atlantic. Our estimate is of export rather than production but dissolution is probably minor in the supersaturated surface ocean and so the two are probably similar. The discrepancy with other estimates could potentially be reconciled if calcification is primarily taking place in deeper parts of the euphotic zone, i.e. below the surface mixed layer [*Poulton et al.*, 2006] or further south in the Atlantic sector of the Southern Ocean (Figure 3-1j). Another explanation is that equatorial upwelling does supply Alk* and it is used too quickly to be seen in the surface concentrations. We suspect that the largest uncertainty in our calculation stems from the assumption that the only flows are NADW and associated net flow through the tropical Atlantic box, which is an oversimplification.

Alk* could also be used to analyze the spatial distribution of $CaCO_3$ export. Calculation of Alk* on different depth and/or density levels may help resolve the question about where in the oceans most $CaCO_3$ is produced and exported. In the surface layer at least, the steepest horizontal gradients in Alk* are at mid latitudes of 30º-40º (Figure 3-1m, n and o). This concurs with satellite observations of highest particulate inorganic carbon (PIC; coccoliths) concentrations in surface waters at high latitudes [*Iglesias-Rodríguez et al.*, 2002; *Balch et al.*, 2005; *Moore et al.*, 2012]. Likewise, *Jin et al.* [2006] found high $CaCO_3$ export at 40º latitude using global nutrient and alkalinity observations and a biogeochemical model; however, the authors also found an equally large peak in export at the equator. A peak in

export at the equator would not show up in Alk* if the simultaneous impacts of upwelling and export cancelled each other out. Sediment trap compilations [*Berelson et al.*, 2007] and theoretical calculations [*Sarmiento et al.*, 2002], indicate highest rain ratios (highest $CaCO_3$ export) towards the equator; however, there was no peak at mid latitudes.

Table 3-3. Estimates of Annual Production of Particulate Inorganic Carbon in the Atlantic Ocean Basin

	Pg PIC yr^{-1}
Lee (2001)	0.43
Poulton et al. (2006)	0.69[a]
Berelson et al. (2007)	0.11-0.35
Our estimate	0.03

[a]Flux estimate from data collected during northern hemisphere spring (southern hemisphere autumn).

Alk* could also be used to validate biogeochemical models and improve model quantifications of $CaCO_3$ fluxes. The broad patterns in Alk* should be reproduced in high-resolution global carbon cycle models if correctly formulated. The degree of agreement with Alk* can be used as a check of the representations of ocean physics and $CaCO_3$ formation and dissolution. It may also be possible to improve methods for deducing $CaCO_3$ particle fluxes from ocean alkalinity data, by basing the inversion method on this method for Alk*.

Finally, if ocean acidification leads to large reductions in calcification then an effect on ocean alkalinity may be detectable by 2040 [*Ilyina et al.*, 2009]. This may be more accurately determined using Alk* rather than measured alkalinity as the method corrects for changes in the water cycle [*Huntington*, 2006 and references therein] and productivity [e.g. *Bopp et al.*, 2001; *Gregg et al.*, 2003; *Behrenfeld et al.*, 2006], which are also forecast to change. Time-series are often located close to the coast, because of ease of access, and consequently are frequently affected by river inputs. Alk* is less variable than potential alkalinity in river-affected areas. This is because the standard deviation is reduced by the

river correction (Table 3-2), making long term trends easier to detect (higher signal-to-noise ratio). This is illustrated in a simplistic way (Figure 3-9) in an example using data from the area of the Atlantic affected by the Amazon River outflow and an increase of 30 µmol kg^{-1} by 2040 [*Ilyina et al.*, 2009]. Following *Ilyina et al.* [2009], the trend is deemed to be detected when the magnitude of the change due to the trend exceeds the standard deviation of the data. According to this method (more sophisticated methods would be used in reality), the long-term trend is detectable by 2040 using Alk* but not until 2060 using potential alkalinity.

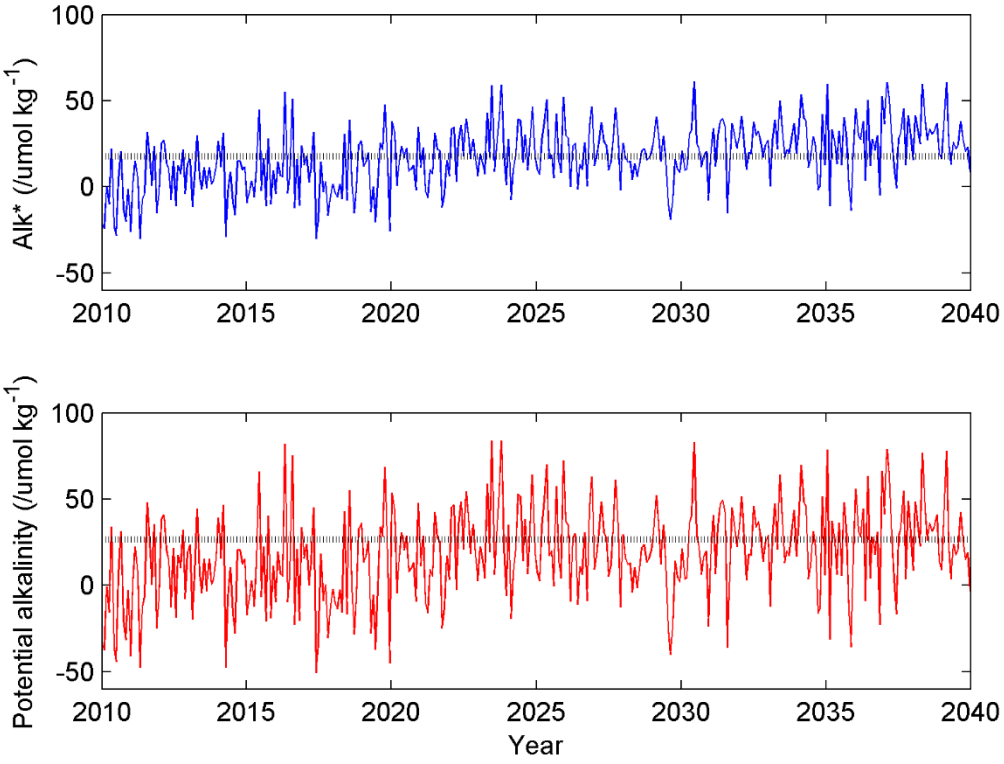

Figure 3-9. Modelled *Alk** in an area of the ocean affected intermittently by the Amazon River outflow. Alk* is shown both with river adjustment included (top) and without it (bottom). The simulated data was produced using a random number generator to produce random numbers from a normal distribution with a standard deviation (dashed line) of 16.5 µmol kg^{-1} (top panel) and 25.6 µmol kg-1 (bottom panel). These standard deviations are the standard deviations of the actual Alk* values in the region affected by the Amazon (Table 3-2), depending on whether adjusted to take account of Amazon alkalinity or not. An

alkalinity increase over time of 30 µmol kg^{-1} from 2010 until 2040 was added to the random numbers to produce the simulated data. Data sampling frequency of 30 days.

3.6 Conclusions

In this study we derive a tracer for the ocean $CaCO_3$ cycle by subtracting the influences of other processes from the global surface alkalinity data, specifically (a) the hydrological cycle, (b) riverine discharge, and (c) the biological cycling of nutrients. On a regional scale, adjustment for the individual alkalinities of nearby large rivers was found to be particularly important in bringing anomalous values 'into line' in areas such as the tropical Atlantic Ocean, the Bay of Bengal and the Labrador Sea. The coherent geographic pattern revealed by our alkalinity tracer shows a constant value across the low latitudes of all major ocean basins, and well-defined, large magnitude increases of ~85 and ~110 µmol kg^{-1} towards the North Pacific and Southern Ocean respectively. The surface North Atlantic and North Atlantic Deep Water inherit low residual alkalinity from their source waters in the Atlantic subtropical gyres. Comparisons to nutrient distributions and calcium data strongly suggest that these patterns in the residual alkalinity are caused by $CaCO_3$ cycling, i.e. upwelling mainly at high latitudes of deep water into which $CaCO_3$ has dissolved, and $CaCO_3$ export elsewhere that reduces Alk* with increasing distance from the centers of upwelling. This residual alkalinity (Alk*) therefore has considerable potential as a tracer of $CaCO_3$ cycling. This new tracer is likely to have many applications, including in quantification and localization of $CaCO_3$ export.

Chapter 4: Analysis of longitudinal variations in North Pacific alkalinity to improve predictive algorithms

This chapter published as Fry, C.H., T. Tyrrell, E.P. Achterberg (2016), Analysis of longitudinal variations in North Pacific alkalinity to improve predictive algorithms. Global Biogeochem. Cy., 30, 1493–1508. T. Tyrrell and E.P. Achterberg provided feedback on the methods and the manuscript. The writing of the chapter and all analysis and production of figures was performed by C.H. Fry.

4.1 Abstract

The causes of natural variation in alkalinity in the North Pacific surface ocean need to be investigated to understand the carbon cycle and to improve predictive algorithms. We used GLODAPv2 to test hypotheses on the causes of three longitudinal phenomena in Alk*, a tracer of calcium carbonate cycling. These phenomena are: (a) an increase from east to west between 45ºN and 55ºN, (b) an increase from west to east between 25ºN and 40ºN, and (c) a minor increase from west to east in the equatorial upwelling region. Between 45ºN and 55ºN, Alk* is higher on the western than on the eastern side and this is associated with denser isopycnals with higher Alk* lying at shallower depths. Between 25ºN and 40ºN, upwelling along the North American continental shelf causes higher Alk* in the east. Along the equator, a strong east-west trend was not observed, even though the upwelling on the eastern side of the basin is more intense, because the water brought to the surface is not high in Alk*. We created two algorithms to predict alkalinity, one for the entire Pacific Ocean north of 30ºS and one for the eastern margin. The Pacific Ocean algorithm is more accurate than the commonly-used algorithm published by *Lee et al*. [2006], of similar accuracy to the best previously published algorithm by *Sasse et al.* [2013], and is less biased with longitude than other algorithms in the subpolar North Pacific. Our eastern margin algorithm is more accurate than previously published algorithms.

4.2 Introduction

Total alkalinity, hereafter referred to as alkalinity, is typically determined as part of seawater carbonate chemistry observations. Alkalinity is the excess of proton acceptors

over proton donors [*Wolf-Gladrow et al.*, 2007]. It is one of four measurable carbonate chemistry variables, with the others being dissolved inorganic carbon, pH, and the partial pressure of carbon dioxide (pCO_2). We can calculate the entire carbonate system with any two of these variables, along with temperature, pressure, salinity, phosphate, and silicate concentrations. Alkalinity is useful because it behaves in a conservative manner when water masses mix and is independent of changes in temperature and pressure, unlike pCO_2 and pH [*Dyrssen and Sillén*, 1967; *Wolf-Gladrow et al.*, 2007]. This allows us to develop linear relationships to predict alkalinity from common hydrographic measurements, like temperature and salinity. These relationships can then be used to constrain the carbonate system from standard measurements when a carbonate variable is unavailable. This approach is more difficult for pCO_2 and pH due to their non-linear relationship with temperature and salinity.

The main causes of variation in surface ocean alkalinity are dilution and concentration as a result of precipitation, evaporation, river discharge, and sea ice formation and melt [*Millero et al.*, 1998b; *Friis et al.*, 2003; *Cai et al.*, 2010]. Since these processes also strongly influence ocean salinity, alkalinity is often considered a function of salinity due to its strongly conservative nature [e.g. *Chen and Millero*, 1979; *Millero et al.*, 1998b; *Lee et al.*, 2006; *Land et al.*, 2015]. However, alkalinity is also affected by non-conservative processes, for example, biological organic matter production and calcification [*Brewer and Goldman*, 1976; *Wolf-Gladrow et al.*, 2007; *Kwon et al.*, 2009]. It is therefore important to determine the causes of local non-conservative deviations in alkalinity (variations from the relationship with salinity) to improve our understanding of the controls on ocean carbonate chemistry and its role in climate change and ocean acidification.

The North Pacific, from the equator to the Bering Sea, is a region of the global ocean where the controls on alkalinity are not yet well understood. *Chen and Pytkowicz* [1979] first identified a longitudinal gradient in salinity-normalized alkalinity in the subpolar North Pacific and in this area, unlike in other regions, *Lee et al.* [2006] could not model the distribution of surface ocean alkalinity using salinity and temperature alone, and used longitude as an additional predictor variable. The results matched the observed alkalinity variations, but the approach was no longer mechanistic.

Physical processes are known to be important drivers of surface ocean alkalinity, including for example, upwelling of deep water with enhanced alkalinity *Fry et al.* [2015]. To capture these physical processes, *Takatani et al.* [2014] included sea surface height as an independent predictor variable for alkalinity in the Pacific Ocean. This is because sea

surface height can be used to distinguish between water bodies with potentially different alkalinities. The relationships in *Takatani et al.* [2014] improved on *Lee et al.* [2006] and reduced bias in the western North Pacific from a mean difference between the measured and predicted values of -12.7 µmol kg^{-1} (root mean square error (rms) of 16.7 µmol kg^{-1}), obtained using the relationship presented by *Lee et al.* [2006], to a mean difference of -0.2 µmol kg^{-1} (rms of 6.2 µmol kg^{-1}). For the subpolar North Pacific (north of 30ºN and < 20 ºC), these authors also used two equations where *Lee et al.* [2006] used only one. Longitude was not included explicitly as a predictor variable but the application of one equation in the east and one in the west allowed the effect of longitude to be included indirectly. Therefore, the increased accuracy of *Takatani et al.* [2014] could be caused by the use of additional variables and equations (allowing a greater degree of tuning of the algorithm), rather than because sea surface height is a superior predictor variable.

Sasse et al. [2013] improved on *Lee et al.* [2006] by using more predictor variables (temperature, salinity, dissolved oxygen, silicate, and phosphate), while dividing the ocean into the same regions as *Lee et al.* [2006]. They compared the results of their multiple linear regression with a Self-Organizing Multiple Linear Output (SOMLO); however, this did not improve the prediction of alkalinity in the North Pacific. The accuracy of the SOMLO was only 2.7% greater in the North Pacific (temperature < 20ºC, salinity between 31 and 35) and was 2.1% less accurate in the equatorial Pacific. They commented that there are few non-linearities in the carbonate system; therefore, using a non-linear model does not provide an improvement. Henceforth we only refer to the multiple linear regression by *Sasse et al.* [2013].

In the tropical ocean, both *Millero et al.* [1998b] and *Lee et al.* [2006] noted that the eastern equatorial upwelling region had a higher salinity-normalized alkalinity than the rest of the tropical oceans. *Fry et al.* [2015] and *Ishii et al.* [2004], on the other hand, did not observe any longitudinal variation in salinity-normalized alkalinity in these ocean regions. However, it is possible that a different relationship from the rest of the tropical region is still required. Some of the predictor variables may be affected by the equatorial upwelling and, although alkalinity is not, the relationship between alkalinity and the predictor variables is changed by the upwelling. For example, if upwelling waters are colder than non-upwelling waters but do not contain elevated Alk* values (see below for Alk* definition), then the relationship with the predictor (temperature) may change and a new equation is necessary even though Alk* values are not different from those outside the upwelling region.

The study of the factors controlling variability of the oceanic carbonate system is important because of its central role in climate change and ocean acidification. There is, however, a limited amount of alkalinity data compared to other hydrographic measurements such as temperature, salinity, and nutrients (GLODAPv2 has about 42 thousand casts whereas the World Ocean Database contains over 3 million casts). As a result of the insufficient temporal and spatial coverage of the global ocean, algorithms are employed to predict alkalinity values using commonly measured variables such as temperature and salinity. These algorithms therefore provide greater alkalinity coverage of the ocean, and are also of importance for verification of biogeochemical models as it is difficult to model alkalinity fields with a high level of accuracy.

We have recently introduced Alk* (Equation 4-1) as a tracer of calcification, dissolution of calcium carbonate, and the movement of the dissolution products via physical circulation [*Fry et al.*, 2015]. Alk* illuminates these processes as it removes other common controlling factors of variation, namely evaporation and precipitation, river inputs, and biological uptake and release of ions.

$$\text{Alk} * = \frac{Alk_m + 1.36 \times NO_3^- - Alk_r}{S} \times 35 + Alk_r - 2300 \quad (4\text{-}1)$$

where Alk_m is measured alkalinity (µmol kg^{-1}), NO_3^- is nitrate concentration (µmol kg^{-1}), Alk_r is identified river alkalinity (µmol kg^{-1}) in ocean areas affected by river inputs, and S is salinity.

The aim of our work is to determine the factors controlling alkalinity in the surface waters of the North Pacific Ocean. We test a series of hypotheses that explore longitudinal variations in Alk* in the zonal bands 45ºN - 55ºN, 25ºN - 40ºN, and 15ºS - 10ºN. We then derive two algorithms that predict alkalinity in surface waters, for both the entire Pacific Ocean north of 30ºS, and also in the eastern margin of the North Pacific. Each algorithm consists of three equations and the relevant definitions of how to choose which equation to use for each location.

4.3 Hypotheses

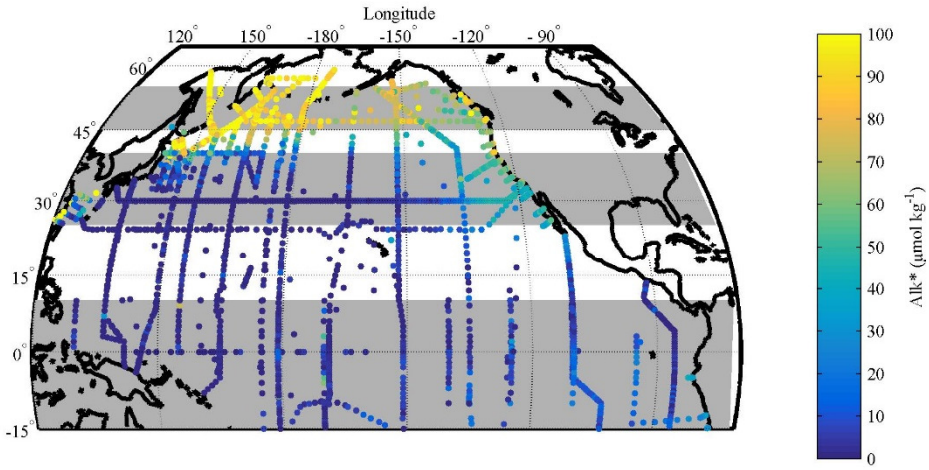

Figure 4-1. Alk* in the surface waters (<30 m) of the North Pacific using data from the GLODAPv2 database. No rivers were included in the calculation of the Alk* values. The three areas shaded in grey indicate the areas of the three phenomena investigated in this study.

The Alk* distribution in the surface waters of the North Pacific shows distinct longitudinal gradients at different latitudes (Figure 4-1): (1) between 45ºN and 55ºN, Alk* is higher in the west than the east (Figure 4-2a); (2) between 25ºN and 40ºN, Alk* at the eastern edge of the Pacific is higher than further west (Figure 4-2b); and (3) in the eastern equatorial Pacific there is only a minor increase in Alk* despite a pronounced reported increase in salinity-normalized alkalinity [*Millero et al.*, 1998b; *Lee et al.*, 2006] (Figure 4-2c). The differences between east and west in all three latitudinal bands are significant (Table 4-1). The divide is situated further east for the 30ºN zonal band as we are looking to explain a localized feature and a more central divide would bias the t-test results. We developed a series of hypotheses for each of the phenomena (the gradients just described), and tested the hypotheses using observational data. For all three latitudinal bands, we considered the alternative possibility of the patterns being caused by errors in data such as a bias of one cruise or random error in a few data points.

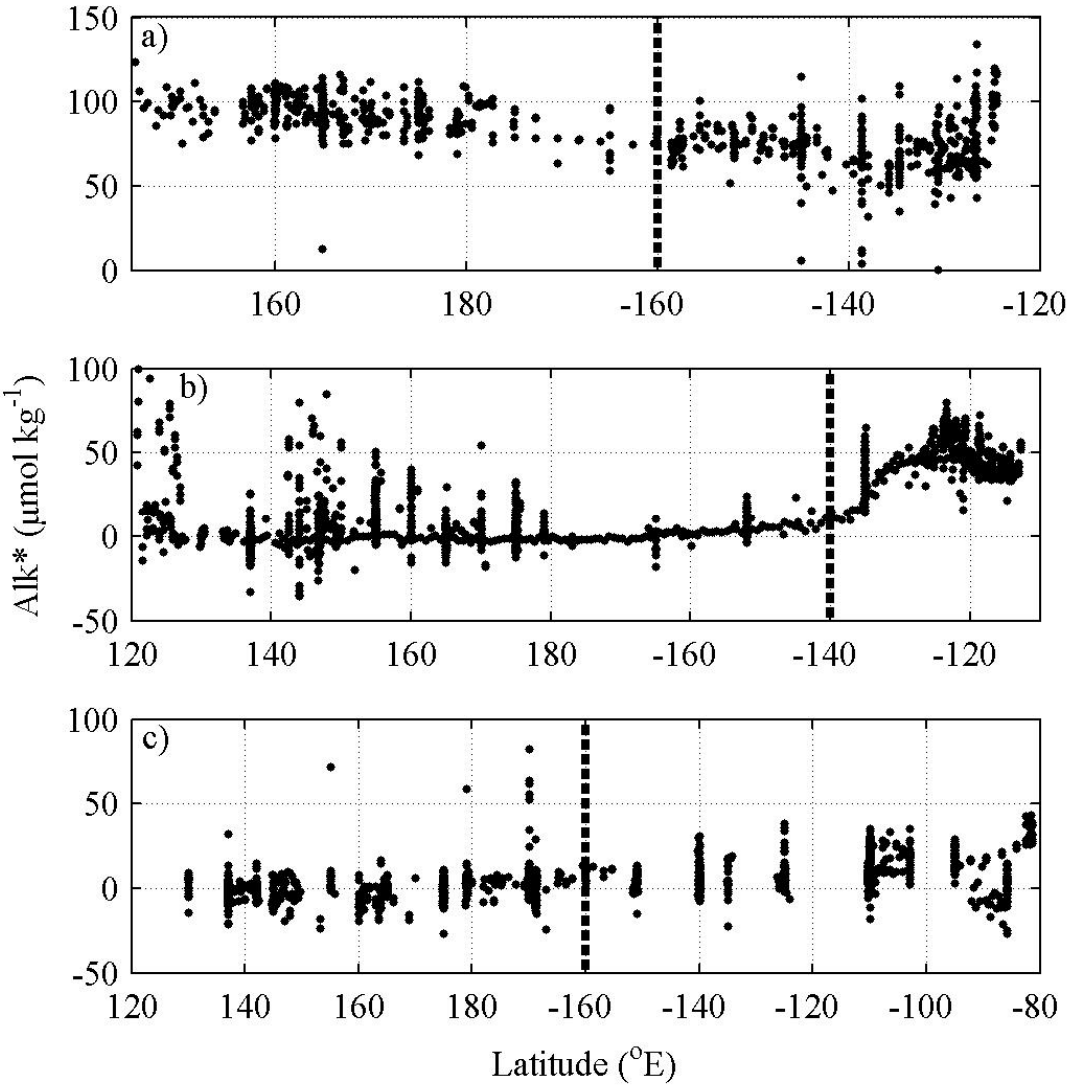

Figure 4-2. Longitudinal variations in Alk* along the three longitudinal bands presented in Figure 4-1: (a) 45ºN to 55ºN, (b) 25ºN to 40ºN, and (c) 15ºS to 10ºN. The dashed lines represent the longitudinal divide between east and west. For phenomenon 1 (a) and 3 (c), 160ºW was used because is it approximately central in the basin. Phenomenon 2 (b) is a local feature so 140ºW was used to separate data in the local area from the rest of the basin.

Phenomenon 1: Between 45ºN and 55ºN, Alk* is higher in the northwest Pacific than in the northeast Pacific.

Hypotheses:

1.1 Winter mixing yields higher Alk* values to the west, as it reaches greater depths than on the eastern side.

1.2 Denser isopycnals with older water containing elevated Alk* are closer to the surface on the western side.

1.3 Anaerobic processes in shelf sediments (which enhance Alk*) exert a stronger influence on the western side.

Table 4-1. Alk* difference from east to west in the North Pacific.

Band	Longitudinal divide between east and west	p[a]	Degrees of freedom	t-stat[b]	Mean in west (µmol kg^{-1})	Mean in east (µmol kg^{-1})
45ºN - 55ºN	160ºW	<0.001	931	23.6	95.3	72.2
25ºN - 40ºN	140ºW	<0.001	1602	-24.1	9.5	46.9
15ºS - 10ºN	160ºW	<0.001	1619	-20.0	0.8	10.7

[a]Probability with the null hypothesis for each band is that the means of both boxes are equal. [b]Two-sample two-tailed t-test.

Phenomenon 2: Between 25ºN and 40ºN, Alk* is higher towards the eastern edge of the Pacific than further west.

Hypotheses:

2.1 Previously unidentified outflow from North American rivers affects Alk*.

2.2 Upwelling increases Alk* along the North American coast.

2.3 High Alk* waters are transported southwards from the northeast Pacific by the California Current, but this process does not occur in the northwest Pacific where the northward flowing Kuroshio Current dominates.

Phenomenon 3: In the equatorial Pacific region, there is little increase in Alk* from the west to the east.

Hypotheses:

3.1 In the majority of phases of the El-Niño-Southern-Oscillation (ENSO) there is limited upwelling of Alk*.

3.2 The upwelled waters do not come from a sufficiently great depth to contain enhanced Alk*.

3.3 High Alk* waters are upwelled but calcification and export rapidly remove Alk* from the surface ocean.

4.4 Methodology

Alkalinity and other variables were obtained from the GLODAPv2 database [*Olsen et al.*, 2016]. Data from depths of less than 30 m were defined as being from the surface mixed layer. Alk* was calculated using Equation 4-1 and no correction for riverine alkalinity inputs was applied because no substantial areas influenced by rivers have previously been identified in the North Pacific [*Fry et al.*, 2015]. Shelf areas are included in our approach, which is different to our previous study [*Fry et al.*, 2015]. The typical accuracy of alkalinity measurements is 3 µmol kg^{-1} [*Dickson et al.*, 2003], and 3.02 µmol kg^{-1} for Alk* [*Fry et al.*, 2015]. Annual mean dissolved oxygen and nitrate gridded to 1° was obtained from the World Ocean Atlas 2013 [*Garcia et al.*, 2014a, 2014b]. Mixed layer depth data were obtained from the National Oceanic and Atmospheric Administration (NOAA) [*Monterey and Levitus*, 1997]. The mixed layer depth data were gridded to 0.5° for each month and mixed layer depth was defined using a variable potential density criterion corresponding to a change in temperature of 0.5 ºC [*Monterey and Levitus*, 1997]. The maximum mixed layer depth used was the largest of the monthly values for each gridpoint. The resulting maximum mixed layer depths occurred in the northern hemisphere winter, with February the most common month for the deepest mixed layer. The effect and strength of the ENSO was tested using a Multivariate ENSO Index from NOAA [http://www.esrl.noaa.gov/psd/enso/mei/]. The index is produced monthly and calculated using the current and previous month.

Unless otherwise stated, the areas analyzed are: 45ºN to 55ºN for phenomenon 1, 25ºN to 40ºN for phenomenon 2, and 15ºS to 10ºN for phenomenon 3. The chosen area for phenomenon 3 (equatorial region) is asymmetrical across the equator because the peak in nitrate occurs south of the equator in the Pacific Ocean [*Garcia et al.*, 2014b] as a result of geographic asymmetry [*Xie and Philander*, 1994].

4.5 Results and discussion

4.5.1 Alk* variations along approximately 50ºN in the north Pacific

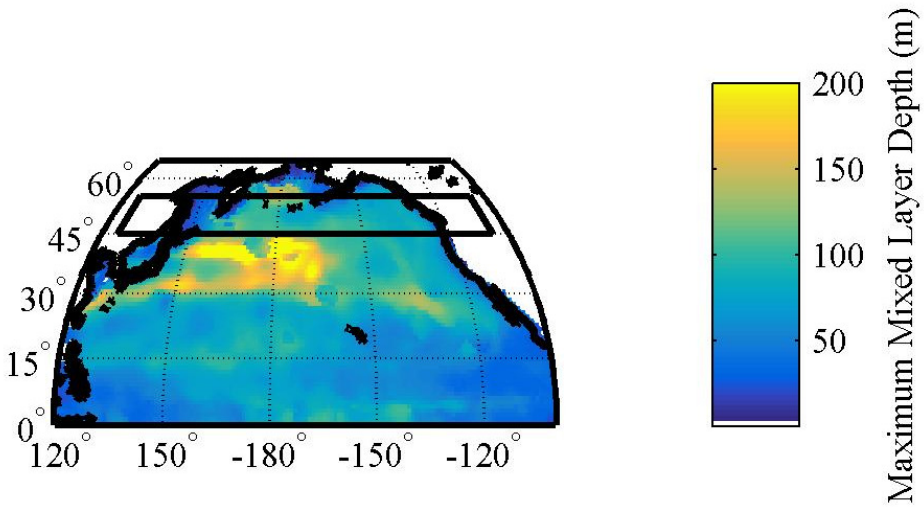

Figure 4-3. Maximum mixed layer depths in the North Pacific Ocean. The black box marks the area defined as phenomenon 1.

The maximum mixed layer depths at 40ºN are greater in the west than the east (Figure 4-3). However, the area of interest (the black box) is to the north of the region of the greatest maximum mixed layer depths. The relationship between maximum mixed layer depth and the surface Alk* is weak ($R^2 = 0.0578$, N = 3889) (Figure 4-4). Therefore, surface Alk* appears to be unrelated to the maximum mixed layer depth (refuting hypothesis 1.1).

Alk* appears to follow the lines of potential density, with denser waters containing higher Alk* occurring closer to the surface in the west than in the east (right side of Figure 4-5a compared to right side of Figure 4-5b). The depths of isopycnals and Alk* concentrations in the west and the east are presented in Table 4-2. These show that the mean depth of isopycnals is shallower in the west than the east of the North Pacific and this is matched by shallower mean depths of Alk* concentrations in the west than in the east. Further, the Pearson's r correlation coefficient between potential density and Alk* is 0.890 in the region of phenomenon 1 which shows there is a strong positive correlation. These observations confirm Hypothesis 1.2; Alk* in the surface ocean is affected by entrainment of waters from dense isopycnal layers.

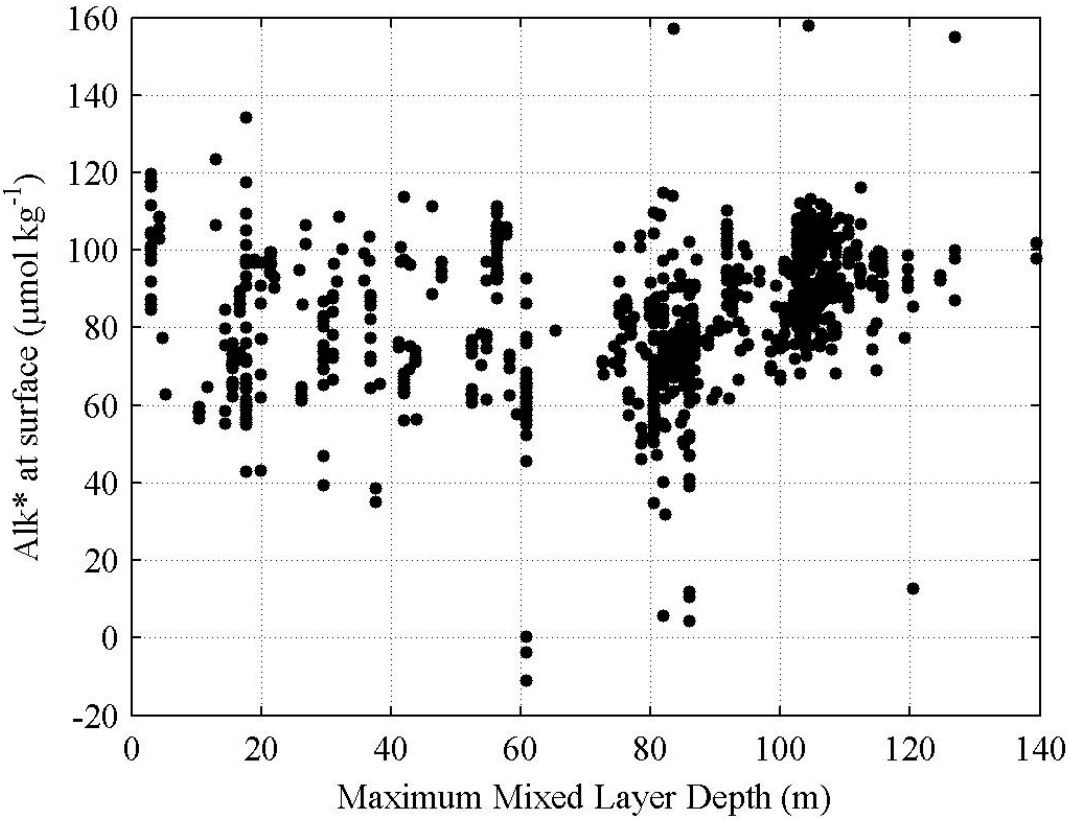

Figure 4-4. Alk* in surface waters of the North Pacific between 45ºN and 55ºN as a function of maximum mixed layer depth.

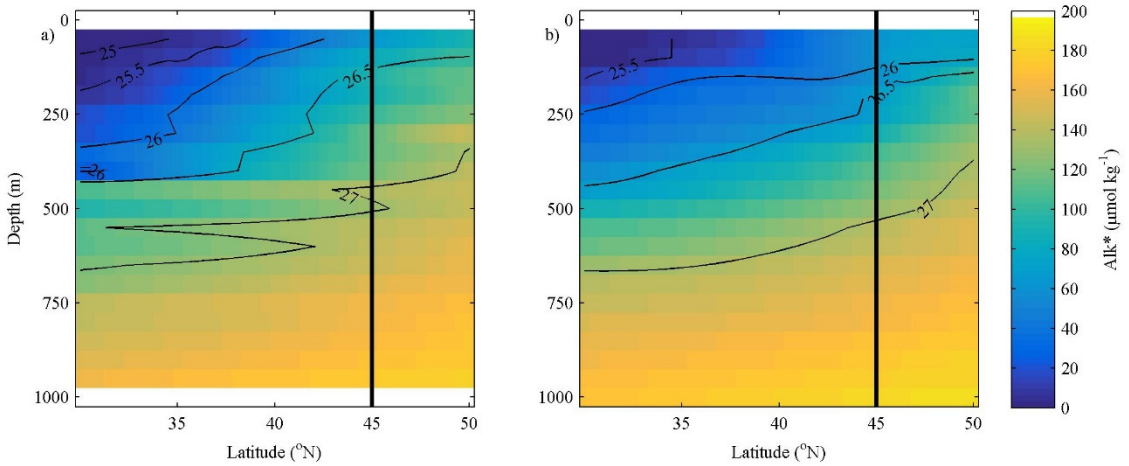

Figure 4-5. Meridional sections of Alk* (µmol kg^{-1}, color) and potential density (σ_θ, contours) at (a) 165ºE (WOCE cruise P13N in 1992) and (b) 135ºW (WOCE cruise P16N in 2006) obtained from GLODAPv2. The vertical black line represents the southern edge of the area of phenomenon 1.

Table 4-2. Mean depths (m) of different σ_θ and Alk* values[a] in the east compared with the west for the latitudinal region between 45ºN and 55ºN.

	Mean depth at which $\sigma_\theta = 26$	Mean depth at which $\sigma_\theta = 27$	Mean depth at which Alk* = 100	Mean depth at which Alk* = 150
West of 160ºW	28	328	46	399
East of 160ºW	101	412	172	528

[a]Data were interpolated using a smoothing spline where the smoothing parameter is p = 0.5.

Sulfate uptake affects alkalinity by changing the charge balance of seawater. This causes alkalinity to increase in order to counteract the change [*Wolf-Gladrow et al.*, 2007]. Sulfate reduction is an anaerobic process; therefore, if this process contributes to phenomenon 1 (Hypothesis 1.3), we would also expect lower dissolved oxygen concentrations in the western region of the North Pacific zonal band compared with the eastern region. However, anoxia is not prevalent in surface waters due to rapid exchange processes of oxygen with the atmosphere. Using the World Ocean Atlas, the dissolved oxygen concentrations in the surface waters in the west are higher (mean =7.1 ml L^{-1}, standard deviation = 0.4 ml L^{-1}) than in the east (mean = 6.5 ml L^{-1}, standard deviation = 0.6 ml L^{-1}). The east and west North Pacific between 45ºN and 55ºN have different oxygen concentrations at all depths (2-sample t-tests, $p < 0.001$). However, the difference at 100 m is opposite to what is required for Hypotheses 1.3 to be accepted (oxygen is higher in the west than the east). There is a band of low oxygen concentrations along the Aleutian Arc at about 200 m, a region where sulfate reduction in sediments has been observed [*Hein et al.*, 1979; *Elvert et al.*, 2000]. However, the Aleutian Arc is not where the highest Alk* is observed and the area seems to have decreased oxygen levels (<2 ml L^{-1}) only below 200 m.

The east-west Alk* gradient occurs in measurements from many cruises. The gradient is therefore unlikely to be an artefact caused by measurement error on any single cruise. However, all Japanese cruises in GLODAPv2 had a systematic adjustment applied to their alkalinity data of + 6 µmol kg^{-1}. This was done in order to make the deep water values of the Japanese cruises consistent with data from other countries at crossover stations. If this

adjustment was incorrect then it could have created the observed east-west trend, as the Japanese cruises took place mainly in the western North Pacific. To test this possibility, we subtracted 6 µmol kg^{-1} from all the Japanese alkalinity data, reversing the adjustment in GLODAPv2. This reduced the mean Alk* value in the west from 95.8 (Table 4-1) to 89.9 µmol kg^{-1} and the mean Alk* value in the east from 72.2 to 71.0 µmol kg^{-1}. Therefore a significant east-west gradient remained, showing that the adjustment in GLODAPv2 was not the cause of the east-west trend.

Our data suggest that the alkalinity variation in the surface waters of the North Pacific, between 45ºN and 55ºN, is caused by denser isopycnals with higher Alk* occurring at shallower depths on the western side than on the eastern side (Hypothesis 1.2). This east-west difference is likely driven by Ekman pumping which brings deeper water closer to the surface on the western side [*Talley*, 1985, 1988].

4.5.2 Alk* variations along about 30ºN in the North Pacific

Table 4-3. The criteria for delineation of surface waters.

Area	Salinity	Alkalinity (µmol kg^{-1})	Alk* (µmol kg^{-1})
Subpolar	32.5 ± 0.2	2184 ± 18	68 ± 17
Tropical	35.0 ± 0.3	2304 ± 23	9 ± 9
Upwelling	>33		>50
River	<32	<2170	

Between 25ºN and 40ºN, Alk* concentrations are higher in the eastern coastal region than in the open ocean (Figure 4-6). Along the coast at about 45ºN, the Alk* is elevated (approximately 80 µmol kg^{-1}) and the salinity and alkalinity are low (about 32 and 2180 µmol kg^{-1}, respectively), suggesting that this enhanced Alk* is caused by unaccounted for riverine inputs. But in the area of interest along the coast (25-40ºN), the salinity and alkalinity are both higher than the average of all the data between 25-50ºN (33.5 versus a mean of 32.7 and 2244 µmol kg^{-1} versus a mean of 2216 µmol kg^{-1}) and the temperature is lower than offshore (14.3 ºC versus 17.9 ºC offshore). This indicates that the enhanced Alk* is caused by upwelling.

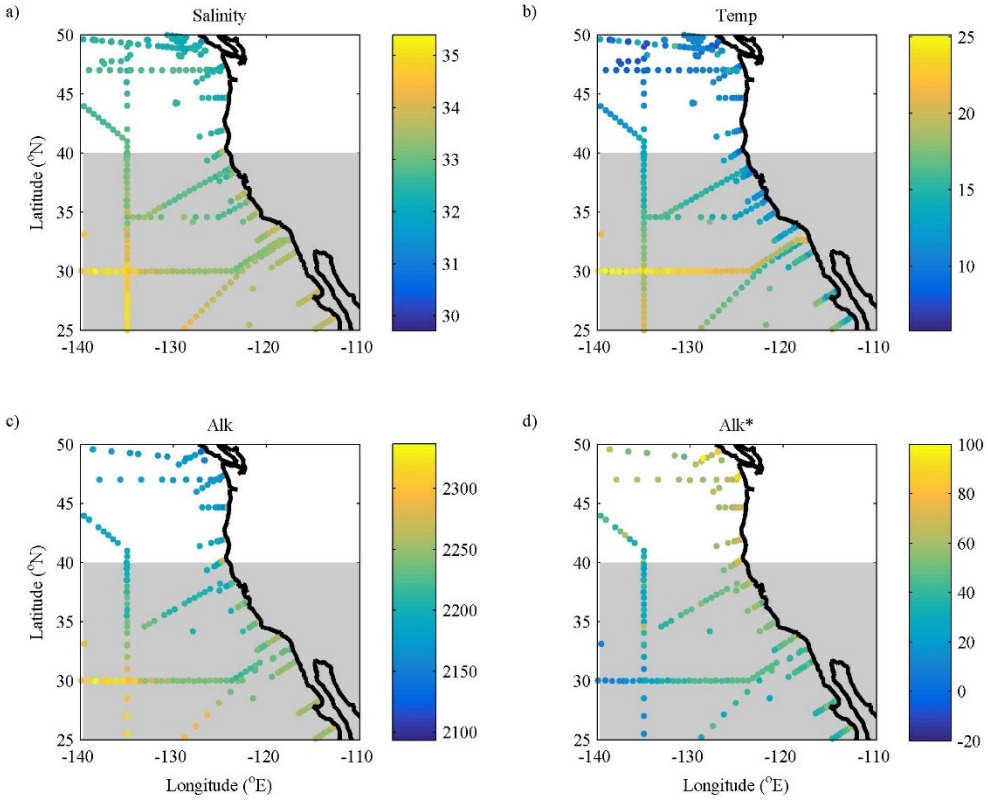

Figure 4-6. The distribution of (a) salinity, (b) temperature (ºC), (c) alkalinity (µmol kg^{-1}), and (d) Alk* (µmol kg^{-1}) in the surface waters of the North Pacific Ocean close to the North American continent. The grey shaded area represents the area of phenomenon 2.

We partitioned the eastern data into four groups to represent subpolar, tropical, upwelling, and river-influenced waters (Table 4-3 and Figure 4-7). The properties of offshore subpolar and tropical water were derived by using data within regional boxes and calculating the mean and standard deviations. These boxes were defined as: between 45ºN and 55ºN and 130ºW and 150ºW for the subpolar box; and between 15ºN and 25ºN and 120ºW and 150ºW for the tropical box. Water was flagged as subpolar or tropical influenced if its salinity, alkalinity, and Alk* were all within one standard deviation of the mean of the defined box.

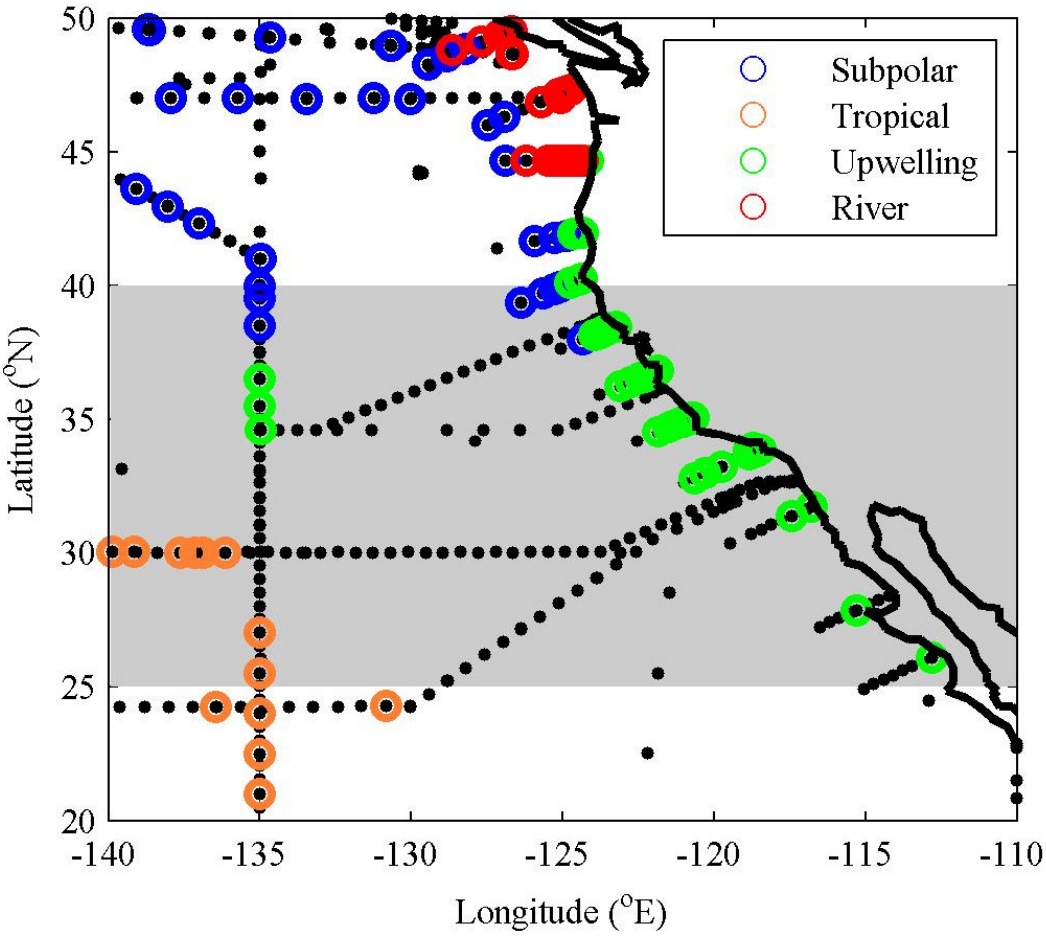

Figure 4-7. The distribution of data points determined by waters of different origin: subpolar, tropical, upwelling, and river. The grey shaded area represents the area of investigated for phenomenon 2.

Figure 4-7 shows that the groups are distributed in geographical clusters according to where each set of forcing factors had the strongest influence. For example, river-influenced points are situated in the coastal region. This provides evidence that all three factors enhance Alk* in different areas. Away from the coast, a small amount of mixing between subpolar water and tropical gyre waters takes place (Hypothesis 2.3). In the coastal region, upwelling increases Alk* in the south (25-42ºN) and river inputs increases Alk* in the north (42-50ºN) (Figure 4-7). However, the river-influenced waters are to the north of the area we have highlighted as anomalous, hence ruling out hypothesis 2.1 for the latitudinal region under investigation.

Phenomenon 2 is unlikely to be due to random error because it is derived from a large and coherent dataset from a range of cruises. The different surface waters identified in this dataset also agree with those reported by *Jiang et al.* [2014]: low temperature, high salinity water upwelling off the tropical coast and water from the Columbia and Fraser rivers (both

with alkalinities of about 1000 µmol kg^{-1} [*Park et al.*, 1969; *Dahm et al.*, 1981; *Mora*, 1983; *Amiotte Suchet et al.*, 2003]) influencing regions near the coastline further north. *Jiang et al.* [2014] also reported lower salinities (<32.5) in the California Current than in the open ocean (>32.5), which is in agreement with our definitions of subpolar and tropical waters (Table 4-3).

Figure 4-1 and Figure 4-2 show a few anomalously high Alk* values adjacent to the East China Sea at 30ºN (21 points with an Alk* greater than 100 µmol kg^{-1}), although the average is not much different from elsewhere, unlike towards the eastern side. Alk* in the East China Sea is likely to be influenced by the river alkalinity inputs from the Yangtze and Yellow rivers [*Chen*, 1996; *Tsunogai et al.*, 1997; *Kang et al.*, 2013] and sulfate reduction due to eutrophication [*Chen and Wang*, 1999; *Chen*, 2002; *Lin et al.*, 2002b; *Cai et al.*, 2011].

In conclusion, we find that Alk* is enhanced in the eastern North Pacific around 30ºN through upwelling of deeper waters with enhanced dissolved calcium carbonate concentrations (Alk* > 50 µmol kg^{-1}) (Hypothesis 2.2). Previous research indicated that the upwelling may be seasonal in spring and summer around 35ºN [*Huyer*, 1983; *Hauri et al.*, 2013] and is caused by Ekman transport from wind stress [*Huyer*, 1983] and is linked to the North Pacific Gyre Oscillation [*Di Lorenzo et al.*, 2008]. Studies project that strengthening of the North Pacific Gyre Oscillation, caused by climate change, will increase future wind stress [*Bond et al.*, 2003; *Douglass et al.*, 2006; *Cummins and Freeland*, 2007]. This implies that enhanced Alk* may occur in this region in the future due to increased upwelling.

4.5.3 Alk* variations in the Equatorial Pacific

In the equatorial Pacific, Alk* increases from the west to the east by 9.1 µmol kg^{-1} (Table 4-1). There is a significant difference in Alk* (greater than the uncertainty in Alk*: 3.02 µmol kg^{-1}) between El Niño (ENSO Index > 0.5) and La Niña years (ENSO index < 0.5) which is also observed in the nitrate and silicate concentrations (Table 4-4). However, there is only a weak correlation between ENSO index and Alk* ($R^2 = 0.12$, N = 810) while temperature (x) is a strong predictor ($R^2 = 0.63$, N = 810) of Alk* (y) (Equation 4-2). This strong correlation between Alk* and temperature indicates that sea surface temperature is a better indicator than the ENSO index for the upwelling strength in this region.

$$y = -2.76x + 81.95 \quad (4\text{-}2)$$

Variations in nutrients and Alk* concentrations can be observed in a meridional section across the known area of upwelling (Figure 4-8). The absence of a meridional increase in Alk* (decrease of 10% in the grey area in Figure 4-8 compared with outside the grey area (20-15ºS & 10-20ºN)) despite a significant increase in nitrate (increase of 490%) in the equatorial region supports Hypothesis 3.2; that the upwelling is not usually from sufficient depth to supply significant Alk*. There is also little increase in silicate concentration (<1%) which indicates that the upwelled waters are derived from depths where remineralization of organic matter has supplied nitrate, but the depths are not sufficient to provide enhanced Alk* (derived from sinking calcium carbonate) and silicate (derived from sinking opal). These results can be compared to those in Table 4-4. The surface concentrations of silicate and Alk* are typically low and similar to those outside the area of upwelling. However, strong upwelling during negative ENSO phases supplies waters from greater depths, increasing surface silicate and Alk*.

Table 4-4. t-test results for effect of El Niño/La Niña status on properties of surface waters of the eastern Equatorial Pacific[a]

Variable	Mean value during El Niño years [b] ($\mu mol\ kg^{-1}$)	Mean value during La Niña years [c] ($\mu mol\ kg^{-1}$)	Percentage increase (%)	Number of El Niño data points	Number of La Niña data points	p [d]
Alk*	10	17	+ 60	880	334	< 0.001
Nitrate	3.4	4.9	+ 40	2196	1185	< 0.001
Silicate	1.5	3.2	+ 113	2037	1099	< 0.001

[a]Two sample, two-tailed, t-test, in the East Equatorial Pacific (east of 160ºW), (15ºS < Latitude < 10ºN). [b]ENSO Index is greater than 0.5. [c]ENSO Index is less than -0.5. [d]The null hypothesis is that the mean Alk* or nutrient values from both time periods are equal; it is rejected for all 3 variables.

This finding is different to that for the eastern North Pacific margin around 30ºN where upwelling has a stronger effect on Alk* than in the eastern Equatorial Pacific. This is because the upwelled waters are older in the eastern North Pacific margin around 30ºN. *Feely et al.* [2008] reported that the upwelled waters are derived from the potential density layer of 26.2 – 26.6, which has a depth of about 175 m offshore. Water at this depth has

high nitrate and silicate concentrations, unlike at the equator (Figure 4-8 and [*Garcia et al.*, 2014b]).

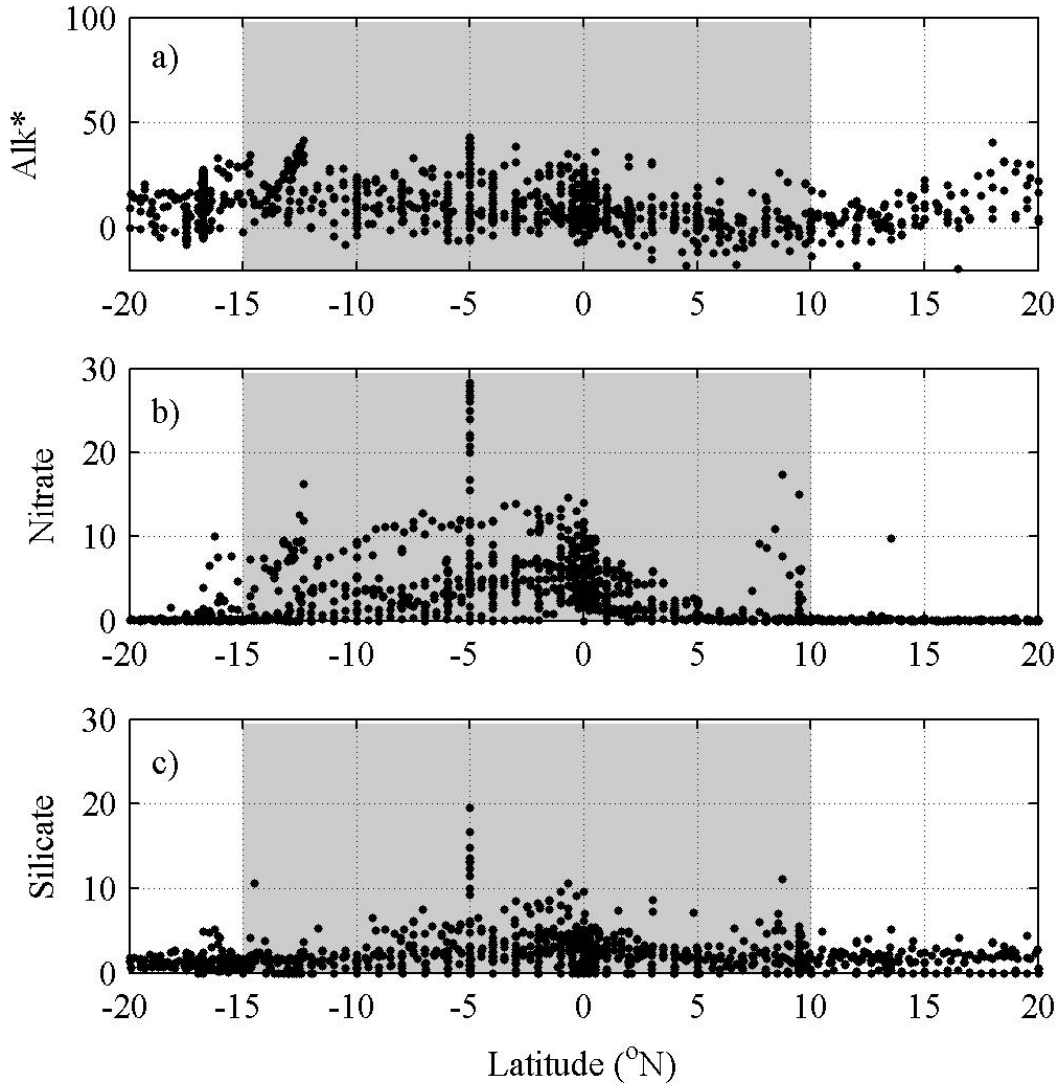

Figure 4-8. Surface (a) Alk* (µmol kg^{-1}), (b) nitrate (µmol kg^{-1}), and (c) silicate (µmol kg^{-1}) in the eastern (east of 160ºW) equatorial Pacific Ocean, plotted versus latitude. The grey bar indicates the area of Phenomenon 3. Values at ~5ºS correspond to values from a short cruise into the center of the intense Chile-Peru upwelling (Figure 4-1).

In contrast to reports of a short turnover time (<10 days) for calcite in the surface ocean [*Balch and Kilpatrick*, 1996], there is little increase in Alk* in the surface compared with nitrate concentration (Figures 4-8 and 4-9), hence ruling against Hypothesis 3.3. It is unlikely that waters high in both nitrate and Alk* are upwelled and then calcification and export rapidly remove the Alk* before the nitrate.

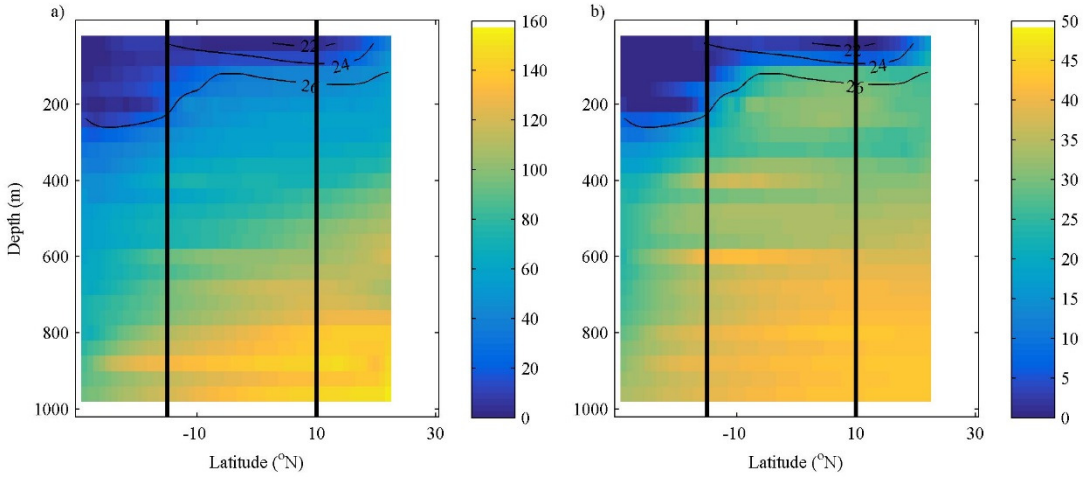

Figure 4-9. Meridional sections of (a) Alk* (µmol kg^{-1}), and (b) nitrate concentration (µmol kg^{-1}) across the equator on WOCE cruise P18 in 1994 (along approximately 105ºW). Potential density (σ_θ) contours are added. The black lines show the limits to the area of Phenomenon 3.

An increase in nitrate is apparent at around 200 m depth in the meridional section (Figure 4-9), whereas Alk* increases more gradually with depth. It is therefore likely that waters are usually upwelled with enhanced nitrate concentrations but low Alk*.

In conclusion, the evidence indicates that the cause for the small average increase in Alk* from west to east (10 µmol kg^{-1}) is that the shallow depths from which waters are usually upwelled contain low concentrations of Alk* (Hypothesis 3.2). The significant difference between El Niño and La Niña conditions (Table 4-4) indicates that stronger upwelling during La Niña years brings up deeper water, resulting in increase surface Alk* (Hypothesis 3.1). These findings are similar to observations by *Ishii et al.* [2004] who observed no increase in normalized alkalinity from west to east, possibly because the years they sampled featured positive ENSO index values (lowest ENSO index = -0.21 but most months above 1).

4.5.4 Improved predictive algorithms

Our investigation shows that the enhanced Alk* in the Northwestern compared with the Northeastern subarctic Pacific at about 50ºN is associated with denser isopycnals (e.g. σ_θ = 27.0) reaching closer to the surface, which is probably caused by more intense Ekman pumping [*Talley*, 1985, 1988]. A predictive algorithm for surface alkalinity that identifies supply of deep waters should therefore improve predictive skill compared to an algorithm that does not identify recently entrained deep waters. To incorporate this mechanistic

understanding into predictive algorithms, we propose potential density (σ_θ), or some other measure of seawater density, as a predictor variable rather than temperature alone. Sub-surface potential density is likely to give more accurate results because physical processes acting on the surface (e.g. evaporation, precipitation, warming and cooling) can change the water density; however, the algorithm would be more difficult to apply if it depended on variables obtained at other depths.

Our analysis of 30ºN shows that upwelling of deep waters increases surface alkalinity and highlights the difficulty in predicting alkalinity in regions where multiple water bodies meet, such as offshore of California and Mexico, as shown by *Jiang et al.* [2014]. More complex algorithms should be used in order to accurately predict the alkalinity when studying this area. Previous attempts to characterize the carbonate system have been made in this region using temperature, oxygen, salinity, and potential temperature [*Juranek et al.*, 2009; *Alin et al.*, 2012]. However, these algorithms did not include surface waters because they are more difficult to predict.

Finally, in the equatorial Pacific we argued that the surface Alk* is affected only by the strength of upwelling as this determines the depth from which the upwelled water is derived. Because nitrate and silicate are also affected by the strength of the upwelling (as indicated by the ENSO index; e.g. see Table 4-4) it is possible to parameterize the variations in Alk* using more commonly measured nutrient concentrations.

Using the GLODAPv2 database, we created two algorithms using predictive equations; one algorithm of three equations covers the entire Pacific Ocean between 30ºS and 65ºN, and another separate algorithm, also of three equations, covers the region between 25ºN and 50ºN and 140ºW and 110ºW (Table 4-5).

We divided each algorithm into regions with different equations. For the basin-wide Pacific Ocean algorithm, we first split the basin into above or below 10ºN. We then optimized the way to divide each area into two regions by sequentially splitting all the data by temperature for every degree from 0ºC to 30ºC and calculating the Pearson's r correlation coefficient (r) of a simple multiple linear regression (using nitrate, phosphate, silicate, salinity, potential density, and temperature) for each temperature. In the eastern North Pacific margin, we separated the areas into river influenced (salinity < 32), upwelling influenced (salinity > 33 and temperature < 20ºC), and open ocean (remaining data) as identified in section 4.2.

We transformed the nitrate, phosphate, and silicate concentrations to a normal distribution by taking natural logarithms. We transformed the other predictor variables by subtracting the mean values from salinity, potential density, and temperature (34.02, 23.4, and 21.20ºC respectively for the Pacific Ocean algorithm or 32.76, 24.6, and 12.80ºC respectively for the eastern margin). All subsequent analysis was performed on the transformed variables.

In the entire region (north of 30ºS), we tested for collinearity between the predictor variables by calculating the Variance Inflation Factor (VIF). A lower VIF signifies less collinearity between the tested variable and the other predictor variables and we deemed values lower than 4 to be acceptable. The collinearity of variables was high so we removed temperature and phosphate. The final VIFs were 3.24 for nitrate, 2.47 for surface potential density, 1.46 for salinity, and 3.55 for silicate. We then correlated the combinations of predictor variables with longitude in the subpolar North Pacific (north of 40ºN) and chose to include potential density squared as it had the most significant (furthest from zero) correlation with longitude in this region ($r = -0.362$). This value supports our conclusions in section 4.1 that the variation in Alk* is influenced by denser, deeper water containing dissolved calcium carbonate products. When using the predictor variables of nitrate, salinity, surface potential density, potential density squared, and silicate all the coefficients are significant with a probability value smaller than 0.001 which reduces to less than $1x10^{-10}$ when silicate is removed due to the covariance between nitrate and silicate. These probabilities indicate that all the predictor variables help to constrain alkalinity; however, there is moderate covariance between nitrate and silicate. Table 4-6 summarizes the input variables and their uncertainty.

Then in each region for each algorithm, we ran a 10-fold cross-validation using least squares multiple linear regression both with and without silicate. This was done to produce a robust fit of the predictor variables to alkalinity. For the 10-fold cross validation, we randomly split the data 10 times into two groups. Group 1 consisted of 90% of the data in the region, and this was used to produce the multiple linear regressions both including and excluding silicate. Group 2, containing 10% of the data in the region was used to test the accuracy of the equations which we measured using the root mean square deviation (rms) and the r coefficient. The inclusion of silicate did not improve the fit of the multiple linear regression, so we used the equation without it. We also increased the MLR coefficient of salinity in the northern low temperature region to reduce the bias with longitude. This increased the rms; however, it also increase the r in the region. The final statistical results

were then compared with previously reported algorithms by *Millero et al.* [1998b], *Lee et al.* [2006], and *Sasse et al.* [2013] using the GLODAPv2 database (Table 4-5).

Table 4-5. Predictions of surface water alkalinity in the North Pacific.

Algorithm	Equations[a]	Measure of Algorithm Predictive Capability[b]		
		n	rms	r
Pacific Ocean[c]		4541	14.1	0.970
> 24 ºC	2246.4 + 0.20 N + 65.58 S + 2.31 σ_θ + 0.50 σ_θ^2	1513	7.2	0.989
≤ 24 ºC & > 10ºN	2281.6 + 1.93 N + 45.23 S – 11.98 σ_θ + 4.68 σ_θ^2	2623	16.9	0.910
≤ 24 ºC & ≤ 10ºN	2248.1 + 0.56 N + 67.11 S + 4.77 σ_θ – 1.42 σ_θ^2	405	8.4	0.973
Sasse et al. 2013	4 equations using salinity, temperature, oxygen, silicate, and phosphate[e]	4626	12.4	0.977
Lee et al. 2006	4 equations using salinity and temperature and longitude[e]	5773	14.2	0.969
Millero et al. 1998b	3 equations using salinity and temperature[f]	5977	25.0	0.928
Eastern margin[d]		477	7.03	0.991
< 32 Sal	2191.2 + 2.27 N + 43.69 S – 19.64 σ_θ – 1.55 σ_θ^2	58	8.55	0.936
> 33 Sal & < 20 ºC	2194.8 – 0.19 N + 59.19 S + 0.13 σ_θ + 3.77 σ_θ^2	361	6.17	0.946

Other data	2191.6 + 2.42 N + 44.22 S – 22.32 σ_θ – 2.99 σ_θ^2	58	8.92	0.910
Sasse et al. 2013	2 equations using salinity, temperature, oxygen, silicate, and phosphate[e]	745	13.0	0.953
Lee et al. 2006	2 equations using salinity and temperature and longitude[e]	770	22.1	0.945
Millero et al. 1998b	2 equations using salinity and temperature[f]	831	27.1	0.912

[a] in which S is salinity minus the mean (34.14 for the North Pacific and 32.76 for the eastern margin), N is the natural logarithm of the nitrate concentration, and σ_θ is surface potential density minus the mean (23.2 or 24.6 for the North Pacific or eastern margin respectively). [b]n is the number of data points, rms is the root mean square error, and *r* is the Pearson's product moment correlation coefficient. [c]from 30ºS to 65ºN and < 30 m depth. [d]from 25 to 50ºN and 140 to 110ºW and < 30 m depth. [e]equations for the North Pacific, the (Sub)tropics, and the equatorial Pacific, and Southern Ocean depending on latitude, longitude, and temperature. [f]equations for the North Pacific, the gyres, and the equatorial Pacific depending on latitude, longitude, and temperature.

Table 4-6. Variables and their uncertainty used in our predictive algorithm obtained from GLODAPv2.

Variable	Uncertainty
Nitrate	2% of measurement[a]
Salinity	0.005[a]
Potential Density	0.005[b]

[a]the minimum adjustment level of GLODAPv2 [*Olsen et al.,* 2016]. [b][*Jackett et al.,* 2006]

Our prediction for the Pacific Ocean accounts for more variability than the algorithms by *Lee et al.* [2006] and *Millero et al.* [1998b] but not more than the algorithm by *Sasse et al.* [2013]. For the entire Pacific, the r of our algorithm is 0.970 compared to 0.928, 0.969, and

0.977 for algorithms by *Millero et al.* [1998b], *Lee et al.* [2006], and *Sasse et al.* [2013] respectively, and the rms of our algorithm is 14.1 µmol kg^{-1} compared to 25.0, 14.2, and 12.4 µmol kg^{-1} for algorithms by *Millero et al.* [1998b], *Lee et al.* [2006], and *Sasse et al.* [2013] respectively.

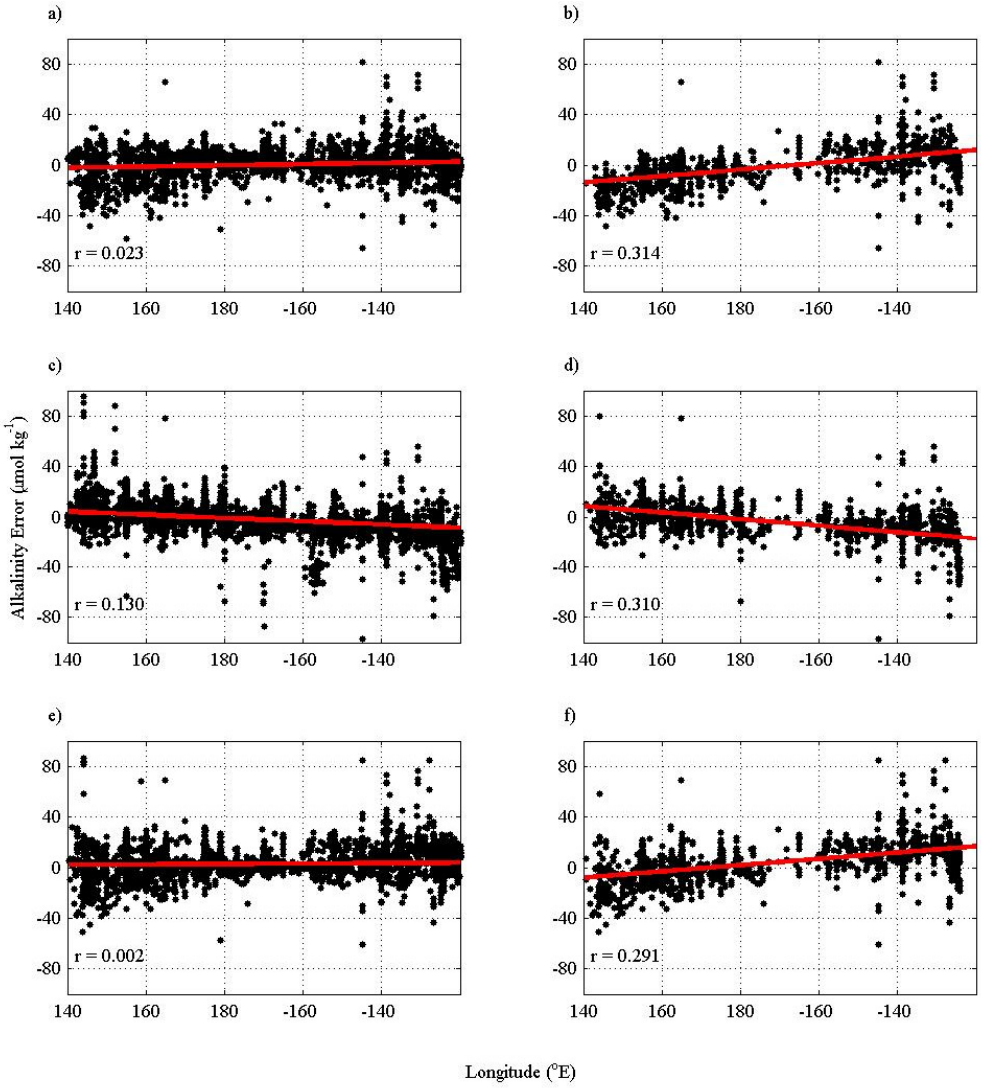

Figure 4-10. Predicted alkalinity minus measured alkalinity from the *Sasse et al.* [2013] algorithm in (a) the entire Pacific Ocean (north of 30ºS), and (b) the high latitude subarctic North Pacific (north 40ºN), the same areas (c) and (d) using the algorithm by *Lee et al.* [2006], and for the same areas (e) and (f) using our algorithm for the entire Pacific Ocean algorithm. The solid red lines are the best-fit straight lines.

The algorithm for the whole Pacific is also an improvement in terms of simplicity; it uses only three equations to cover the Pacific Ocean north of 30ºS, rather than the four

equations used by *Lee et al.* [2006] and *Sasse et al.* [2013]. The ability to make predictions of similar accuracy (first 2 significant figures of the r value are the same) as previous attempts, with fewer equations as used by *Lee et al.* [2006], and without using longitude as an artificial predictor, suggests that our algorithms correspond more closely to the underlying mechanistic reality. Because our algorithm for the Pacific Ocean has fewer equations, it is also simpler and therefore easier to apply.

Residuals for our Pacific Ocean algorithm show no relationship with year ($R^2 = 0.020$, N = 860) or with ENSO index ($R^2 = 0.014$, N = 860) in equatorial waters, showing that it performs well in both El Niño and La Niña years. Our Pacific Ocean algorithm, without longitude as a predictor variable, is not biased (r = 0.002, N = 4541) with longitude for the whole area (Figure 4-10e). But, the same algorithm applied in the subpolar North Pacific is biased (r = 0.291, N = 1662) with longitude (Figure 4-10f). However, the r value (Alk* residual versus longitude) is less than that for both the algorithms by *Sasse et al.* [2013] and by *Lee et al.* [2006]. When using the *Lee et al.* [2006] algorithm, the residuals (Figure 4-10c and 26d) increase from east to west even in the subpolar North Pacific where longitude was used as an additional variable to reduce this bias.

Figure 4-11 shows the relationship between the residuals and longitude in the areas of each of the phenomena. The subpolar North Pacific (45 -55ºN) has the strongest bias (r = 0.635) with longitude despite the use of squared potential density and an increased salinity coefficient to specifically reduce bias in this region. This bias is still less than the bias of the *Sasse et al.* [2013] algorithm in the same region (r = 0.874). The resulting gradient in the residual from west-to-east is an increase 19 µmol kg^{-1} which is 4 µmol kg^{-1} less than the magnitude of the original gradient in alkalinity in the subpolar North Pacific. The increase from west-to-east is because our algorithm underpedicts in the high alkalinity north-west and overpredicts in the lower alkalinity north-east. The direction of our bias is similar to the bias from the algorithm by *Sasse et al.* [2013], but opposite to the algorithm by *Lee et al.* [2006] which underpredicts the low alkalinity in the west. We conclude that using in-situ parameters may limit the ability of a predictive algorithm to capture the east-west gradient in the subpolar North Pacific; therefore, model based approaches could improve the coverage of data in this region in the future. The regions of phenomenon 2 and 3 have little bias with longitude (r < 0.001 and 0.047 respectively) and the gradient in residuals at 30ºN is a decrease from west-to-east of 2 µmol kg^{-1} (from 7.1 µmol kg^{-1} to 5.3µmol kg^{-1}) and the residuals along the equator increase by 0.56 µmol kg^{-1} (from -0.6

µmol kg^{-1} to -0.04 µmol kg^{-1}). These statistics show little bias and therefore our entire Pacific Ocean algorithm models the natural variation in these regions.

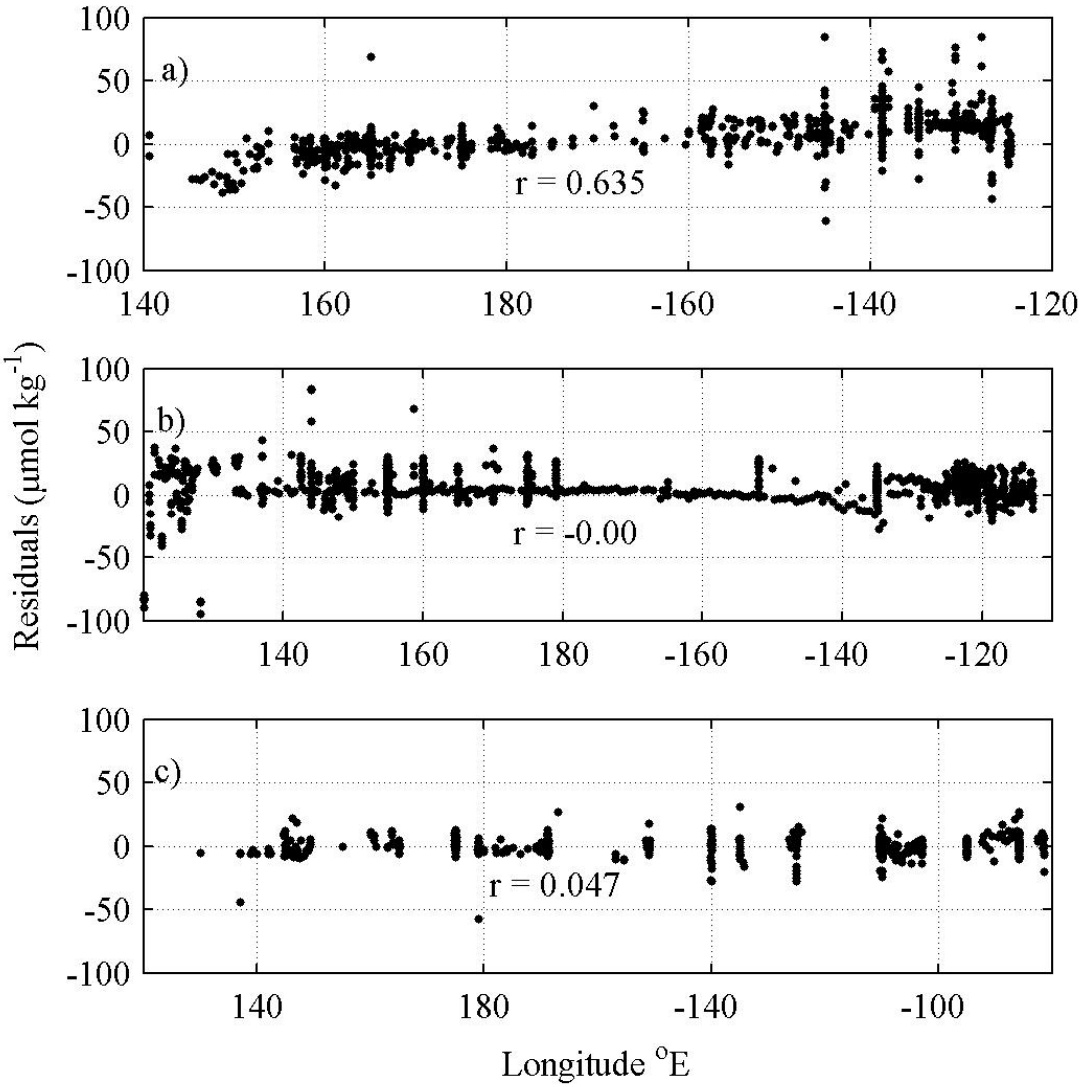

Figure 4-11. Residual alkalinity (predicted alkalinity minus measured alkalinity) using the Pacific Ocean algorithm in (a) the region of phenomenon 1 (45 - 55ºN), (b) the region of phenomenon 2 (25 - 40ºN), and (c) the region of phenomenon 3 (15ºS - 10ºN).

For the eastern margin, our algorithm is more accurate than previous algorithms; the r increased from 0.912, 0.945, and 0.953 (for the algorithms by *Millero et al.* [1998b], *Lee et al.* [2006], and *Sasse et al.* [2013] respectively) to 0.991, and rms error decreased from 27.1, 22.1, and 13.0 µmol kg^{-1} to 7.03 µmol kg^{-1}. This is partly because our algorithm is designed specifically for the area whereas the others were not.

4.5.5 Possible future changes in alkalinity

An improved mechanistic understanding of carbonate chemistry in the North Pacific will be helpful for estimating future changes in alkalinity and calcium carbonate saturation state. There is evidence that climate change is causing winds to strengthen which may increase upwelling along the North American coast [*Bakun*, 1990; *Hauri et al.*, 2013; *Sydeman et al.*, 2014]. Upwelled waters in this area have enhanced Alk* from dissolution of calcium carbonate minerals at depth (Figure 4-6); therefore, future increases in wind strength could cause a local increase in Alk*. Changes in ocean circulation could also affect alkalinity concentrations in the equatorial Pacific; climate change may cause El Niño conditions to occur more frequently by strengthening of the equatorial thermocline [*Timmermann et al.*, 1999; *Yeh et al.*, 2009]. Because upwelling of alkalinity seems to occur only during La Niña events, if they occur less frequently in future then it is likely that less alkalinity will be upwelled in the equatorial Pacific.

4.6 Conclusions

Analysis of data from GLODAPv2 and other datasets allowed us to test a series of hypotheses on the causes of longitudinal variations in Alk* in the North Pacific. At 50ºN, the major cause of variation was found to be denser isopycnals (with higher Alk*) coming closer to the surface on the western side. At about 30ºN, the higher Alk* close to the eastern margin is caused predominantly by upwelling off the North American continent. But in the eastern equatorial Pacific, upwelling does not increase the surface Alk* to significantly higher than in the west. Alk* is, however, higher in the east during La Niña years, probably because stronger upwelling during these periods brings water to the surface from greater depths, depths at which Alk* is elevated.

We created two algorithms (entire Pacific Ocean, and eastern margin of the North Pacific) to predict alkalinity using salinity, nitrate, and potential density. The Pacific Ocean algorithm is of similar accuracy to the best previous algorithm by *Sasse et al.* [2013] (r value of 0.973 for our algorithm versus 0.970 for their algorithm). However, our algorithm is less biased with longitude in the subpolar North Pacific (north of 40ºN) with an r value of 0.291 between the residuals and longitude compared to 0.314 by *Sasse et al.'s* [2013] algorithm. Our algorithm for the eastern margin of the North Pacific is more accurate than previously published algorithms (r = 0.991 compared to 0.953 from *Sasse et al.* [2013]).

Chapter 5: Export of calcium carbonate in the Southern Ocean

M. Mazloff provided access to model data and assisted with the Gaussian-Markov objective mapping. T. Tyrrell and E.P. Achterberg provided feedback on the methods and the manuscript. The writing of the chapter and all analysis and production of figures was performed by C.H. Fry.

5.1 Abstract

There is evidence of substantial export of calcium carbonate in the Southern Ocean; however, we have limited understanding of the controlling processes and the spatial distribution because existing methods yield estimates with large uncertainties. We describe here a method for calculating export from a tracer of calcium carbonate cycling and then demonstrate its use with data from GLODAPv2 and modelled water velocities. The ability of this method to accurately quantify calcium carbonate export is limited by the lack of simultaneous measurements of Alk* and water velocity. However, we do produce an estimate of the geographical distribution and rate of export of calcium carbonate in the region between 75ºS and 30ºS. We find that the intensity of export peaks around the Subantarctic Front and Polar Front and decreases both southwards and northwards from this region. We estimate the summer and autumn export flux from the Southern Ocean to be approximately 0.31 Pg C yr^{-1} which constitutes between 17% and 77% of current estimates of global calcium carbonate export. The observed spatial distribution agrees well with satellite observations of a "Great Calcite Belt" of coccolithophores in the Southern Ocean.

5.2 Introduction

Calcium carbonate export is the rate at which calcium carbonate sinks out of the surface layer of the ocean. A more accurate estimate of calcium carbonate export is needed because current global estimates are only poorly constrained, lying within a large range of 0.4-1.8 Pg PIC yr^{-1} [*Berelson et al.*, 2007]. More accurate quantifications of calcium carbonate export will help towards a better understanding of the carbon cycle. Calcification affects the global carbon cycle by reducing the air-sea flux of carbon dioxide from the atmosphere [*Barker et al.*, 2003]; however, the export of calcium carbonate also influences

the export of organic carbon through ballasting particles to greater depths [*Armstrong et al.*, 2002; *Klaas and Archer*, 2002; *Berelson et al.*, 2007]. Greater research is also needed to predict future changes in the carbon cycle because ocean acidification may reduce the rates of calcification and export of calcium carbonate [*Caldeira and Wickett,* 2005; *Orr et al.*, 2005; *Doney et al.*, 2009]. Therefore, it is important to gain a better quantitative and mechanistic understanding of calcium carbonate cycling in order to better understand current controls on air-sea fluxes of carbon dioxide and in order to be better able to predict which parts of the ocean will be more severely impacted by ocean acidification.

Several methods have been used to quantify calcium carbonate export and calcification. Sediment traps collect sinking debris and produce a direct measurement of calcium carbonate export [*Honjo et al.*, 2000, 2008; *Schiebel*, 2002]. However, sediment traps often underestimate export due to preservation issues. For example, calcium carbonate can dissolve within traps situated below the carbonate compensation depth and zooplankton and detritivores can change the composition of the material in the buckets. Also, advection of water can cause a sediment trap not to reflect the surface ocean production of calcification [*Honjo et al.*, 2008]. Finally, the sediment trap measurements are taken at specific points in time and space; therefore, there can be errors when the measured values are extrapolated to represent large areas of the ocean [*Trull et al.*, 2001].

Calcium carbonate export can also be estimated from the alkalinity distribution. These studies generally use simplified modelled circulation and observed three-dimensional alkalinity fields. Several studies have used an alkalinity tracer with water mass age estimates from chlorofluorocarbons (CFCs) and carbon-14 to estimate the rate of dissolution of calcium carbonate [*Milliman et al.*, 1999; *Feely et al.*, 2002a, 2004; *Chung*, 2003]. However, their use of apparent oxygen utilization and water age tracers means the method is only applicable to calculating calcium carbonate dissolution at depth and, therefore, does not show directly where the export takes place. Using a method that only works below the surface layer also means that their estimates are susceptible to anaerobic increases in alkalinity from sediments [*Chen*, 2002]. *Lee* [2001] used the seasonal changes in estimated salinity-normalised alkalinity over the warming period (spring) of 1990 to calculate spring calcification. They then extrapolated the estimated spring calcification, using sediment trap data, to estimate yearly calcification. Their method does not account for advection (potentially biasing results from within the Antarctic Circumpolar Current, the largest ocean current on Earth [*Orsi et al.*, 1995]) or seasonal changes in the water

mass; however, it does produce estimates of where the production and export of calcium carbonate takes place.

The export of calcium carbonate can also be inferred from measurements of calcification in the surface ocean [*Poulton et al.*, 2010, 2013; *Charalampopoulou et al.*, 2016]. The benefit of these is that they are direct measurements of the rate of carbon uptake to form new calcium carbonate and provide an upper limit for the export of calcium carbonate (the calcium carbonate must be produced before it can be exported). However, the measurements are few and far between and are still subject to the same errors as sediment traps when extrapolating sparse measurements to represent large areas of ocean.

Algorithms using satellite data can also be used to predict calcification. For example, *Balch et al.* [2007] produced a multiple linear regression using sample depth, particulate inorganic carbon (PIC) concentration, chlorophyll, day length, and temperature. Satellites observe large swathes of the ocean surface and therefore produce regional estimates of calcification. However, satellite derived chlorophyll and PIC only represent the surface meter of the ocean (where nearly all of the light emitted from the ocean comes from) and they rely on light leaving the ocean being able to reach the satellite which requires cloud free conditions and more sunlight than is available during the high latitude winter [*Beaufort et al.*, 2008; *Freeman and Lovenduski*, 2015]. Finally, PIC satellite products reflect the distribution of bloom-forming coccolithophores rather than all calcifiers [*Cubillos et al.*, 2007; *Mohan et al.*, 2008; *Holligan et al.*, 2010] and the presence of other suspended particles in the water can interfere with the quality of the satellite product [*Broerse et al.*, 2003; *Tyrrell and Merico*, 2004; *Balch et al.*, 2005].

One area where calcium carbonate export is poorly constrained is in the Southern Ocean. Calcifiers were first recorded in the Southern Ocean in the early sixties. *McIntyre and Bé* [1967] found that *Emiliania huxleyi* dominated in Subantarctic waters, in places comprising almost 100% of the coccolithophore community by number. These authors also noted that the species was not found in waters colder than 2ºC (i.e. not south of about 65ºS). The first studies of calcium carbonate export used sediment traps. These records began in 1983, and found highest export in the Polar Frontal Zone and lowest export in sea-ice areas [*Wefer and Fischer*, 1991]. Later sediment trap studies showed high concentrations of calcifiers, mainly the coccolithophore *Emiliania huxleyi*, around the Subantarctic and Polar Fronts with decreasing concentrations south of the Polar Front [*Honjo et al.*, 2000, 2008; *Trull et al.*, 2001; *Schiebel*, 2002; *Salter et al.*, 2007]. With the development of satellite algorithms for estimating the distribution of standing stocks of

particulate inorganic carbon, the spatial extent of calcification could be calculated [*Balch et al.*, 2005, 2011]. The new satellite information showed a region of calcification in the Southern Ocean between 30ºS and 60ºS, which became known as the "Great Calcite Belt" [*Balch et al.*, 2011]. *Charalampopoulou et al.* [2016] were the first to measure and report in situ calcification rates in the Southern Ocean and their measured rates were between 0.04 and 2.4 g C m^{-2} yr^{-1}. Like the studies above, they observed higher calcification rates between the Subantarctic Front and the Polar Front in Drake Passage and decreasing calcification south of the Polar Front.

Increasing anthropogenic carbon dioxide may affect the export of calcium carbonate in the Southern Ocean. Studies have suggested a reduction in calcification in the Southern Ocean [*Moy et al.*, 2009; *Freeman and Lovenduski*, 2015] and that in the Southern Ocean aragonite-forming pteropods are subject to dissolution as a result of ocean acidification [*Orr et al.*, 2005; *Bednaršek et al.*, 2012]. The Southern Ocean plays a major role in the resupply of nutrients to the global surface ocean through convective processes [*Sarmiento et al.*, 2004]; therefore, changes in convection and the processes that influence the concentration of nutrients in the Southern Ocean could impact the biogeochemical rates elsewhere in the global ocean.

The aim of this paper is to introduce a method, using an in-situ alkalinity tracer, to quantify and map calcium carbonate export in the Southern Ocean. This approach yields rates and distributions of calcium carbonate export in the Southern Ocean, which, as with other methods are subject to uncertainties.

5.3 The Tracer-Velocity Method

The concentrations of silicic acid, nitrate, and phosphate are enhanced in the surface waters of the Southern Ocean and decrease equatorwards [*Sarmiento et al.*, 2004; *Sarmiento and Gruber*, 2006]. The decrease in silicic acid concentrations commences furthest south at around 60ºS. This is related to an enhanced silicic acid to nitrate uptake ratio by diatoms [*Sarmiento et al.*, 2004], possibly caused by iron limitation [*Hutchins and Bruland*, 1998; *Coale et al.*, 2004], and/or sinking of empty diatom frustules [*Assmy et al.*, 2013], or by a greater resupply of nitrate relative to silicic acid during winter mixing as silicic acid is exported to greater depths [*Holzer et al.*, 2014]. The decline in surface water nitrate and phosphate commences further north at about 45ºS. We have previously (Chapter 3) defined a new tracer of calcium carbonate cycling by removing the influence on alkalinity of

evaporation, precipitation, river input, and the production and dissolution of organic matter. This new tracer of calcium carbonate cycling (Alk*) also decreases at about 45ºS (Chapter 3) which suggests that the declines in nitrate, phosphate, and Alk* could all be due to biological production and associated calcification.

In the Southern Ocean, the gradient in Alk* with latitude could be used to calculate calcification and the export of calcium carbonate. Here, we demonstrate how the rate of export could be calculated from a mapped product of the gradient in the tracer (Alk*) together with mapped products of the spatial variation in northwards and eastwards surface water velocity.

Because of the general shortage of data in the remote Southern Ocean, we apply this method on a coarse grid (2º latitude by 10º longitude). The mapped gradient in the carbonate cycle tracer (hereafter assumed to be Alk*) must be converted from values per degree to values per meter by dividing by the number of meters in either 2º latitude for the northwards difference (Δv) or 10º longitude for the eastwards difference (Δu) at the latitude of the grid cell (this calculation yields values with units of µmol kg^{-1} m^{-1}). The vector of the Alk* gradient is then produced by calculating the magnitude (A, µmol kg^{-1} m^{-1}) and angle of the gradient compared to due east (θ) by combing the two Alk* difference grids (Equations 5-1 and 5-2). The angle from east is calculated as positive for 180º anticlockwise and negative for 180º clockwise.

$$A = \sqrt{\Delta v^2 + \Delta u^2} \tag{5-1}$$

$$\theta = \tan^{-1}\left(\frac{\Delta v}{\Delta u}\right) \tag{5-2}$$

The vector of water velocity is produced from the gridded water velocity fields by calculating the magnitude (M, $m\ s^{-1}$) and angle of the velocity compared to due east (φ) by combing the two water velocity grids (V and U; Equations 5-3 and 5-4).

$$M = \sqrt{V^2 + U^2} \tag{5-3}$$

$$\varphi = \tan^{-1}\left(\frac{V}{U}\right) \tag{5-4}$$

Next the two vectors, for Alk* gradient and water velocity, are combined (Equation 5-5), to calculate the gradient in Alk* along the direction of water movement (ΔA, µmol kg^{-1} m^{-1}). This is then scaled by the magnitude of the water velocity (Equation 5-6; the faster the water is moving, the more intensely the biogeochemical process must be operating in order

to produce a given spatial rate of change) to calculate the temporal rate of change in Alk* within the moving water (*F,* µmol kg^{-1} s^{-1}).

$$\Delta A = A.\cos(\theta - \varphi) \quad (5\text{-}5)$$

$$F = M.\Delta A \quad (5\text{-}6)$$

An estimate of the reduction in Alk* concentration through mixing is calculated using Equations 5-7 and 5-8. The second derivative of the Alk* gradient of each cell is calculated by subtracting the value of the eastwards neighbor cell (*Δu(j+1)*, µmol kg^{-1} m^{-1}) in the matrix from the value of the westwards neighbor cell (*Δu(j-1)*, µmol kg^{-1} m^{-1}) for the eastwards direction and by subtracting the value of the northwards neighbor cell in the matrix (*Δv(j+1)*, µmol kg^{-1} m^{-1}) from the value of the southwards neighbor cell (*Δv(j-1)*, µmol kg^{-1} m^{-1}) for the northwards direction and assuming the effective diffusivity to be 1000 m^2 s^{-1}. The second derivative is then divided by the number of meters in two degree latitude (2*lt*, m) or ten degrees longitude (10*ln*, m) times the number of degrees in four degrees longitude (*4lt,* m) or twenty degrees longitude (*20ln*, m), which represents the distance between the two boxes used to calculate the difference.

$$Dv(j) = 1000(\Delta v(j-1) - \Delta v(j+1))/(2lt \times 4lt) \quad (5\text{-}7)$$

$$Du(j) = 1000(\Delta u(j-1) - \Delta u(j+1))/(10ln \times 20ln) \quad (5\text{-}8)$$

Next the total estimated contribution from mixing (*Du* + *Dv*, µmol kg^{-1} s^{-1}) is subtracted from the rate of decrease in Alk* (*F*) to calculate the rate of uptake of Alk* by calcification (µmol kg^{-1} s^{-1}). This is halved to find the rate of uptake of carbon into newly-formed calcium carbonate (µmol C kg^{-1} s^{-1}), as the formation of one mole of calcium carbonate requires removal from seawater of two moles of alkalinity. The resulting value is then multiplied by 1025 kg m^{-3} (seawater density) and divided by 10^6 (µmol mol^{-1}) to produce a flux for each grid box in units of mol C m^{-3} s^{-1}. The resulting flux is multiplied by the relative atomic mass of carbon (12 g mol^{-1}) and the number of seconds in summer and autumn to produce a number in units of g m^{-3} yr^{-1}. Finally, the flux is multiplied by the mixed layer depth (MLD) grid (m) to find the flux per unit area (g C m^{-2} yr^{-1}). To produce the total summer and autumn flux, the grid is multiplied by the area of each grid box in meters squared and summed to produce the total amount of carbon exported every year (g C yr^{-1}).

5.4 Application of the Tracer-Velocity Method

To demonstrate the application of the tracer-velocity method, we used GLODAPv2 data to calculate Alk* values and combined it with modelled surface water velocities [*Mazloff et al.*, 2010].

5.4.1 Data sources

Alkalinity and other variables were obtained from the GLODAPv2 database [*Olsen et al.*, 2016]. We used only data from summer and autumn (1st November to 30th April), and the spatial distribution of that data is shown in Figure 5-1. Alk* was calculated from GLODAPv2 using Equation 5-9 (below) with no correction for river alkalinity inputs because almost no rivers flow into the Southern Ocean, and no river-influenced areas have been identified in this ocean region (Chapter 3). The accuracy of observed alkalinity is 3 µmol kg^{-1} [*Dickson et al.*, 2003], leading to a similar propagated error (3.02 µmol kg^{-1}) for Alk* (Chapter 3).

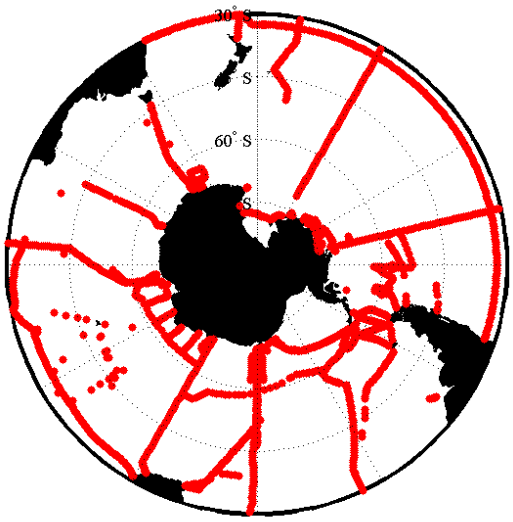

Figure 5-1. Distribution of surface Alk* data between 1st November and 30th April from 2005 to 2010 in the Southern Ocean using GLODAPv2.

Summer and autumn water velocity (m s^{-1}) and mixed layer depth (m) values for locations across the Southern Ocean were obtained from the output of the Southern Ocean State Estimate (SOSE) model [*Mazloff et al.*, 2010]. SOSE uses the adjoint method to bring the model into agreement with multiple oceanographic and satellite observational datasets of salinity, temperature, and sea surface height. The model is high resolution (1/6º by 1/6º) with 42 depth levels and covers the ocean south of 24.7ºS. Data is currently available from 2005 to 2010 (http://sose.ucsd.edu/sose_stateestimation_data_05to10.html).

The mean positions of the Polar Front, the Subantarctic Front, and the Subtropical Front in the Southern Ocean were obtained from the Australian Antarctic Data Centre [*Orsi et al.*, 1995; *Orsi and Harris*, 2015].

Calcification rates from satellite observations were estimated following the equation by *Balch et al.* [2007], which requires information on particulate inorganic carbon (PIC) and chlorophyll concentrations, and sea surface temperature. These values were all obtained from MODIS (satellite) datasets, using monthly climatologies at 9 km resolution, downloaded from http://oceancolor.gsfc.nasa.gov.

5.4.2 Calcification rates from GLODAPv2 data and SOSE model output

We used Alk* (Equation 5-9) as a tracer for calcification, dissolution of calcium carbonate, and the movement of calcium carbonate dissolution products via physical circulation (Chapter 3). Alk* removes of other common causes of alkalinity variation: evaporation and precipitation, river inputs, and biological uptake and release of ions.

$$Alk^* = \frac{Alk_m + 1.36Nit - Alk_r}{Sal} * 35 - 2300 + Alk_r \quad (5\text{-}9)$$

where Alk_m is measured alkalinity (µmol kg^{-1}), *Nit* is nitrate concentration (µmol kg^{-1}), Alk_r is identified river alkalinity (µmol kg^{-1}) which is 0 for the Southern Ocean, and *Sal* is salinity.

The velocity and mixed layer depth data were subsampled for the dates of the Alk* samples. As a result, each Alk* value is matched with a corresponding eastwards velocity, northwards velocity, and mixed layer depth measurement from the date and grid point of the measurement. The Alk* values, eastwards velocity, northwards velocity, and mixed layer depth values were then gridded and interpolated using Gaussian-Markov objective mapping to 2º latitude and 10º longitude. Alk* was gridded twice. Firstly, it was gridded from 76ºS to 28ºS and 180ºW to 180ºE and secondly, from 75ºS to 29ºS and from 185ºW

to 185ºE. These were used to calculate the northwards and eastwards gradients in Alk* respectively. Parameters used for Alk* were noise variance = 7 (μmol kg^{-1})^2, signal variance =15 (μmol kg^{-1})^2, 10 (μmol kg^{-1})^2, 6 (μmol kg^{-1})^2 for respective Gaussian correlation length scales of 200 km, 1000 km, 6,000 km in latitude and 1000 km, 5000 km, 30,000 km in longitude. The parameters used for eastwards velocity were noise variance = 0.018 (m s^{-1})^2, signal variance = 0.03, 0.2, 0.01 (m s^{-1})^2 for the above Gaussian correlation length scales. The parameters used for northwards velocity were noise variance = 0.005 (m s^{-1})^2, signal variance = 0.01, 0.008, 0.001 (m s^{-1})^2 and the parameters used for mixed layer depth were noise variance = 1 (m)^2, signal variance = 0.6, 0.8, 1.2 (m)^2 for the above Gaussian correlation length scales. The total signal to noise for Alk* is 31/7 = 4.43, whilst it is 3.3, 3.8, and 2.6 for eastwards velocity, northwards velocity, and mixed layer depth respectively.

The northwards and eastwards gradients in Alk* were then calculated using the differences between two adjacent boxes; either the southwards minus northwards for the northwards gradients (μmol kg^{-1} 2º latitude^{-1}) or westwards minus eastwards for the eastwards gradients (μmol kg^{-1} 10º longitude^{-1}). The resulting gridding for both Alk* gradient matrices was to 2º latitude and 10º longitude from 75ºS to 29ºS, with the center of the first grid square being at 74ºS and 175ºW.

5.4.3 Silicification rates from GLODAPv2.

The export of silicon was calculated in the same way as the export of calcium carbonate, but using silicic acid instead of Alk* and using the relevant stoichiometry; the flux was not halved and the number of moles was multiplied instead by the atomic mass of silicon (28 g mol^{-1}).

5.4.4 Calcification rates from MODIS data.

We compared the tracer-velocity method results to satellite estimates of calcification. To produce the satellite predictions of the calcification rate we used the equation by *Balch et al.* [2007]. In the equation we used sea surface temperature from both day and night, a depth of 1 m, and a day length for the 15th day of each month depending on latitude [*Freeman and Lovenduski*, 2015]. The calcification rates for each month in the year were averaged to produce the average annual rate, and then multiplied by duration in order to obtain an estimate of the total annual calcium carbonate export.

5.4.5 Statistical testing of differences between areas

A simpler method was also used, in order to compare against those from the tracer-velocity method and to check the robustness of the main findings of this analysis. Rates of decrease of Alk* and silicic acid were calculated north, south, and in the vicinity of the Polar Front. Data from 23 cruises that crossed the Polar Front were used to calculate the mean change per latitude for >3º north of, within 3º latitude of, and >3º south of the Polar Front for each cruise. No account was taken of velocities or direction of flow in this comparison. We used paired t-tests to calculate whether there was a significant difference between (a) Alk* and silicic acid gradients south of the Polar Front versus those around the Polar Front, (b) around the Polar Front versus north of the Polar Front, and (c) south of the Polar Front versus north of the Polar Front.

5.5 Results and Discussion

5.5.1 Results of application using GLODAPv2 and SOSE

The Alk* gradient was combined with modeled Southern Ocean circulation [*Mazloff et al.*, 2010]. The distribution of the data used to test the tracer-velocity method is shown in Figure 5-2. Figure 5-3 shows the results of applying the different steps in the calculation of export.

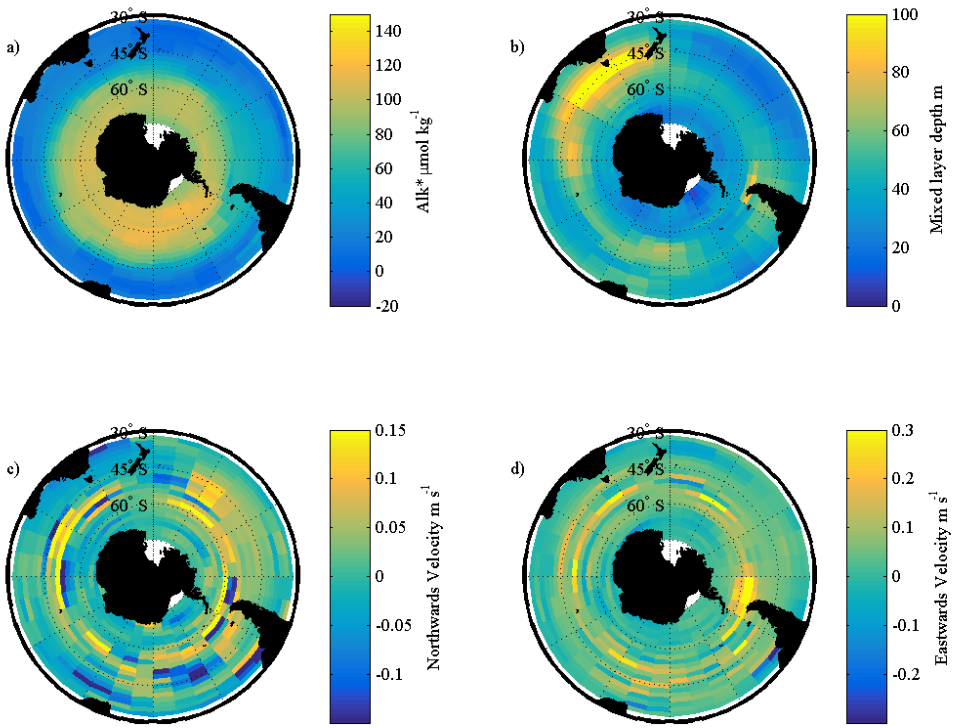

Figure 5-2. Distribution of several properties in the Southern Ocean (November to April): (a) Alk*, (b) mixed layer depth, (c) northwards velocity component, and (d) the eastwards velocity component (note different color scale compared to (c)). All properties are gridded to 10º longitude and 2º latitude.

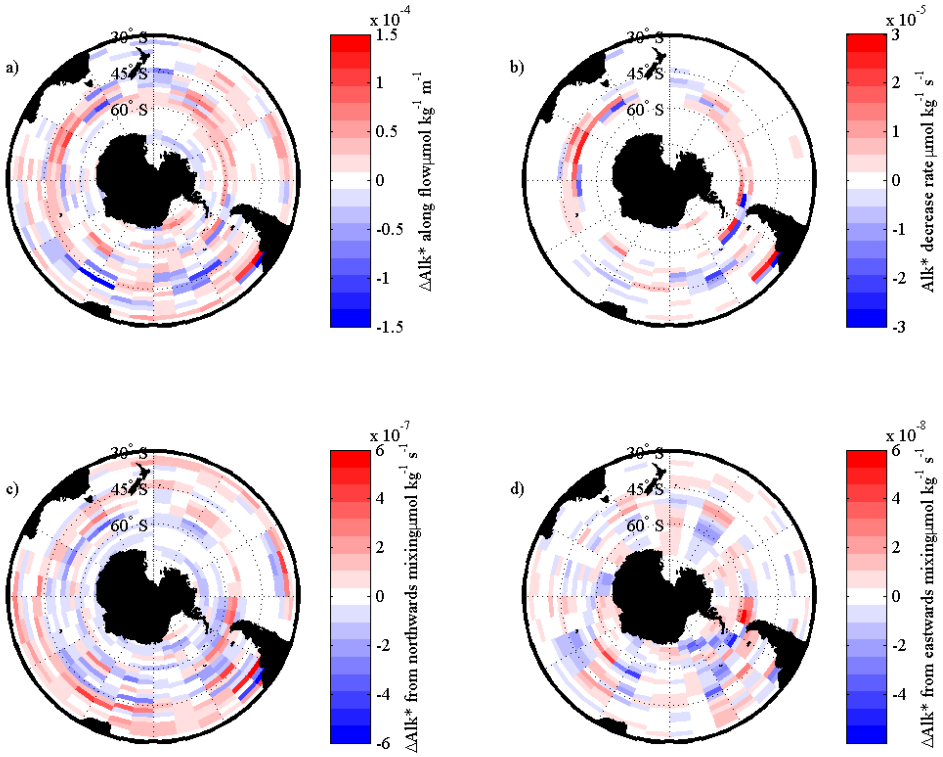

Figure 5-3. Intermediate stages in the calculation of export: (a) spatial rate of decrease of Alk* along the direction of water flow (µmol kg^{-1} m^{-1}), (b) temporal rate of Alk* decrease (µmol kg^{-1} s^{-1}), (c) temporal rate of Alk* decrease due to northwards mixing component (µmol kg^{-1} s^{-1}), (d) temporal rate of Alk* decrease due to eastwards mixing component (µmol kg^{-1} s^{-1}). Note that the color scale bar is different for each plot.

We used the decrease in Alk* together with the modeled circulation (Figure 5-2) [*Mazloff et al.*, 2010] to map export (Figure 5-4) and infer 0.31 Pg C yr^{-1} of export of calcium carbonate in the Southern Ocean (between 30ºS and 75ºS) in summer and autumn. The regions where the greatest export is calculated (and also the regions of greatest variation in calculated export) (Figure 5-4) are close to and between the Polar and Subantarctic Fronts. Export variation then decreases from the Subantarctic Front to the Subtropical Front. Export of calcium carbonate is also close to zero almost everywhere south of the Polar Front.

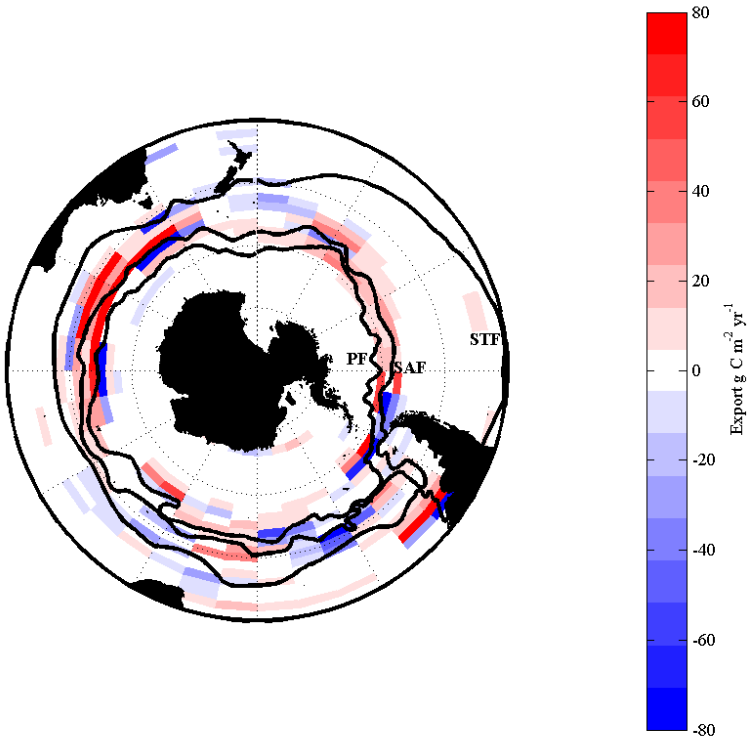

Figure 5-4. Calculated export of $CaCO_3$ (g C m^{-2} yr^{1}) in the Southern Ocean in summer and autumn as estimated from our tracer-velocity technique using GLODAPv2 and SOSE. PF is the Polar Front, SAF is the Subantarctic Front, and STF is the Subtropical Front.

Using a similar method with silicate rather than Alk* produces a biogenic silica export estimate of 0.45 Pg Si yr^{-1} (Figure 5-5). Comparing the geographical pattern of calcium carbonate export (Figure 5-4) to that of silica export shows that the export of silica takes place further south, with the latitude of the highest mean export being 58ºS for biogenic silica and 50ºS for calcium carbonate. There is also a greater proportion of export of biogenic silica than calcium carbonate south of the Polar Front. Silica export is reported to occur mainly south of the Polar Front [*Buesseler et al.*, 2001]. But our calculation of export in the Southern Ocean (0.45 Pg Si yr^{-1}) is lower than previous estimates of a total of 2 Pg Si yr^{-1} [*Fripiat et al.*, 2011], with mean export in the range of 28-252 g Si m^{-2} yr^{-1} [*Buesseler et al.*, 2001; *Jin et al.*, 2006; *Fripiat et al.*, 2011], whereas our mean export is 3.2 g Si m^{-2} yr^{-1} due to "negative export" of silica in some areas.

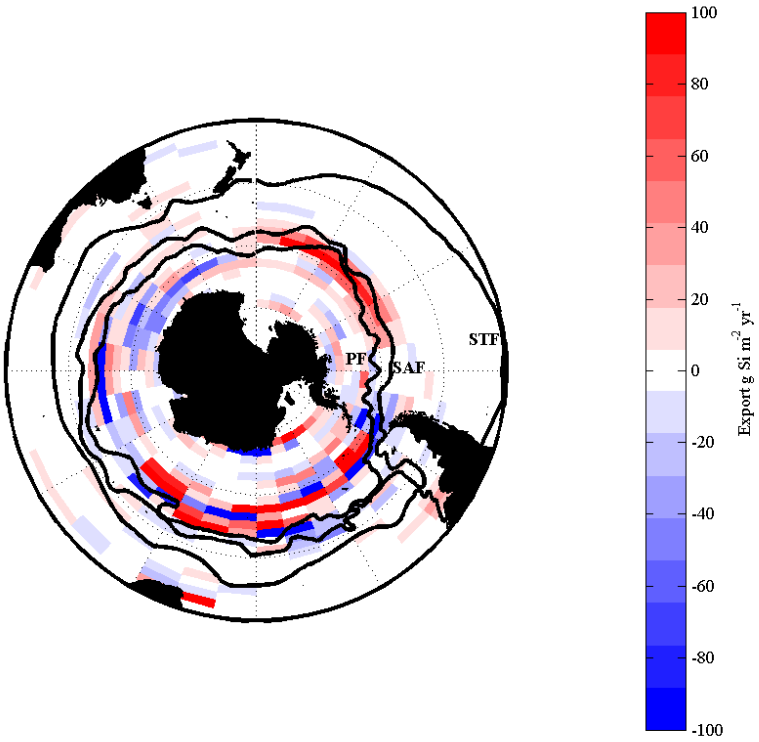

Figure 5-5. Export of biogenic silica (g Si m^{-2} yr^{-1}) in the Southern Ocean in summer and autumn as estimated from our technique using GLODAPv2 and SOSE. PF is the Polar Front, SAF is the Subantarctic Front, and STF is the Subtropical Front.

In north-south transects crossing the Polar Front, there is a significant difference (Table 5-1) between the rate of decrease in Alk* south of the front (mean decrease >3º south of the Polar Front = 0.5 µmol kg^{-1} ºlat^{-1}; σ = 1.8 µmol kg^{-1} ºlat^{-1}) and around the Polar Front (mean decrease within 3º latitude of the Polar Front = 3.0 µmol kg^{-1} ºlat^{-1}; σ = 4.5 µmol kg^{-1} ºlat^{-1}). There is also a significant difference between the rate of decrease in Alk* north of the front (mean decrease >3º north of the Polar Front = 4.2 µmol kg^{-1} ºlat^{-1}; σ = 3.8 µmol kg^{-1} ºlat^{-1}) and south of the front (Table 5-1); however, there is no significant difference between the decrease around the Polar Front and the decrease >3º north of the Polar Front. This suggests that the Polar Front is the boundary between the region of little calcium carbonate export (south of the Polar Front) and significant calcium carbonate export (close to the Polar Front and northwards). In the Pacific section of the Southern Ocean, the Subtropical Front is more than 15º latitude north of the Subantarctic Front and this area reveals that the rates of Alk* decrease and export of calcium carbonate are much greater near both the Polar and Subantarctic Fronts compared to lower rates between the

Subantarctic and Subtropical Fronts and near the Subtropical Front (Figure 5-4). This agrees with sediment trap studies that find the areas of highest calcium carbonate export around the Polar Front [*Wefer and Fischer*, 1991; *Honjo et al.*, 2000, 2008; *Salter et al.*, 2007]. The regions with a decrease in Alk* are also seen to be different from the regions with a decrease is silicic acid which decreases by 3.3 µmol kg^{-1} $°lat^{-1}$ (σ = 3.6 µmol kg^{-1} $°lat^{-1}$) in the region >3° south of the Polar Front, 3.0 µmol kg^{-1} $°lat^{-1}$ (σ = 4.5 µmol kg^{-1} $°lat^{-1}$) in the region within 3° latitude of the Polar Front, and 1.1 µmol kg^{-1} $°lat^{-1}$ (σ = 1.4 µmol kg^{-1} $°lat^{-1}$) in the region >3° north of the Polar Front. The only significant difference in the decreases in silicic acid is between >3° north of the Polar Front and >3° south of the Polar Front (Table 5-1). This suggests that the export of biogenic silica is greatest south of the Polar Front and is much lower north of the Polar Front, which supports our map of silica export generated using the tracer-velocity method (Figure 5-5) and previous reports of silica export [*Buesseler et al.*, 2001].

Table 5-1. P-values for 2 tailed, paired, t-tests between the rates of decrease in Alk* or silicic acid in different regions of the Southern Ocean (as calculated on 23 cruise transects, N=23). Significant differences are indicated by bold font.

Subsets to be compared		For Alk*	For silicic acid
Subset A	Subset B		
>3° south of the Polar Front	Within 3° of the Polar Front	**0.03**	0.76
>3° north of the Polar Front	Within 3° of the Polar Front	0.42	0.09
>3° south of the Polar Front	>3° north of the Polar Front	**<0.01**	**0.02**

5.5.2 Strengths and weaknesses of the tracer-velocity method

The advantage of combining surface gradients in a tracer of calcium carbonate cycling with modeled ocean circulation is that it provides an estimate of biogeochemical rates that factors in, rather than ignores, water motion. This allows the export of calcium carbonate to be mapped, highlighting area of low production and export and areas of high production

and export. This method also provides an independent method to calculate export that can be compared with estimates from other methods such as sediment traps.

The major issue with using the tracer-velocity method is that concurrent measurements of Alk* and water velocity are needed. For example, Figure 5-3a shows the change in Alk* along the direction in flow. There are large areas of blue highlighting an increase in Alk* along the direction of flow. Although upwelling events could potentially cause an increase in Alk*, it is unlikely to cause such a widespread effect. Instead, the effect is likely caused by the Alk* measurements and the ocean circulation not being truly concurrent despite using the ocean circulation modeled for the time Alk* was sampled. To improve this error, Alk* could be calculated from modeled alkalinity, nitrate, and salinity; however, not all models produce process-based alkalinity and this method could not then be used to test the accuracy of modeled calcification. A greater density of in-situ Alk* data values could help reduce this error. As will be discussed further in Chapter 6, Alk* could be predicted using nitrate and salinity measurements from Autonomous Underwater Vehicles [*Johnson and Coletti,* 2002].

Our estimation method may underestimate the extents of both biogenic silica and calcium carbonate export. Our approach may underestimate the extent export by overly smoothing gradients or by using a large scale grid and therefore not accounting for small scale variations in Alk* or silicic acid. This may cause our method to only show large scale export and miss small scale variations caused by small scale export.

Another source of error is from the variation in the timing of the in-situ sampling. For example, some Alk* values may come from late spring, before substantial calcification has taken place and at a time when the in-situ conditions are likely to strongly reflect entrainment of deep water into the surface layer during the immediately preceding winter, whereas other data may come from late summer after calcification. If the upstream value is from late summer and the downstream one from late spring then Alk* may appear to increase along the flow path, giving rise to a negative estimation of calcification.

To estimate the error caused by various assumptions, we calculated the total export with and without those assumptions (Table 5-2). The removal of the contribution of mixing to the Alk* decrease (*Du* and *Dv*) only changes the estimate of export by 0.005 Pg C yr^{-1}. To test the errors that MLD could contribute to total export, we calculated the total export by multiplying by a fixed depth of 48 m (mean MLD of all Alk* sampling points). This altered the total export by 0.024 Pg C yr^{-1}. A greater decrease is observed when using an

alternative tracer for the calcium carbonate cycle. *Carter et al.* [2014] produced a version of Alk* which is slightly different to that in Chapter 3. The lower estimate (by 0.094 Pg C yr^{-1}) using *Carter et al.* [2014]'s Alk* could be caused by the use of a different salinity correction method or by using 1.26 as the ratio between nitrate uptake and the effect on alkalinity [*Kanamori and Ikegami,* 1982]. We used instead a theoretically derived ratio of 1.36 [*Wolf-Gladrow et al.*, 2007], which tends to increase gradients in the Southern Ocean. A much wider range of total calcium carbonate export is observed if the input fields are varied, with estimates up to 0.18 Pg C yr^{-1} lower depending on the assumptions used. This is consistent with the biggest disadvantage of the method; the need for simultaneous measurements of Alk* and water velocity. The lowest export is calculated using a simplified linear interpolation to create the Alk*, MLD, and velocity fields. An estimate of export using all summer and autumn GLODAPv2 data and the mean summer and autumn velocity fields also produces a low value. Increasing the smoothing of the Gaussian-Markov objective mapping by increasing the noise until the signal to noise ratio = 2, also decreased the total calcium carbonate estimate by 0.045 Pg C yr^{-1}.

Table 5-2. Total summer and autumn calcium carbonate export using different methods and assumptions.

Method	$CaCO_3$ export (Pg C yr^{-1})
Total export of calcium carbonate	0.31
Without subtracting mixing	0.31
With constant MLD (48 m)	0.29
With *Carter et al.* [2014] Alk* algorithm	0.21
With linear interpolation	0.13
With smoothing (signal to noise = 2)	0.26
Using all GLODAPv2 and mean summer and autumn velocity fields	0.15

5.5.3 How does our distribution compare to other studies?

Sediment trap observations in the Southern Ocean produce export estimates that range from 0.096 to 230 g C m^{-2} yr^{-1} [*Wefer and Fischer*, 1991; *Honjo et al.*, 2000, 2008; *Trull et al.*, 2001; *Schiebel*, 2002; *Salter et al.*, 2007]. But the techniques to extrapolate from the sediment trap period to a yearly flux vary and therefore the error on this data is large. The highest export in this range is extrapolated from the summer south of the Subantarctic Front [*Salter et al.*, 2007] and the lowest is in a seasonally ice covered area [*Honjo et al.*, 2008]. The studies agree that the area of highest export is around the Subantarctic Front and the Polar Front [*Honjo et al.*, 2000, 2008; *Trull et al.*, 2001], which is consistent with our findings of the areas of greatest export. The mean export from the sediment trap data [*Wefer and Fischer*, 1991; *Honjo et al.*, 2000, 2008; *Trull et al.*, 2001; *Schiebel*, 2002; *Salter et al.*, 2007] is 24 g m^{-2} yr^{-1} which produces a total of 2.7 Pg C yr^{-1} over the Southern Ocean when multiplied over the area between 75ºS and 30ºS. The total and mean export are higher than ours (mean = 2.3 g C m^{-2} yr^{-1}, total = 0.31 Pg C yr^{-1}); however, our mean export is within the range of the sediment trap data (0.096 to 230 g m^{-2} yr^{-1} [*Wefer and Fischer*, 1991; *Honjo et al.*, 2000, 2008; *Trull et al.*, 2001; *Schiebel*, 2002; *Salter et al.*, 2007]). As well as lacking simultaneous measurement of Alk* and water velocity, our calculation also included more data from further north and south where the export is low rather than extrapolating from data mostly from spring around the frontal zones. On the other hand, we would expect the sediment trap data to underestimate export as there is likely to be calcium carbonate dissolution as the mean depths of the sediment traps were about 1500 m which is deep enough for dissolution in the Southern Ocean (at 1500 m the saturation state of calcite (Ω) is always < 1). Also, there could be error in the sediment trap data from the extrapolation from a few points or from problems such as advection, sample preservation, or zooplankton feeding in the buckets [*Honjo et al.*, 2008].

There is only one set of in situ measurements of calcification rates in the Southern Ocean. In the Drake Passage, *Charalampopoulou et al.* [2016] measured calcite production to be between 0.04 and 2.4 g C m^{-2} yr^{-1} in February 2009. They measured high calcite production around the Subantarctic Front and south of the Falkland Islands. Due to errors in our method, our analysis produces a mean of -0.06 g C m^{-2} yr^{-1} for the area around the Drake Passage (71ºS-55ºS, 70ºW-50ºW). However, our mean export of 2.3 g C m^{-2} yr^{-1} for the whole of the Southern Ocean is closer to the values measured by *Charalampopoulou et al.* [2016].

Calcification in the Southern Ocean has previously been estimated by *Balch et al.* [2007] who used sample depth, PIC concentration, chlorophyll, day length, and temperature to produce a multiple linear regression. When using satellite estimates of temperature, PIC and chlorophyll concentration, they found high calcification in the Southern Ocean, up to 0.8 Pg C yr^{-1}. However, the R^2 value of their equation is 0.27 which indicates that much of the variability is missed. Figure 5-6 shows calcification estimated using MODIS PIC, chlorophyll and sea surface temperature on a 9 km grid. The PIC and chlorophyll concentrations have been updated since the creation of the equation. The distribution of calcification is similar to ours in that the area of highest export/calcification is around the Polar and Subantarctic fronts (Figure 5-4). But the Pearson's r correlation coefficient between our estimate and their estimate is 0.09 (N = 465). The difference may be caused by our estimate being for export and their estimate being for calcification; however, if both estimates were accurate, one would expect greater correlation. The major difference is likely caused by our method not using concurrent measurements of Alk* and water velocity. Satellite derived predictions could also cause error because the calcification estimate from the satellite data is reflective of a depth of 1 m averaged during cloud free conditions whereas the Alk* estimate and the water velocity use the mixed layer depth. Satellite-based methods predict significant amounts of calcification taking place south of the Polar Front because satellite maps of PIC standing stocks suggest high concentrations in the region. However, neither coccolithophore in situ counts [*Holligan et al.*, 2010; *Malinverno et al.*, 2015] nor in situ calcification rate measurements [*Charalampopoulou et al.*, 2016] support high rates south of the Polar Front. Our results (Figure 5-4) using alkalinity-based analysis also do not support the satellite-based estimates south of the Polar Front.

Freeman and Lovenduski [2015] also used the equation by *Balch et al.* [2007] to project calcification. They calculated a mean summer production of 30.0 ± 0.3 g C m^{-2} yr^{-1} which is higher than our summer and autumn average export of 2.3 g C m^{-2} yr^{-1}. Their calculations are subject to be same issues as described for *Balch et al.* [2007].

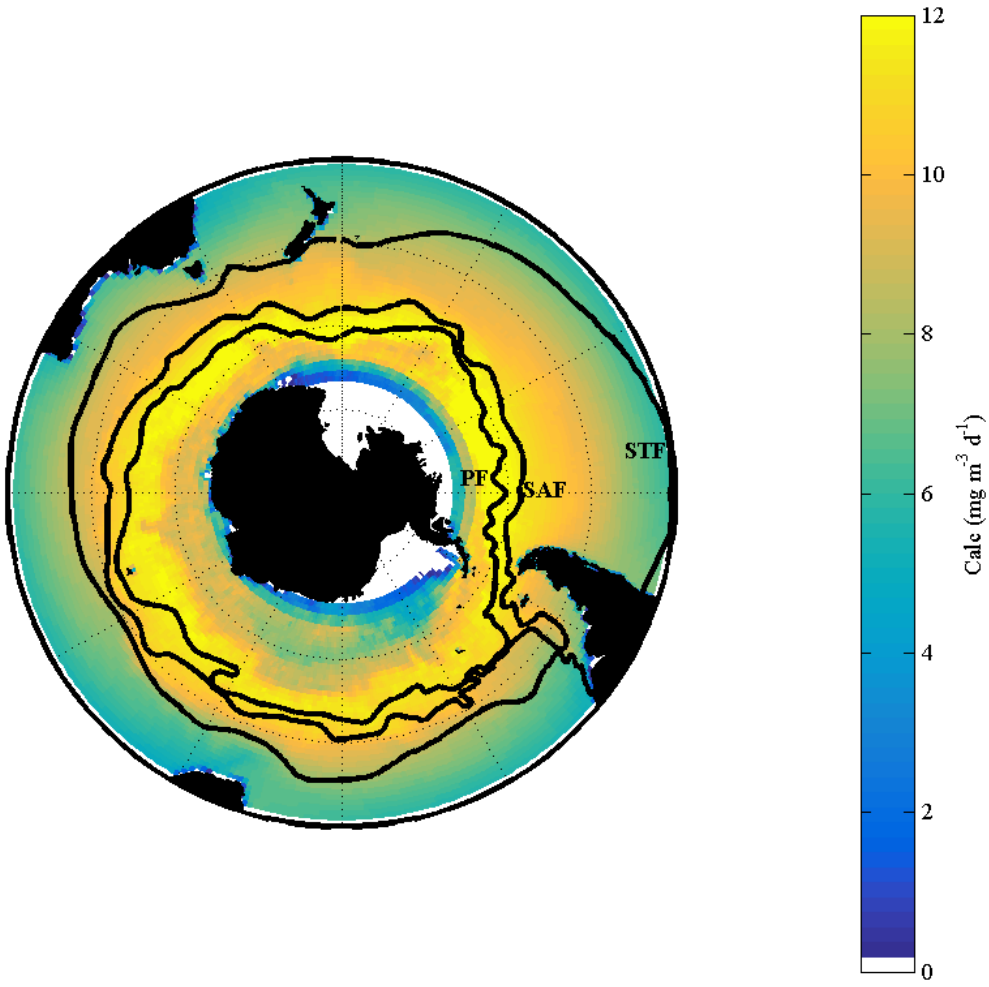

Figure 5-6. Calcification rate (mg m^{-3} d^{-1}) in the Southern Ocean (south of 30ºS) estimated from a multiple linear regression [*Balch et al.*, 2007]. The black line labelled with PF is the Polar Front, SAF is the Subantarctic Front, and STF is the Subtropical Front.

The major calcifiers in the Southern Ocean are bloom forming coccolithophores [*Cubillos et al.*, 2007; *Mohan et al.*, 2008; *Holligan et al.*, 2010]. Evidence from sediment traps shows dominance by coccoliths made of calcite north of the Polar Front, whereas aragonite building pteropods mainly dominate calcium carbonate export south of the Polar Front [*Honjo et al.*, 2000]. Studies of species assemblages [*Gravalosa et al.*, 2008; *Mohan et al.*, 2008; *Holligan et al.*, 2010] have found high concentrations of coccolithophores in the Southern Ocean north of the Polar Front but decreasing concentrations south of the Polar Front. *Malinerno et al.* [2015] analyzed coccolithophore abundance along a transect from New Zealand to the Ross Sea and found the distribution of coccolithophores, in particularly *Emiliania huxleyi,* showed a distribution that is similar to ours of export with high concentrations in the Polar Frontal Zone (between the Polar Front and the Subantartic

Front). *Holligan et al.* [2010] found that south of the Polar Front the level of coccolithophores is undetectable; however, eddies may bring water southwards from further north containing blooms of coccolithophores. Our calculation of export (Figure 5-4) shows low activity south of the Polar Front.

Berelson et al. [2007] compiled many estimates of calcium carbonate export. They concluded that global ocean export is between 0.4 and 1.8 Pg PIC yr^{-1}. Our estimate of approximately 0.31 Pg PIC yr^{-1} is between 17% and 77% of this range. However, our estimates using different assumptions (Table 5-2) are between 7% and 79% of this range.

5.5.4 What mechanisms could explain the spatial distribution of calcification?

One hypothesis to explain the patterns of export in Figure 5-4 and Figure 5-5 is that once diatoms use up the silicic acid, non-silicifiers can take advantage of the remaining nitrate as they are no longer outcompeted [*Margalef*, 1978; *Tyrrell and Merico*, 2004]. From the Antarctic continent the concentration of nutrients decreases northwards. Silicate reaches subtropical concentrations in the Polar Frontal Zone (between the Polar Front and the Subantartic Front). *Sarmiento et al.* [2004] found that the Polar Front marked the boundary between the silicate-rich and silicate-poor waters. *Balch et al.* [2011] also found the water within a calcifier bloom had an extremely low silicate to nitrate ratio. But *Hopkins et al.* [2015] report diatom and coccolithophore blooms coinciding, which conflicts with this interpretation.

An alternate hypothesis is that the range of coccolithophores is controlled by temperature. Water south of the Polar Front is colder than further north which could explain why there is a southern limit to coccolithophore growth. Studies of coccolithophores [*Neori and Holm-Hansen*, 1982; *Gravalosa et al.*, 2008; *Mohan et al.*, 2008] suggest that temperature limits the southern extent of the coccolithophores and nutrients controls the northern limit.

5.5.5 Implications and Future research

Improved estimates of calcium carbonate export are needed in order to better understand the magnitude of the possible effect of ocean acidification and to better understand the carbon cycle. Our research supports the existence of a belt of calcium carbonate production in the Southern Ocean, similar to that reported by *Balch et al.* [2005; 2011]. As calcium carbonate dissolution increases with lower pH, ocean acidification has the potential to affect calcification in this region, especially as cool waters and upwelling of carbon-rich

deep water [*Orr et al.*, 2005] means that the effects of ocean acidification may be already being seen in susceptible species [*Orr et al.*, 2005; *Bednaršek et al.*, 2012]. *Moy et al.* [2009] suggest that there has been a 30-35% reduction in calcification of planktonic foraminifera *Globigerina bulloides* in the Southern Ocean since the pre-industrial age. *Freeman and Lovenduski* [2015] found a decline of 3.9 ± 1.3% in basin-wide summer calcification measured by satellite from 1998 to 2004. The effects of reduced calcification may cause changes in the organic carbon cycle of the ocean as calcium carbonate is a major ballast for exporting material out to the photic zone [*Armstrong et al.*, 2002; *Klaas and Archer*, 2002; *Berelson et al.*, 2007].

Our understanding of the strengths and weaknesses of the tracer-velocity approach would benefit from more seasonal data. Seasonal research should include measurements through the year of alkalinity, calcification rate, and calcifier species abundances, as well as of export. Using our method with improved future sampling of Alk* could produce better estimates of the geographical distribution and rate of calcium carbonate export to improve our understanding of the carbon cycle in the Southern Ocean.

In this chapter, we introduce a novel method for assessing the rate and distribution of the calcium carbonate export flux. However, the tracer-velocity method depends on the quantity and concurrent timing of the Alk* and velocity measurements. Although this method may indicate where calcification and export are likely to have taken place, this method is less accurate in estimating the exact quantity of calcium carbonate exported. This method is likely to become more powerful in the future as more data becomes available.

Chapter 6: Conclusion and future work

6.1 Overview of thesis

This chapter summarizes the previous chapters of this thesis and suggests future work. In Chapter 1, the carbon cycle and past research into ocean alkalinity were summarized. It was also explained how research into the ocean calcium carbonate cycle is important to understand climate change and ocean acidification. In Chapter 2, the development and the quality control procedures of the large carbon databases used in this thesis were described. In Chapter 3, a tracer of the calcium carbonate cycle called Alk* was developed. In Chapter 4, the tracer was used to analyze zonal variations in the North Pacific and to produce algorithms that predict alkalinity in the surface of the Pacific Ocean. In Chapter 5, a method was developed, using in-situ Alk* and modeled velocity measurements, to estimate calcium carbonate export.

6.2 Summary of findings

To investigate the causes of alkalinity variations in the surface ocean, Alk*, a tracer of ocean calcium carbonate cycling, was created. Its distribution in the ocean was calculated using GLODAP, CARINA, and PACIFICA data. The calcium carbonate cycle was defined as the production and dissolution of calcium carbonate combined with the redistribution of dissolution products through physical processes. The Alk* tracer was produced by removing the variation in measured alkalinity caused by evaporation and precipitation, river inputs, and the production and dissolution of organic matter. Equation 6-1 shows the calculation of Alk* where Alk_m is measured alkalinity (µmol kg^{-1}), Alk_r is river alkalinity (µmol kg^{-1}), NO_3^- is the nitrate concentration (µmol kg^{-1}), and S is salinity.

$$\text{Alk}* = \frac{Alk_m - Alk_r + 1.36 \times NO_3^-}{S} \times 35 + Alk_r - 2300 \quad (6\text{-}1)$$

Rivers were found to have a significant impact on the alkalinity concentration in the tropical Atlantic Ocean, the Labrador Sea, and the Bay of Bengal. The impact of rivers was on a regional scale, especially in the Bay of Bengal where multiple large rivers enter the sea. It is also expected that other areas, where there are currently few data, will show the influence of river input including the Congo River plume in the Atlantic Ocean and the Pearl and Mekong rivers in the South China Sea [*Cao and Dai*, 2011; *Kang et al.*, 2013].

Surface Alk* values are low in the low latitudes of all basins with an increase of about 85 µmol kg^{-1} from the tropical Pacific to the North Pacific and an increase of approximately 110 µmol kg^{-1} from the tropical ocean to the Southern Ocean. These enhanced values in the North Pacific and the Southern Ocean are caused by the upwelling and winter entrainment of water containing the dissolution products of calcium carbonate. The Alk* value of the surface water then decreases as Alk* is removed through calcification and export of calcium carbonate, which subsequently dissolves at depth, increasing the Alk* concentration in the deep oceans.

During the development of Alk* in Chapter 3, it was found that many processes affect alkalinity. In Table 6-1, the potential impact that different processes have on the surface alkalinity have been estimated. The biggest impact is caused by evaporation and precipitation which affects large areas of the surface ocean through dilution and concentration. However, rivers and the upwelling of the dissolution products of calcium carbonate can also cause large local increases in alkalinity compared with salinity.

Table 6-1. Potential impact of different processes on surface ocean alkalinity.

Process	Potential magnitude of impact
Evaporation and precipitation	200 µmol kg^{-1}[a]
Rivers	100 µmol kg^{-1}[b]
Biological uptake of ions	25 µmol kg^{-1}[b]
Calcium carbonate cycling	150 µmol kg^{-1}[c]

[a]range of variation in alkalinity measurements, [b]difference between the salinity-normalized alkalinity and the Alk* value in regions affected by the process, [c]range of surface Alk* values.

In Chapter 4, Alk* was used with the new database, GLODAPv2, to analyze alkalinity variations in the surface of the North Pacific. Three longitudinal gradients were identified: (1) an increase from east to west between 45ºN and 55ºN, (2) an increase from west to east between 25ºN and 40ºN, and (3) little of a predicted increase [*Millero et al.*, 1998b; *Lee et al.*, 2006] from west to east between 15ºS and 10ºN. Hypotheses that could explain each zonal gradient were tested.

The results of the hypothesis testing indicated that, from 45ºN to 55ºN, the major cause of variation is denser isopycnals (with higher Alk*) coming closer to the surface on the western side than on the eastern side. Between 25ºN and 40ºN, the higher Alk* close to the eastern margin is caused by upwelling off the North American continent. In contrast, in the eastern equatorial Pacific upwelling does not greatly increase the surface Alk* value. However, Alk* is higher in the east during La Niña years, which is probably because stronger upwelling during these periods brings water to the surface from greater depths where Alk* is elevated.

Two algorithms to predict alkalinity were then created, one with three equations for the entire Pacific Ocean, and one with three equations for the eastern margin of the North Pacific. Multiple linear regression was used with the predictor variables of salinity, nitrate, and potential density. The accuracy of the Pacific Ocean algorithm is similar to the best previous algorithm; the algorithm created in Chapter 4 has a Pearson's r correlation coefficient of 0.970 whereas the algorithm by *Sasse et al.* [2013] has an r value of 0.977. However, the Pacific Ocean algorithm from Chapter 4 is less biased with longitude in the North Pacific north of 40ºN. In this region, there is an r value of 0.291 between the residuals and longitude whereas the algorithm by *Sasse et al.* [2013] has an r value of 0.314. The Pacific Ocean algorithm in Chapter 4 also uses fewer equations and variables than the algorithm by *Sasse et al.* [2013] and is therefore easier to apply. The algorithm created for the eastern margin of the North Pacific is more accurate than the algorithm by *Sasse et al.* [2013]; the algorithm has an r value of 0.991 whereas *Sasse et al.* [2013] have an r value of 0.953, although their algorithm was not optimized for that specific region.

A method to estimate the export of calcium carbonate from the surface ocean was created. It was demonstrated in the Southern Ocean with calculated Alk* from GLODAPv2 and water velocity estimates from the Southern Ocean State Estimate model [*Mazloff et al.*, 2010]. The method produced an estimate of the geographical distribution and rate of the export of calcium carbonate between 75ºS and 30ºS in summer and autumn; however, the accuracy of the method was limited by the lack of concurrent measurements of Alk* and water velocity. The results showed export of calcium carbonate was potentially highest around the Subantarctic Front and the Polar Front and was lower both southwards and northwards of these fronts. The calcium carbonate export was then compared with the silicon export estimated using the same method. It was found that the export of calcium carbonate occurs northwards of the silicon export, as expected from other biological and biogeochemical data. The distribution of export validates the satellite evidence of a Great

Calcite Belt of coccolithophores between 30ºS and 60ºS. The total amount calcium carbonate exported from November to April between 75ºS and 30ºS is estimated to be 0.31 Pg C yr^{-1}.

6.3 Future work

The results in this thesis advance scientific understanding of the causes of alkalinity variation in the global surface ocean, including calcium carbonate cycling, and show how alkalinity can be used to analyze different water bodies and calculate calcium carbonate export. However, further studies could improve the accuracy of Alk* and improve the use of Alk* in further investigations of the carbon cycle and ocean acidification.

6.3.1 Improved understanding of how river inputs affect ocean alkalinity

Figure 3-1e compared with Figure 3-1b shows how river alkalinity inputs can cause large scale variation in Alk*. To improve the accuracy of Alk* globally and locally, more measurements of alkalinity fluxes from more rivers are needed. The largest and also the most well studied river is the Amazon [*Amiotte Suchet et al.*, 2003; *Körtzinger*, 2003; *Cooley and Yager*, 2006; *Cooley et al.*, 2007; *Cai et al.*, 2010]; however, most of the other 25 largest rivers [*Kang et al.*, 2013] are either not measured or are only poorly studied. An investigation of river alkalinity with monthly transects from low salinity to open ocean salinity would answer many questions; such as: “How does the alkalinity of rivers vary through an estuary?” also, “What impact does organic alkalinity have in coastal waters [*Kim et al.*, 2006; *Hofmann et al.*, 2011; *Koeve and Oschlies*, 2012]?” and, “What is the final value of the river alkalinity as it enters the sea and so what is the river-alkalinity correction needed in Alk*?”. Monthly transects would ideally be performed on multiple rivers with different catchment geologies. Studying river alkalinity would also improve scientific understanding of the seasonal variation in alkalinity fluxes and how river alkalinity varies with runoff. For example, during heavy rainfall the alkalinity could be diluted in the river. Alternatively, greater rainfall could cause greater erosion raising the alkalinity concentration or the total alkalinity flux.

The final salinity-alkalinity relationship, derived from monthly transects on a river, could be used to improve the local accuracy of Alk* by inputting a more accurate average Alk_r value or by using different Alk_r values for each month. Alternatively, the relationship between alkalinity and salinity in the surface ocean around a river outflow can be used to inform the local Alk_r value which can then be included in the Alk* equation. This latter

technique is less direct, but may be better at capturing end-of-river processes that can perturb alkalinity, such as denitrification and sulphate reduction [*Brewer and Goldman,* 1976; *Wolf-Gladrow et al.*, 2007; *Cai et al.*, 2010]. The salinity concentration in the surface ocean can also be used to identify where to apply the local Alk_r value (i.e. only where low salinity values indicate river influence).

6.3.2 Improved understanding of how sea ice formation and melting affect alkalinity

Ikaite, with the chemical formula of $CaCO_3 \cdot 6H_2O$, is a carbonate mineral that forms in sea-ice. Just as river alkalinity affects ocean alkalinity, ikaite also affects regional alkalinity. The Alk* equation could therefore be improved through the inclusion of ikaite. The production and dissolution of ikaite causes the alkalinity-salinity relationship to deviate from the usual proportional relationship [*Nomura et al.*, 2013]; the production of ice containing ikaite reduces the alkalinity and increases the salinity of the surrounding water. Dissolution of ice containing ikaite decreases the salinity and relatively increases the alkalinity of the surrounding water. These processes induce changes in Alk* in sea-ice areas that are not related to the calcium carbonate cycle and the variation is caused by the salinity correction which assumes that as salinity decreases, the alkalinity decreases in proportion. The associated error could be high in the Arctic Sea which has large areas of sea ice and will have more data coverage in future [*Lauvset et al.*, 2014]. Alk* would have to be adjusted to account for the deviations in the salinity-normalization; however, the precise relationship between salinity changes and alkalinity need to be understood. Current measurements of alkalinity in sea ice range from 100 to 1352 $\mu mol\ kg^{-1}$ [*Rysgaard et al.*, 2012b, 2013; *Nomura et al.*, 2013], but sea ice does not always have negligible salinity [*Rysgaard et al.*, 2013]. To accurately add ikaite to the Alk* equation, it is important to know if there is a relationship between sea-ice salinity and ikaite content. For this, more data on ikaite concentrations and characteristics are needed, as well as more salinity measurements in sea ice.

6.3.3 Alk* analysis applied to time-series

Alk* varies with changes in the calcium carbonate cycle (production and dissolution of calcium carbonate, and ocean circulation that redistributes dissolution effects). So, it could be used to analyze the causes of seasonal variations in alkalinity in time series. Seasonal or monthly time series could show changes in Alk* caused by physical processes or blooms

of species. For example, seasonal analysis might also show changes in Alk* caused by circulation such as deeper winter mixing; Alk* could show that during winter there is deeper mixing which could entrain deeper waters with higher dissolved calcium carbonate and so higher Alk*. The Alk* could then decrease in spring and summer when the mixed layer depth decreases and calcification takes up alkalinity and reduces Alk*, decreasing the surface concentration. On a shorter timescale, a small bloom may impact the Alk* in a specific area, temporarily depleting Alk*. The changes in Alk* could be compared to the magnitude and fluctuations in nutrients, such as silicate or nitrate. This could inform us of bloom phenology and the succession of species over a bloom or a whole season.

Figure 6-1 shows a seasonal cycle in Alk*, with higher values in winter and lower values in summer. The seasonal cycle in Alk* is also correlated with nitrate (R^2=0.5 with Alk*, compared with 0.05 for alkalinity, n=106). But, to undertake global scale analysis like this more data are needed; on the Carbon Dioxide Information Analysis Center (CDIAC) website (http://cdiac.ornl.gov/oceans/time_series_moorings.html) there are 19 time series measuring alkalinity and only 5 of those contain monthly measurement at greater than 30º latitude, which is where there is likely to be significant seasonal changes.

In the same way as Alk* could be used to analyze short-term changes in the calcium carbonate cycle, multiyear analysis of Alk* using time series could also show useful long-term trends. The types of trends that could be observed using Alk* could be changes in overturning such as seen by *Byrne et al.* [2010] in the North Pacific. For example, in the future the ocean may become increasingly stratified and this could cause less nutrients [*Behrenfeld et al.*, 2006] and Alk* to be upwelled. This may decrease the gradient in Alk* observed between the polar and tropical regions (Figure 3-1). Alk* could also be used to monitor long-term changes in calcification rates. Ocean acidification could adversely affect calcifiers [*Doney et al.*, 2009; *Steinacher et al.*, 2009; *Bednaršek et al.*, 2012] and so the rates of calcification and calcium carbonate export could decrease. Such a shift could be accompanied by increased Alk* values in specific areas or by a reduced decrease in Alk* as water moves from polar to tropical regions (Figure 3-1). Figure 3-9 shows that Alk* is better than raw alkalinity at detecting trends in the calcium carbonate system.

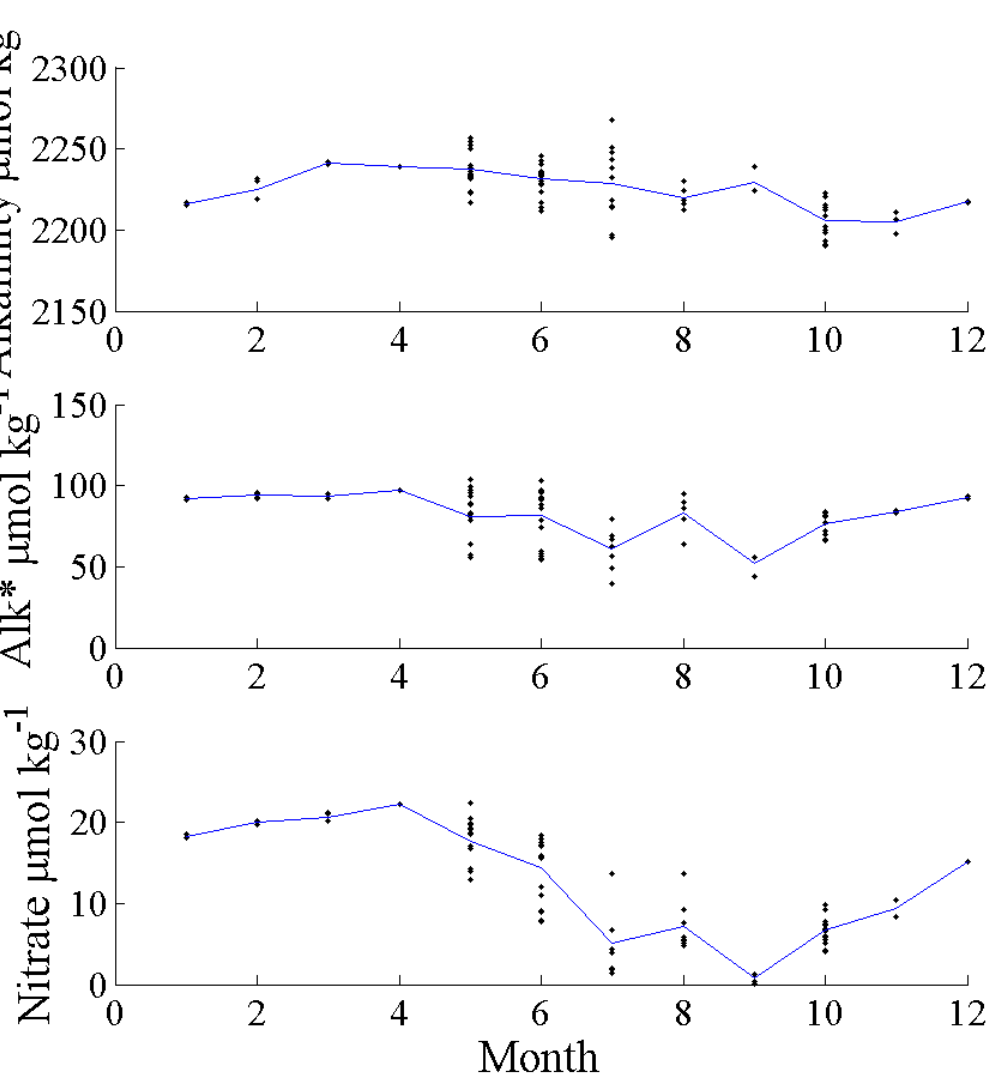

Figure 6-1. Alkalinity (µmol kg-1), Alk* (µmol kg-1), and nitrate (µmol kg-1) measurements (black dots) from the KNOT site in the Pacific Ocean at 44ºN 154ºE. The blue line connects the monthly mean.

The Bermuda Atlantic Time-series (BATS) and Hawaii Ocean Time series (HOT) are long-term, monthly time series which both contain measurements of alkalinity. Although they are not ideally placed to show seasonal variability, being at low- and mid-latitude locations where seasonal cycles are not as pronounced, the pH values at both sites show a trend of increasing acidity over time [*Dore et al.*, 2009; *Takahashi et al.*, 2014]. Most of the variations in alkalinity in these datasets are due to changes in water mass [*Sabine et al.*, 1995; *Bates et al.*, 1996]. However, individual drawdown events of 15-25 µmol kg^{-1} caused by calcification have occurred at BATS [*Bates et al.*, 1996]. Future research could correlate pH and the saturation state of calcium carbonate with Alk* to show the effects of ocean acidification. For example, future sampling may show fewer individual calcification events or events of a lower magnitude effect.

6.3.4 Combining Alk* with models

In Chapter 5, modeled ocean circulation was used with Alk* to calculate the export of calcium carbonate in the Southern Ocean. Further studies could use Alk* with inverse models, or models could verify their representation of calcification by comparing modeled Alk* to a global data product. Comparing modeled Alk* to a climatological map of Alk*, could show where the model accurately represents the calcium carbonate cycle and where it is less accurately represented. Feedback from this comparison could be used to improve modeled calcification and export of calcium carbonate in the ocean, for example, identifying where in situ Alk* is greater at mid-depth than the modeled Alk* could highlight areas of greater export. This feedback could show the levels of calcification, and other biological activity, needed to reproduce the observed Alk* fields. Identifying areas with the greatest uncertainty may help to refine the global estimate of calcification which is currently estimated only rather loosely, with a large range (0.5-1.6 Pg PIC yr^{-1} [*Berelson et al.*, 2007]). Modeled calcification could also highlight the areas of the ocean where further in situ studies of calcification could provide the most information and so models could be used to plan cruise routes. For example, modeled calcification could identify areas of high calcium carbonate production which also have a low pH and therefore where ocean acidification may have the greatest impact on the community structure. This could be used to plan biological surveys of the area and test the robustness of the community to ocean acidification. Improving the modeled Alk* could also help to refine the biogeochemical processes in models and improve predictions of local air-sea fluxes because fluxes are affected by the state of the ocean carbonate system. For instance, alkalinity is a major control on surface pCO_2, and hence air-sea gas exchange, therefore improving the modeling of some of the processes affecting alkalinity, such as the calcium carbonate cycle, could improve the local modeling of air-sea carbon dioxide fluxes.

6.3.5 Using Alk* to refine predicative algorithms for alkalinity

In Chapter 4, two algorithms to predict alkalinity in the Pacific Ocean north of 30ºS were created. A processed-based algorithm for predicting alkalinity in the entire ocean, at all depths, could also be produced using Alk*. Alk* could be used to represent evaporation, precipitation, river input, and biological uptake of ions. The rest of the variation, mainly from the calcium carbonate cycle, could be statistically modeled using relationships with nutrients, such as nitrate, which is also used by calcifiers, or silicate, which dissolves at a more similar depth to calcium carbonate (Chapter 4). Alternatively, the remaining variation

could be modeled with a more complex neural network [*Sasse et al.*, 2013; *Velo et al.*, 2013; *Carter et al.*, 2016]. Using a larger dataset, e.g. GLODAPv2 [*Olsen et al.*, 2016], would also improve and update an algorithm compared with the *Lee et al.* [2006] algorithm because GLODAPv2 covers more coastal areas and the Arctic Sea. The result of using Alk* and GLODAPv2 would be a more accurate and process-based algorithm with the potential to respond to future changes in processes which affect alkalinity.

The use of nitrate may help to refine predicative algorithms (Chapter 4; [*McNeil et al.*, 2007]) and in the future nitrate may also be measured using autonomous underwater vehicles (AUVs) [*Johnson and Coletti,* 2002]. *Carter et al.* [2016] produced a Locally Interpolated Alkalinity Regression (LIAR) which uses salinity plus any or none of: potential temperature, apparent oxygen utilization, total dissolved nitrate, and total silicate to predict alkalinity in the ocean. Their most accurate algorithm uses all of the parameters. These algorithms are designed to be used to interpolate alkalinity around available cruise data to avoid discontinuities between regression equations for separate areas; however, their algorithms could also be used on data from AUVs including data from Argo floats equipped with biogeochemical sensors, such as nitrate and oxygen. Using AUVs, the entire carbonate system could also be estimated if, in the future, alkalinity and pH sensors of sufficient accuracy are developed [*Bresnahan et al.*, 2014].

6.4 Final remarks

To further scientific knowledge, the aims of this thesis were to understand the controlling processes on alkalinity in the surface ocean and the causes of the large-scale regional variations. Five objectives were identified:

1. Identify the magnitude of variations in surface ocean alkalinity caused by different major processes, such as evaporation and precipitation, river inputs, organic matter production, upwelling, and production of calcium carbonate.
2. Identify in which areas surface alkalinity is most affected by each of the major processes in objective 1.
3. Explain the causes of longitudinal variations in alkalinity and salinity-normalized alkalinity in the North Pacific which have previously proven difficult to ascertain [*Lee et al.,* 2006].
4. Produce an algorithm to predict alkalinity in the surface ocean of the North Pacific that is an improvement upon the algorithm by *Lee et al.* [2006].

5. Produce a new method to map and quantify the production of calcium carbonate in the subpolar frontal region of the Southern Ocean using a tracer of calcium carbonate cycling.

This thesis meets these objectives in Chapters 3, 4 and 5. In Chapter 3, the major causes of surface variability in alkalinity are identified and their impact quantified (Table 6-1). The areas most affected by each of the major processes are illustrated in Figure 3-1. In Chapter 4, hypotheses are explored to identify the causes of longitudinal variations in the North Pacific and then an improved algorithm was created for predicting alkalinity in the Pacific Ocean north of 30ºS. In Chapter 5, a new method for calculating the export of calcium carbonate in the Southern Ocean is demonstrated.

By meeting these objectives, this thesis improves predictive algorithms, and furthers scientific understanding of the causes of both local and large-scale variations in alkalinity including calcification and the export of calcium carbonate.

List of References

Aagard, K., and E. C. Carmack (1989), The role of sea ice and other fresh water in the Arctic circulation, *J. Geophys. Res.*, *94*(1), 14,414-485,498, doi:10.1029/JC094iC10p14485.

Alin, S. R., R. A. Feely, A. G. Dickson, J. M. Hernández-Ayón, L. W. Juranek, M. D. Ohman, and R. Goericke (2012), Robust empirical relationships for estimating the carbonate system in the southern California Current System and application to CalCOFI hydrographic cruise data (2005–2011), *J. Geophys. Res.*, *117*, C05033, doi:10.1029/2011JC007511.

Allen, M. R., and W. J. Ingram (2002), Constraints on future changes in climate and the hydrologic cycle., *Nature*, *419*(6903), 224–32, doi:10.1038/nature01092.

Álvarez, M., T. Tanhua, H. Brix, C. Lo Monaco, N. Metzl, E. L. McDonagh, and H. L. Bryden (2011), Decadal biogeochemical changes in the subtropical Indian Ocean associated with Subantarctic Mode Water, *J. Geophys. Res. Ocean.*, *116*(9), 1–13, doi:10.1029/2010JC006475.

Aminot, A., and D. Kirkwood (1995), Report on the results of the fifth ICES intercomparison exercise for nutrients in sea water, Copenhagen, Denmark.

Amiotte Suchet, P., J.-K. Probst, and W. Ludwig (2003), Worldwide distribution of continental rock lithology: Implications for the atmospheric/soil CO2 uptake by continental weathering and alkalinity river transport to the oceans, *Global Biogeochem. Cycles*, *17*(2), 1038, doi:10.1029/2002GB001891.

Anderson, D. H., and R. J. Robinson (1946), Rapid Electrometric Determination of Alkalinity of Sea Water Using Glass Electrode, *Ind. Eng. Chem. Anal. Ed.*, *18*(12), 767–769, doi:10.1021/i560160a011.

Armstrong, R. A., C. Lee, J. I. Hedges, S. Honjo, and S. G. Wakeham (2002), A new, mechanistic model for organic carbon fluxes in the ocean based on the quantitative association of POC with ballast minerals, *Deep Sea Res. Part II Top. Stud. Oceanogr.*, *49*, 219–236, doi:10.1016/S0967-0645(01)00101-1.

Assmy, P. et al. (2013), Thick-shelled, grazer-protected diatoms decouple ocean carbon and silicon cycles in the iron-limited Antarctic Circumpolar Current, *Proc. Natl. Acad. Sci.*, *110*(51), 20633–20638, doi:10.1073/pnas.1309345110.

Bakker, D. C. E. et al. (2014), An update to the surface ocean CO2 atlas (SOCAT version 2), *Earth Syst. Sci. Data*, *6*(1), 69–90, doi:10.5194/essd-6-69-2014.

Bakun, A. (1990), Global climate change and intensification of coastal ocean upwelling, *Science*, *247*, 198–201, doi:10.1126/science.247.4939.198.

Balch, W., D. Drapeau, B. Bowler, and E. Booth (2007), Prediction of pelagic calcification rates using satellite measurements, *Deep Sea Res. Part II Top. Stud. Oceanogr.*, *54*(5–7), 478–495, doi:10.1016/j.dsr2.2006.12.006.

Balch, W. M., and K. Kilpatrick (1996), Calcification rates in the equatorial Pacific along 140 degrees W, *Deep. Res. Part II*, *43*(4–6), 971–993, doi:10.1016/0967-0645(96)00032-X.

Balch, W. M., H. R. Gordon, B. C. Bowler, D. T. Drapeau, and E. S. Booth (2005), Calcium carbonate measurements in the surface global ocean based on Moderate-Resolution Imaging Spectroradiometer data, *J. Geophys. Res.*, *110*, C07001, doi:10.1029/2004JC002560.

Balch, W. M., D. T. Drapeau, B. C. Bowler, E. Lyczskowski, E. S. Booth, and D. Alley (2011), The contribution of coccolithophores to the optical and inorganic carbon budgets during the Southern Ocean Gas Exchange Experiment: New evidence in support of the "Great Calcite Belt" hypothesis, *J. Geophys. Res.*, *116*, C00F06, doi:10.1029/2011JC006941.

Barbero, L., J. Boutin, L. Merlivat, N. Martin, T. Takahashi, S. C. Sutherland, and R. Wanninkhof (2011), Importance of water mass formation regions for the air-sea CO2 flux estimate in the Southern Ocean, *Global Biogeochem. Cycles*, *25*, GB1005, doi:10.1029/2010GB003818.

Barker, S., J. A. Higgins, and H. Elderfield (2003), The future of the carbon cycle: review, calcification response, ballast and feedback on atmospheric CO2, *Philos. Trans. A. Math. Phys. Eng. Sci.*, *361*(1810), 1977–99, doi:10.1098/rsta.2003.1238.

Barnett, J., and W. N. Adger (2007), Climate change, human security and violent conflict, *Polit. Geogr.*, *26*(6), 639–655, doi:10.1016/j.polgeo.2007.03.003.

Bates, N. R., A. F. Michaels, and A. H. Knap (1996), Seasonal and interannual variability of oceanic carbon dioxide species at the U.S. JGOFS Bermuda Atlantic Time-series Study (BATS) site, *Deep Sea Res. Part II Top. Stud. Oceanogr.*, *43*(2–3), 347–383, doi:10.1016/0967-0645(95)00093-3.

Bates, N. R., A. C. Pequignet, and C. L. Sabine (2006), Ocean carbon cycling in the Indian Ocean: 1. Spatiotemporal variability of inorganic carbon and air-sea CO2 gas exchange, *Global Biogeochem. Cycles*, *20*, GB3020, doi:10.1029/2005GB002491.

Beaufort, L., M. Couapel, N. Buchet, H. Claustre, and C. Goyet (2008), Calcite production by coccolithophores in the south east Pacific Ocean, *Biogeosciences*, *5*, 1101–1117.

Bednaršek, N. et al. (2012), Extensive dissolution of live pteropods in the Southern Ocean, *Nat. Geosci.*, *5*(11), 1–5, doi:10.1038/ngeo1635.

Behrenfeld, M. J., R. T. O'Malley, D. a Siegel, C. R. McClain, J. L. Sarmiento, G. C. Feldman, A. J. Milligan, P. G. Falkowski, R. M. Letelier, and E. S. Boss (2006), Climate-driven trends in contemporary ocean productivity., *Nature*, *444*(7120), 752–755, doi:10.1038/nature05317.

Berelson, W. M., W. M. Balch, R. Najjar, R. A. Feely, C. Sabine, and K. Lee (2007), Relating estimates of CaCO3 production, export, and dissolution in the water column to measurements of CaCO3 rain into sediment traps and dissolution on the sea floor: A revised global carbonate budget, *Global Biogeochem. Cycles*, *21*, GB1024, doi:10.1029/2006GB002803.

Bockmon, E. E., and A. G. Dickson (2015), An inter-laboratory comparison assessing the quality of seawater carbon dioxide measurements, *Mar. Chem.*, *171*, 36–43, doi:10.1016/j.marchem.2015.02.002.

Bond, N. A., J. E. Overland, M. Spillane, and P. Stabeno (2003), Recent shifts in the state of the North Pacific, *Geophys. Res. Lett.*, *30*(23), 2–5, doi:10.1029/2003GL018597.

Bopp, L., P. Monfray, O. Aumont, J. L. Dufresne, H. Le Treut, G. Madec, L. Terray, and J. C. Orr (2001), Potential impact of climate change on marine export production, *Global Biogeochem. Cycles*, *15*(1), 81–99.

Bostock, H. C., B. W. Hayward, H. L. Neil, K. I. Currie, and G. B. Dunbar (2011), Deep-water carbonate concentrations in the southwest Pacific, *Deep Sea Res. Part I Oceanogr. Res. Pap.*, *58*, 72–85, doi:10.1016/j.dsr.2010.11.010.

de Boyer Montégut, C. (2004), Mixed layer depth over the global ocean: An examination of profile data and a profile-based climatology, *J. Geophys. Res.*, *109*(C12), C12003, doi:10.1029/2004JC002378.

Bradshaw, A. L., and P. G. Brewer (1988), High precision measurements of alkalinity and total carbon dioxide in seawater by potentiometric titration. 2. Measurements on standard solutions, *Mar. Chem.*, *24*(2), 155–162, doi:10.1016/0304-4203(88)90046-1.

Bradshaw, A. L., P. G. Brewer, D. K. Shafer, and R. T. Williams (1981), Measurements of total carbon dioxide and alkalinity by potentiometric titration in the GEOSECS program, *Earth Planet. Sci. Lett.*, *55*, 99–115, doi:10.1016/0012-821X(81)90090-X.

Brady, P. V, and S. A. Carroll (1994), Direct effects of CO2 and temperature on silicate weathering: Possible implications for climate control, *Geochim. Cosmochim. Acta, 58*(8), 1853–1856, doi:10.1016/0016-7037(94)90543-6.

Bresnahan, P. J., T. R. Martz, Y. Takeshita, K. S. Johnson, and M. LaShomb (2014), Best practices for autonomous measurement of seawater pH with the Honeywell Durafet, *Methods Oceanogr.*, *9*, 44–60, doi:10.1016/j.mio.2014.08.003.

Brewer, P. G., and J. C. Goldman (1976), Alkalinity changes generated by phytoplankton growth, *Limnol. Oceanogr.*, *21*(1), 108–117, doi:10.4319/lo.1976.21.1.0108.

Brewer, P. G., G. T. F. Wong, M. P. Bacon, and W. Spencer, Derek (1975), An oceanic calcium problem?, *Earth Planet. Sci. Lett.*, *26*, 81–87.

Brewer, P. G., K. W. Bruland, R. W. Eppley, and J. J. McCarthy (1986a), The Global Ocean Flux Study (GOFS): Status of the U.S. GOFS Program, *Eos, Trans. Am. Geophys. Union*, *67*(44), 827–832, doi:10.1029/EO067i044p00827.

Brewer, P. G., T. Takahashi, and R. T. Williams (1986b), Transient Tracers in the Oceans (TTO) - Hydrographic data and carbon dioxide systems with revised carbon chemistry data. NDP-004/R1, Oak Ridge, Tennessee.

Brewer, P. G., D. M. Glover, C. Goyet, and D. K. Shafer (1995), The pH of the North Atlantic Ocean: Improvements to the global model for sound absorption, *J. Geophys. Research*, *100*(C5), 8761–8776, doi:10.1029/95JC00306.

Broerse, A. T. C., T. Tyrrell, J. R. Young, A. J. Poulton, A. Merico, W. M. Balchc, and P. I. Miller (2003), The cause of bright waters in the Bering Sea in winter, *Cont. Shelf Res.*, *23*(16), 1579–1596, doi:10.1016/j.csr.2003.07.001.

Buesseler, K. O., L. Ball, J. Andrews, J. K. Cochran, D. J. Hirschberg, M. P. Bacon, A. Fleer, and M. Brzezinski (2001), Upper ocean export of particulate organic carbon and biogenic silica in the Southern Ocean along 170??W, *Deep. Res. Part II Top. Stud. Oceanogr.*, *48*(19–20), 4275–4297, doi:10.1016/S0967-0645(01)00089-3.

Byrne, R. H., S. Mecking, R. A. Feely, and X. Liu (2010), Direct observations of basin-wide acidification of the North Pacific Ocean, *Geophys. Res. Lett.*, *37*(2), n/a-n/a, doi:10.1029/2009GL040999.

Cai, W., and Y. Wang (1998), The chemistry, fluxes, and sources of carbon dioxide in estuarine waters of the Satilla and Altamaha Rivers, Georgia, *Limnol. Oceanogr.*, *43*(4), 657–668.

Cai, W.-J., X. Hu, W.-J. Huang, L.-Q. Jiang, Y. Wang, T.-H. Peng, and X. Zhang (2010), Alkalinity distribution in the western North Atlantic Ocean margins, *J. Geophys. Res.*, *115*, C08014, doi:10.1029/2009JC005482.

Cai, W.-J. et al. (2011), Acidification of subsurface coastal waters enhanced by eutrophication, *Nat. Geosci.*, *4*(11), 766–770, doi:10.1038/ngeo1297.

Caldeira, K., and M. E. Wickett (2005), Ocean model predictions of chemistry changes from carbon dioxide emissions to the atmosphere and ocean, *J. Geophys. Res.*, *110,* C09S04, doi:10.1029/2004JC002671.

Caminade, C., S. Kovats, J. Rocklov, A. M. Tompkins, A. P. Morse, and F. J. Colón-gonzález (2014), Impact of climate change on global malaria distribution, *Postdam Inst. Clim. Impact Res.*, *111*(9), 3686–3291, doi:10.1073/pnas.1302089111.

Cao, Z., and M. Dai (2011), Shallow-depth CaCO3 dissolution: Evidence from excess calcium in the South China Sea and its export to the Pacific Ocean, *Global Biogeochem. Cycles*, *25*(2), GB2019, doi:10.1029/2009GB003690.

Cao, Z., M. Dai, N. Zheng, D. Wang, Q. Li, W. Zhai, F. Meng, and J. Gan (2011), Dynamics of the carbonate system in a large continental shelf system under the influence of both a river plume and coastal upwelling, *J. Geophys. Res.*, *116*, G02010, doi:10.1029/2010JG001596.

Carter, B. R., J. R. Toggweiler, R. M. Key, and J. L. Sarmiento (2014), Processes determining the marine alkalinity and calcium carbonate saturation state distributions, *Biogeosciences*, *11*(24), 7349–7362, doi:10.5194/bg-11-7349-2014.

Carter, B. R., N. L. Williams, A. R. Gray, and R. A. Feely (2016), Locally interpolated alkalinity regression for global alkalinity estimation, *Limnol. Oceanogr. Methods*, *14*(4), 268–277, doi:10.1002/lom3.10087.

Castro Ortiz, C. A. (1994), Sea-level rise and its impact on Bangladesh, *Ocean Coast. Manag.*, *23*(3), 249–270, doi:10.1016/0964-5691(94)90022-1.

Charalampopoulou, A., A. J. Poulton, D. C. E. Bakker, M. I. Lucas, M. C. Stinchcombe, and T. Tyrrell (2016), Environmental drivers of coccolithophore abundance and calcification across Drake Passage (Southern Ocean), *Biogeosciences Discuss.*, (April), 1–39, doi:10.5194/bg-2016-139.

Chen, C.-T. A. (1996), The Kuroshio intermediate water is the major source of nutrients on the East China Sea continental shelf, *Oceanol. Acta*, *19*(5), 523–527.

Chen, C.-T. A. (2002), Shelf-vs. dissolution-generated alkalinity above the chemical lysocline, *Deep Sea Res. Part II Top. Stud. Oceanogr.*, *49*(24–25), 5365–5375, doi:10.1016/S0967-0645(02)00196-0.

Chen, C.-T. A., and R. M. Pytkowicz (1979), On the total CO2-tritation alkalinity oxygen system in the pacific ocean, *Nature*, *281*, 362–365.

Chen, C.-T. A., and S.-L. Wang (1999), Carbon , alkalinity and nutrient budgets on the East China Sea continental shelf, *J. Geophys. Res.*, *104*(C9), 20675–20686, doi:10.1029/1999JC900055.

Chen, G.-T., and F. J. Millero (1979), Gradual increase of oceanic CO2, *Nature*, *277*, 205–206, doi:10.1038/277205a0.

Chierici, M., and A. Fransson (2009), Calcium carbonate saturation in the surface water of the Arctic Ocean: undersaturation in freshwater influenced shelves, *Biogeosciences*, *6*(11), 2421–2431, doi:10.5194/bg-6-2421-2009.

Chung, S.-N. (2003), Calcium carbonate budget in the Atlantic Ocean based on water column inorganic carbon chemistry, *Global Biogeochem. Cycles*, *17*(4), 1093, doi:10.1029/2002GB002001.

Chung, S.-N., G.-H. Park, K. Lee, R. M. Key, F. J. Millero, R. A. Feely, C. L. Sabine, and P. G. Falkowski (2004), Postindustrial enhancement of aragonite undersaturation in the upper tropical and subtropical Atlantic Ocean: The role of fossil fuel CO2, *Limnol. Oceanogr.*, *49*(2), 315–321, doi:10.4319/lo.2004.49.2.0315.

Church, J. A., N. J. White, and J. R. Hunter (2006), Sea-level rise at tropical Pacific and Indian Ocean islands, *Glob. Planet. Change*, *53*(3), 155–168, doi:10.1016/j.gloplacha.2006.04.001.

Clark, D., M. Lamare, and M. Barker (2009), Response of sea urchin pluteus larvae (Echinodermata: Echinoidea) to reduced seawater pH: A comparison among a tropical, temperate, and a polar species, *Mar. Biol.*, *156*(6), 1125–1137, doi:10.1007/s00227-009-1155-8.

Coale, K. H., K. S. Johnson, and F. P. Chavez (2004), Southern Ocean Iron Enrichment Experiment: Carbon Cycling in High- and Low-Si Waters, *Science*, *304*(5669), 408–414, doi:10.1126/science.1089778.

Cooley, S. R., and P. L. Yager (2006), Physical and biological contributions to the western tropical North Atlantic Ocean carbon sink formed by the Amazon River plume, *J. Geophys. Res.*, *111*, C08018, doi:10.1029/2005JC002954.

Cooley, S. R., V. J. Coles, A. Subramaniam, and P. L. Yager (2007), Seasonal variations in the Amazon plume-related atmospheric carbon sink, *Global Biogeochem. Cycles*, *21*, GB3014, doi:10.1029/2006GB002831.

Cooper, L. W., J. W. McClelland, R. M. Holmes, P. A. Raymond, J. J. Gibson, C. K. Guay, and B. J. Peterson (2008), Flow-weighted values of runoff tracers (δ18O, DOC, Ba, alkalinity) from the six largest Arctic rivers, *Geophys. Res. Lett.*, *35*, L18606, doi:10.1029/2008GL035007.

Cornelissen, J. H. C. et al. (2007), Global negative vegetation feedback to climate warming responses of leaf litter decomposition rates in cold biomes, *Ecol. Lett.*, *10*(7), 619–627, doi:10.1111/j.1461-0248.2007.01051.x.

Cross, J. N., J. T. Mathis, N. R. Bates, and R. H. Byrne (2013), Conservative and non-conservative variations of total alkalinity on the southeastern Bering Sea shelf, *Mar. Chem.*, *154*, 100–112, doi:10.1016/j.marchem.2013.05.012.

Cubasch, U., D. Wuebbles, D. Chen, M. C. Facchini, D. Frame, N. Mahowald, and J.-G. Winther (2013), Introduction, *Clim. Chang. 2013 Phys. Sci. Basis. Contrib. Work. Gr. I to Fifth Assess. Rep. Intergov. Panel Clim. Chang.*, 119–158, doi:10.1017/CBO9781107415324.007.

Cubillos, J. C., S. W. Wright, G. Nash, M. F. De Salas, B. Griffiths, B. Tilbrook, A. Poisson, and G. M. Hallegraeff (2007), Calcification morphotypes of the coccolithophorid Emiliania huxleyi in the Southern Ocean: Changes in 2001 to 2006 compared to historical data, *Mar. Ecol. Prog. Ser.*, *348*, 47–54, doi:10.3354/meps07058.

Cummins, P. F., and H. J. Freeland (2007), Variability of the North Pacific Current and its bifurcation, *Prog. Oceanogr.*, *75*(2), 253–265, doi:10.1016/j.pocean.2007.08.006.

Dahm, C. N., S. V. Gregory, and P. Kilho Park (1981), Organic carbon transport in the Columbia River, *Estuar. Coast. Shelf Sci.*, *13*, 645–658, doi:10.1016/S0302-3524(81)80046-1.

Deutsch, C., N. Gruber, R. M. Key, J. L. Sarmiento, and A. Ganachaud (2001), Denitrification and N2 fixation in the Pacific Ocean, *Global Biogeochem. Cycles*, *15*(2), 483–506, doi:10.1029/2000GB001291.

Dickson, A. G. (1981), An exact definition of total alkalinity and a procedure for the estimation of alkalinity and total inorganic carbon from titration data, *Deep. Res.*, *28A*(6), 609–623.

Dickson, A. G. (1992), The development of the alkalinity concept in marine chemistry*, *Mar. Chem.*, *40*(1990), 49–63.

Dickson, A. G. (2010), The carbon dioxide system in seawater : equilibrium chemistry and measurements, in *Guide to best practices for ocean acidification research and data reporting*, edited by U. Riebesell, V. J. Fabry, L. Hansson, and J.-P. Gattuso, Publications Office of the European Union, Luxembourg.

Dickson, A. G., J. D. Afghan, and G. C. Anderson (2003), Reference materials for oceanic CO2 analysis: a method for the certification of total alkalinity, *Mar. Chem.*, *80*, 185–197, doi:10.1016/S0304-4203(02)00133-0.

Dittmar, W. (1884), Report on researches into the composition of ocean-water collected by H.M.S. Challenger during the years 1873-76,

Doney, S. C., V. J. Fabry, R. A. Feely, and J. A. Kleypas (2009), Ocean acidification: the other CO2 problem., *Ann. Rev. Mar. Sci.*, *1*, 169–192, doi:10.1146/annurev.marine.010908.163834.

Dore, J. E., R. Lukas, D. W. Sadler, M. J. Church, and D. M. Karl (2009), Physical and biogeochemical modulation of ocean acidification in the central North Pacific., *Proc. Natl. Acad. Sci. U. S. A.*, *106*(30), 12235–12240, doi:10.1073/pnas.0906044106.

Douglass, E., D. Roemmich, and D. Stammer (2006), Interannual variability in northeast Pacific circulation, *J. Geophys. Res. Ocean.*, *111*, C04001, doi:10.1029/2005JC003015.

Dyrssen, D. (1965), A Gran titration of sea water on board Sagitta, *Acta Chem. Scand.*

Dyrssen, D., and L. G. Sillén (1967), Alkalinity and total carbonate in sea water. A plea for p-T-independent data, *Tellus A*, *1*, 113–121, doi:10.3402/tellusa.v19i1.9755.

Eby, G. N. (2016), *Principles of Environmental Geochemistry,* Waveland Press Inc., Long Grove, Illinois.

Edmond, J. M. (1974), On the dissolution of carbonate and silicate in the deep ocean, *Deep. Res.*, *21*, 455–480.

Elvert, M., E. Suess, J. Greinert, and M. J. Whiticar (2000), Archaea mediating anaerobic methane oxidation in deep-sea sediments at cold seeps of the eastern Aleutian subduction zone, *Org. Geochem.*, *31*, 1175–1187, doi:10.1016/S0146-6380(00)00111-X.

Emerson, S., and J. Hedges (2008), *Chemical Oceanography and the Marine Carbon Cycle,* Cambridge University Press, Cambridge.

Falkowski, P. G. et al. (2000), The global carbon cycle: a test of our knowledge of earth as a system., *Science*, *290*(5490), 291–296, doi:10.1126/science.290.5490.291.

Feely, R. A. et al. (2002a), In situ calcium carbonate dissolution in the Pacific Ocean, *Global Biogeochem. Cycles*, *16*(4), 1144, doi:10.1029/2002GB001866.

Feely, R. A. et al. (2002b), Seasonal and interannual variability of CO2 in the equatorial Pacific, *Deep Sea Res. Part II Top. Stud. Oceanogr.*, *49*, 2443–2469, doi:10.1016/S0967-0645(02)00044-9.

Feely, R. A., C. L. Sabine, K. Lee, W. Berelson, J. Kleypas, V. J. Fabry, and F. J. Millero (2004), Impact of anthropogenic CO2 on the CaCO3 system in the oceans., *Science*, *305*, 362–6, doi:10.1126/science.1097329.

Feely, R. A., C. L. Sabine, J. M. Hernandez-Ayon, D. Ianson, and B. Hales (2008), Evidence for Upwelling of Corrosive "Acidified" Water onto the Continental Shelf, *Science*, *320*, 1490–1492, doi:10.1126/science.1155676.

Feely, R. A., C. L. Sabine, R. H. Byrne, F. J. Millero, A. G. Dickson, R. Wanninkhof, A. Murata, L. A. Miller, and D. Greeley (2012), Decadal changes in the aragonite and calcite saturation state of the Pacific Ocean, *Global Biogeochem. Cycles*, *26*(3), n/a-n/a, doi:10.1029/2011GB004157.

Feely, R. A. et al. (2014), The US repeat hydrography CO2/tracer program (GO-SHIP): Accomplishments from the first decadal survey.

Francois, R., S. Honjo, R. Krishfield, and S. Manganini (2002), Factors controlling the flux of organic carbon to the bathypelagic zone of the ocean, *Global Biogeochem. Cycles, 16*(4), 1087, doi:10.1029/2001GB001722.

Freeman, N. M., and N. S. Lovenduski (2015), Decreased calcification in the Southern Ocean over the satellite record, *Geophys. Res. Lett.*, *42*, 1834–1840, doi:10.1002/2014GL062769.1.

Friis, K., A. Körtzinger, and D. W. R. Wallace (2003), The salinity normalization of marine inorganic carbon chemistry data, *Geophys. Res. Lett.*, *30*(2), 1085, doi:10.1029/2002GL015898.

Fripiat, F., A. J. Cavagna, F. Dehairs, S. Speich, L. André, and D. Cardinal (2011), Silicon pool dynamics and biogenic silica export in the Southern Ocean inferred from Si-isotopes, *Ocean Sci.*, *7*(5), 533–547, doi:10.5194/os-7-533-2011.

Fry, C. H., T. Tyrrell, M. P. Hain, N. R. Bates, and E. P. Achterberg (2015), Analysis of global surface ocean alkalinity to determine controlling processes, *Mar. Chem.*, *174*, 46–57, doi:10.1016/j.marchem.2015.05.003.

Galy, A., and C. France-Lanord (1999), Weathering processes in the Ganges–Brahmaputra basin and the riverine alkalinity budget, *Chem. Geol.*, *159*, 31–60, doi:10.1016/S0009-2541(99)00033-9.

Garcia, H. E., R. A. Locarnini, T. P. Boyer, J. I. Antonov, O. K. Baranova, M. . M. Zweng, J. R. Reagan, and D. R. Johnson (2014a), Volume 2: Dissolved Oxygen, Apparent Oxygen Utilization, and Oxygen Saturation, in *World Ocean Atlas 2013*, edited by S. Levitus and A. Mishonov, p. 27, NOAA Atlas NESDIS 75.

Garcia, H. E., R. A. Locarnini, T. P. Boyer, J. I. Antonov, O. K. Baranova, M. M. Zweng, J. R. Reagan, and D. R. Johnson (2014b), Volume 4: Dissolved Inorganic Nutrients (phosphate, nitrate, silicate), in *World Ocean Atlas 2013*, edited by S. Levitus and A. Mishonov, p. 25, NOAA Atlas NESDIS 76.

Gledhill, D. K., R. Wanninkhof, F. K. Millero, and M. Eakin (2008), Ocean acidification of the Greater Caribbean Region 1996-2006, *J. Geophys. Res. Ocean.*, *113*(10), 1–11, doi:10.1029/2007JC004629.

Goldman, J. C., and P. G. Brewer (1980), Effect of nitrogen source and growth rate on phytoplankton-mediated changes in alkalinity, *Limnol. Oceanogr.*, *25*(2), 352–357, doi:10.4319/lo.1980.25.2.0352.

Gran, G. (1952), Determination of the equivalence point in potentiometric titrations. Part II, *Analyst*.

Gran, G., H. Dahlenborg, S. Laurell, and M. Rottenberg (1950), Determination of the Equivalent Point in Potentiometric Titrations., *Acta Chem. Scand.*, *4*, 559–577, doi:10.3891/acta.chem.scand.04-0559.

Gravalosa, J. M., J.-A. Flores, F. J. Sierro, and R. Gersonde (2008), Sea surface distribution of coccolithophores in the eastern Pacific sector of the Southern Ocean (Bellingshausen and Amundsen Seas) during the late austral summer of 2001, *Mar. Micropaleontol.*, *69*(1), 16–25, doi:10.1016/j.marmicro.2007.11.006.

Gregg, W. W., M. E. Conkright, P. Ginoux, J. E. O'Reilly, and N. W. Casey (2003), Ocean primary production and climate : Global decadal changes, *Geol. Mag.*, *30*(15), 1809, doi:10.1029/2003GL016889.

Gruber, N., J. L. Sarmiento, and T. F. Stocker (1996), An improved method for detecting anthropogenic CO2 in the oceans, *Global Biogeochem. Cycles*, *10*(4), 809–837, doi:10.1029/96GB01608.

Hain, M. P., D. M. Sigman, and G. H. Haug (2010), Carbon dioxide effects of Antarctic stratification, North Atlantic Intermediate Water formation, and subantarctic nutrient

drawdown during the last ice age: Diagnosis and synthesis in a geochemical box model, *Global Biogeochem. Cycles*, *24*(4), GB4023, doi:10.1029/2010GB003790.

Hall, T. M., T. W. N. Haine, and D. W. Waugh (2002), Inferring the concentration of anthropogenic carbon in the ocean from tracers, *Global Biogeochem. Cycles*, *16*(4), 1131, doi:10.1029/2001GB001835.

Hartmann, D. J. et al. (2013), Observations: Atmosphere and Surface, *Clim. Chang. 2013 Phys. Sci. Basis. Contrib. Work. Gr. I to Fifth Assess. Rep. Intergov. Panel Clim. Chang.*, 159–254, doi:10.1017/CBO9781107415324.008.

Harvey, L. D. D. (2008), Mitigating the atmospheric CO2 increase and ocean acidification by adding limestone powder to upwelling regions, *J. Geophys. Res.*, *113*, C04028, doi:10.1029/2007JC004373.

Hauri, C., N. Gruber, M. Vogt, S. C. Doney, R. A. Feely, Z. Lachkar, A. Leinweber, A. M. P. McDonnell, M. Munnich, and G.-K. Plattner (2013), Spatiotemporal variability and long-term trends of ocean acidification in the California Current System, *Biogeosciences*, *10*, 193–216, doi:10.5194/bg-10-193-2013.

Hein, J. R., J. R. O'Neil, and M. G. Jones (1979), Origin of authigenic carbonates in sediment from the deep Bering Sea, *Sedimentology*, *26*, 681–705, doi:10.1111/j.1365-3091.1979.tb00937.x.

Hendrix, C. S., and I. Salehyan (2012), Climate change, rainfall, and social conflict in Africa, *J. Peace Res.*, *49*(1), 35–50, doi:10.1177/0022343311426165.

Hester, K. C., E. T. Peltzer, W. J. Kirkwood, and P. G. Brewer (2008), Unanticipated consequences of ocean acidification: A noisier ocean at lower pH, *Geophys. Res. Lett.*, *35*(19), 1–5, doi:10.1029/2008GL034913.

Hofmann, E. E. et al. (2011), Modeling the dynamics of continental shelf carbon., *Ann. Rev. Mar. Sci.*, *3*, 93–122, doi:10.1146/annurev-marine-120709-142740.

Hofmann, M., and H.-J. Schellnhuber (2009), Oceanic acidification affects marine carbon pump, *Procedings Natl. Acad. Sci.*, *106*(9), 3017–3022, doi:10.1073/pnas.0813384106.

Holligan, P. M., and J. E. Roberstson (1996), Significance of ocean carbonate budgets for the global carbon cycle, *Glob. Chang. Biol.*, *2*(2), 85–95, doi:10.1111/j.1365-2486.1996.tb00053.x.

Holligan, P. M., A. Charalampopoulou, and R. Hutson (2010), Seasonal distributions of the coccolithophore, Emiliania huxleyi, and of particulate inorganic carbon in surface waters of the Scotia Sea, *J. Mar. Syst.*, *82*(4), 195–205, doi:10.1016/j.jmarsys.2010.05.007.

Holzer, M., F. W. Primeau, T. DeVries, and R. Matear (2014), The Southern Ocean silicon trap: Data-constrained estimates of regenerated silicic acid, trapping efficiencies, and global transport paths, *J. Geophys. Res. Ocean.*, *119*(1), 313–331, doi:10.1002/2013JC009356.

Honjo, S., R. Francois, S. Manganini, J. Dymond, and R. Collier (2000), Particle fluxes to the interior of the Southern Ocean in the western Pacific sector along 170W, *Deep. Res. Part II Top. Stud. Oceanogr.*, *47*(15–16), 3521–3548, doi:10.1016/S0967-0645(00)00077-1.

Honjo, S., S. J. Manganini, R. A. Krishfield, and R. Francois (2008), Particulate organic carbon fluxes to the ocean interior and factors controlling the biological pump: A synthesis of global sediment trap programs since 1983, *Prog. Oceanogr.*, *76*(3), 217–285, doi:10.1016/j.pocean.2007.11.003.

Hood, M. (2009), *Ship-based Repeat Hydrography: A Strategy for a Sustained Global Programme*, Intergovernmental Oceanographic Commission of UNESCO and the International CLIVAR Project Office.

Hopkins, J., S. A. Henson, S. C. Painter, T. Tyrrell, and A. J. Poulton (2015), Phenological characteristics of global coccolithophore blooms, *Global Biogeochem. Cycles*, *29*(2), 239–253, doi:10.1002/2014GB004919.

Horibe, Y., K. Endo, and H. Tsubota (1974), Calcium in the South Pacific, and its correlation with carbonate alkalinity, *Earth Planet. Sci. Lett.*, *23*, 136–140.

Hu, X., and W.-J. Cai (2011), An assessment of ocean margin anaerobic processes on oceanic alkalinity budget, *Global Biogeochem. Cycles*, *25*, GB3003, doi:10.1029/2010GB003859.

Huntington, T. G. (2006), Evidence for intensification of the global water cycle: Review and synthesis, *J. Hydrol.*, *319*(1–4), 83–95, doi:10.1016/j.jhydrol.2005.07.003.

Hutchins, D. A., and K. W. Bruland (1998), Iron-limited diatom growth and Si : N uptake ratios in a coastal upwelling regime, *Nature*, *393*(6685), 561–564, doi:Doi 10.1038/31203.

Huyer, A. (1983), Coastal upwelling in the California current system, *Prog. Oceanogr.*, *12*, 259–284, doi:10.1016/0079-6611(83)90010-1.

Iglesias-Rodríguez, M. D., C. W. Brown, S. C. Doney, J. Kleypas, D. Kolber, Z. Kolber, P. K. Hayes, and P. G. Falkowski (2002), Representing key phytoplankton functional groups in ocean carbon cycle models: Coccolithophorids, *Global Biogeochem. Cycles*, *16*(4), 1100, doi:10.1029/2001GB001454.

Ilyina, T., R. E. Zeebe, E. Maier-Reimer, and C. Heinze (2009), Early detection of ocean acidification effects on marine calcification, *Global Biogeochem. Cycles*, *23*(1), 1–11, doi:10.1029/2008GB003278.

Ilyina, T., R. E. Zeebe, and P. G. Brewer (2010), Future ocean increasingly transparent to low-frequency sound owing to carbon dioxide emissions, *Nat. Geosci.*, *3*(1), 18–22, doi:10.1038/ngeo719.

IPCC (2014), Climate Change 2014: Synthesis Report . Contribution of Working Groups I, II and III to the Fifth Assessment Report of the Intergovernmental Panel on Climate Change, edited by R. K. Pachauri and L. A. Meyer, p. 31, Geneva, Switzerland, Switzerland.

Ishii, M., S. Saito, T. Tokieda, T. Kawano, K. Matsumoto, and H. Y. Inoue (2004), Variability of surface layer CO2 parameters in the western and central equatorial Pacific, in *Global Environmental Change in the Ocean and on Land*, edited by M. Shiyomi, H. Kawahata, H. Koizumi, A. Tsuda, and Y. Awaya, pp. 59–94, Terrapub.

Ishijima, K., S. Sugawara, K. Kawamura, G. Hashida, S. Morimoto, S. Murayama, S. Aoki, and T. Nakazawa (2007), Temporal variations of the atmospheric nitrous oxide concentration and its $\delta^{15}N$ and $\delta^{18}O$ for the latter half of the 20th century reconstructed from firn air analyses, *J. Geophys. Res. Atmos.*, *112*(3), doi:10.1029/2006JD007208.

Jackett, D. R., T. J. McDougall, R. Feistel, D. G. Wright, S. M. Griffies (2006), Algorithms for density, potential temperature, conservative temperature, and the freezing teperature of seawater, *J. Atmos. Ocean Tech, 23*(12), 1709-1728, doi:10.1175/JTECH1946.1.

Jiang, Z.-P., T. Tyrrell, D. J. Hydes, M. Dai, and S. E. Hartman (2014), Variability of alkalinity and the alkalinity-salinity relationship in the tropical and subtropical surface ocean, *Global Biogeochem. Cycles*, *28*, doi:10.1002/2013GB004678.

Jin, X., N. Gruber, J. P. Dunne, J. L. Sarmiento, and R. A. Armstrong (2006), Diagnosing the contribution of phytoplankton functional groups to the production and export of particulate organic carbon, CaCO3 , and opal from global nutrient and alkalinity distributions, *Global Biogeochem. Cycles*, *20*, GB2015, doi:10.1029/2005GB002532.

Johnson, G. C., P. E. Robbins, and G. E. Hufford (2001), Systematic Adjustments of Hydrographic Sections for Internal Consistency *, *J. Atmos. Ocean. Technoloy*, *18*, 1234–1244.

Johnson, K. S., and L. J. Coletti (2002), In situ ultraviolet spectrophotometry for high resolution and long-term monitoring of nitrate, bromide and bisulfide in the ocean, *Deep. Res. Part I Oceanogr. Res. Pap.*, *49*(7), 1291–1305, doi:10.1016/S0967-0637(02)00020-1.

Juranek, L. W., R. A. Feely, W. T. Peterson, S. R. Alin, B. Hales, K. Lee, C. L. Sabine, and J. Peterson (2009), A novel method for determination of aragonite saturation state on the continental shelf of central Oregon using multi-parameter relationships with hydrographic data, *Geophys. Res. Lett.*, *36*, L24601, doi:10.1029/2009GL040778.

Kanamori, S., and H. Ikegami (1982), Calcium-alkalinity relationship in the North Pacific, *J. Oceanogr. Soc. Japan*, *38*(2), 57–62, doi:10.1007/BF02110291.

Kang, Y., D. Pan, Y. Bai, X. He, X. Chen, C.-T. A. Chen, and D. Wang (2013), Areas of the global major river plumes, *Acta Oceanol. Sin.*, *32*(1), 79–88, doi:10.1007/s13131-013-0269-5.

Karim, M. F., and N. Mimura (2008), Impacts of climate change and sea-level rise on cyclonic storm surge floods in Bangladesh, *Glob. Environ. Chang.*, *18*(3), 490–500, doi:10.1016/j.gloenvcha.2008.05.002.

Key, R., A. Kozyr, C. L. Sabine, K. Lee, R. Wanninkhof, J. L. Bullister, R. A. Feely, F. J. Millero, C. Mordy, and T.-H. Peng (2004), A global ocean carbon climatology: Results from Global Data Analysis Project (GLODAP), *Global Biogeochem. Cycles*, *18*, GB4031, doi:10.1029/2004GB002247.

Key, R. M. et al. (2010), The CARINA data synthesis project: introduction and overview, *Earth Syst. Sci. Data*, *2*, 105–121, doi:10.5194/essd-2-105-2010.

Khan, T. M. A., D. A. Quadir, T. S. Murty, A. Kabir, F. Aktar, and M. A. Sarker (2002), Relative Sea Level Changes in Maldives and Vulnerability of Land Due to Abnormal Coastal Inundation, *Mar. Geod.*, *25*(1–2), 133–143, doi:10.1080/014904102753516787.

Khatiwala, S. et al. (2013), Global ocean storage of anthropogenic carbon, *Biogeosciences, 10*(4), 2169–2191, doi:10.5194/bg-10-2169-2013.

Kheshgi, H. S. (1995), Sequestering atmospheric carbon-dioxide by incresing ocean alkalinity, *Energy, 20*(9), 915–922, doi:10.1016/0360-5442(95)00035-F.

Kim, H., K. Lee, and W. Choi (2006), Contribution of phytoplankton and bacterial cells to the measured alkalinity of seawater, *Limnol. Oceanogr.*, *51*(1), 331–338.

Kim, H. C., and K. Lee (2009), Significant contribution of dissolved organic matter to seawater alkalinity, *Geophys. Res. Lett.*, *36*(20), 1–5, doi:10.1029/2009GL040271.

King, B. . A., E. Firing, and T. M. Joyce (2001), Shipboard Observations during WOCE, in *Ocean Circulation and Climate*, pp. 99–122, Academic Press.

Klaas, C., and D. E. Archer (2002), Association of sinking organic matter with various types of mineral ballast in the deep sea: Implications for the rain ratio, *Global Biogeochem. Cycles*, *16*(4), 63-1-63–14, doi:10.1029/2001GB001765.

Koeve, W., and A. Oschlies (2012), Potential impact of DOC accumulation on fCO2 and carbonate ion computations in ocean acidification experiments, *Biogeosciences Discuss.*, *8*(2), 3797–3827, doi:10.5194/bgd-8-3797-2011.

Körtzinger, A. (2003), A significant CO2 sink in the tropical Atlantic Ocean associated with the Amazon River plume, *Geophys. Res. Lett.*, *30*(24), 2287, doi:10.1029/2003GL018841.

Körtzinger, A., U. Send, R. S. Lampitt, S. Hartman, D. W. R. Wallace, J. Karstensen, M. G. Villagarcia, O. Llinás, and M. D. DeGrandpre (2008), The seasonal pCO2 cycle at 49°N/16.5°W in the northeastern Atlantic Ocean and what it tells us about biological productivity, *J. Geophys. Res.*, *113*, C04020, doi:10.1029/2007JC004347.

Kovacs, K. M., C. Lydersen, J. E. Overland, and S. E. Moore (2011), Impacts of changing sea-ice conditions on Arctic marine mammals, *Mar. Biodivers.*, *41*(1), 181–194, doi:10.1007/s12526-010-0061-0.

Kump, L. R., S. L. Brantley, and A. M. A. (2000), Chemical weathering, atmospheric CO2, and climate, *Annu. Rev. Earth Planet. Sci, 28*, 611–667, doi:10.1146/annurev.earth.28.1.611.

Kwon, E. Y., F. Primeau, and J. L. Sarmiento (2009), The impact of remineralization depth on the air–sea carbon balance, *Nat. Geosci.*, *2*, 630–635, doi:10.1038/ngeo612.

Lamarche, V. C., D. A. Graybill, H. C. Fritts, and M. R. Rose (1984), Increasing atmospheric carbon dioxide: tree ring evidence for growth enhancement in natural vegetation., *Science*, *225*(4666), 1019–1021, doi:10.1126/science.225.4666.1019.

Land, P. E. et al. (2015), Salinity from Space Unlocks Satellite-Based Assessment of Ocean Acidification, *Environ. Sci. Technol.*, *49*, 1987–1994, doi:10.1021/es504849s.

Landschützer, P., N. Gruber, F. A. Haumann, C. Rödenbeck, D. C. E. Bakker, S. Van Heuven, M. Hoppema, N. Metzl, C. Sweeney, and T. Takahashi (2015), The reinvigoration of the Southern Ocean carbon sink, *Science*, *349*(6253), 1221–1224, doi:10.1126/science.aab2620.

Langdon, C., T. Takahashi, C. Sweeney, D. Chipman, and J. Atkinson (2000), Effect of calcium carbonate saturation state of the calcification rate of an experimental coral reef, *Global Biogeochem. Cycles, 14*(2), 639–654.

Lauvset, S. K., and T. Tanhua (2015), A toolbox for secondary quality control on ocean chemistry and hydrographic data, *Limnol. Oceanogr. Methods*, n/a-n/a, doi:10.1002/lom3.10050.

Lauvset, S. K. et al. (2014), GLODAPv2 - A new and updated global ocean carbon data product, *IMBER Updat. Issue No. 27*.

de Lavergne, C., J. B. Palter, E. D. Galbraith, R. Bernardello, and I. Marinov (2014), Cessation of deep convection in the open Southern Ocean under anthropogenic climate change, *Nat. Clim. Chang.*, *4*(4), 0–4, doi:10.1038/NCLIMATE2132.

Lee, K., L. T. Tong, F. J. Millero, C. L. Sabine, A. G. Dickson, C. Goyet, G.-H. Park, R. Wanninkhof, R. A. Feely, and R. M. Key (2006), Global relationships of total alkalinity with salinity and temperature in surface waters of the world's oceans, *Geophys. Res. Lett.*, *33*, L19605, doi:10.1029/2006GL027207.

Lee, K. (2001), Global net community production estimated from the annual cycle of surface water total dissolved inorganic carbon, *Limnol. Oceanogr., 46*(6), 1287–1297, doi:10.4319/lo.2001.46.6.1287.

Lenton, A., N. Metzl, T. Takahashi, M. Kuchinke, R. J. Matear, T. Roy, S. C. Sutherland, C. Sweeney, and B. Tilbrook (2012), The observed evolution of oceanic pCO2 and its drivers over the last two decades, *Global Biogeochem. Cycles*, *26*, GB2021, doi:10.1029/2011GB004095.

Lewandowska, A., and U. Sommer (2010), Climate change and the spring bloom: A mesocosm study on the influence of light and temperature on phytoplankton and mesozooplankton, *Mar. Ecol. Prog. Ser.*, *405*, 101–111, doi:10.3354/meps08520.

Lin, B., B. A. Wielicki, L. H. Chambers, Y. Hu, and K. M. Xu (2002a), The Iris hypothesis: A negative or positive cloud feedback?, *J. Clim.*, *15*(3), 3–7, doi:10.1175/1520-0442(2002)015<2713:COTIHA>2.0.CO;2.

Lin, S., K. Huang, and S. Chen (2002b), Sulfate reduction and iron sulfide mineral formation in the southern East China Sea continental slope sediment, *Deep Sea Res. Part I Oceanogr. Res. Pap.*, *49*(10), 1837–1852, doi:10.1016/S0967-0637(02)00092-4.

Di Lorenzo, E. et al. (2008), North Pacific Gyre Oscillation links ocean climate and ecosystem change, *Geophys. Res. Lett.*, *35*, L08607, doi:10.1029/2007GL032838.

Lovenduski, N. S., and N. Gruber (2005), Impact of the Southern Annular Mode on Southern Ocean circulation and biology, *Geophys. Res. Lett.*, *32*(11), L11603, doi:10.1029/2005GL022727.

Lovenduski, N. S., N. Gruber, and S. C. Doney (2008), Toward a mechanistic understanding of the decadal trends in the Southern Ocean carbon sink, *Global Biogeochem. Cycles*, *22*(3), GB3016, doi:10.1029/2007GB003139.

Lozier, M. S. (2012), Overturning in the North Atlantic., *Ann. Rev. Mar. Sci.*, *4*, 291–315, doi:10.1146/annurev-marine-120710-100740.

Malinverno, E., M. V Triantaphyllou, and M. D. Dimiza (2015), Coccolithophore assemblage distribution along a temperate to polar gradient in the West Pacific sector of the Southern Ocean (January 2005), *Micropaleontology*, *61*(6), 489–506.

Margalef, R. (1978), Life-forms of phytoplankton as survival alternatives in an unstable environment, *Oceanol. Acta*, *1*(4), 493–509.

Marsili, L. (1725), Histoire physique de la mer. Ouvrage enrichi de figures dessinées d'après le naturel.

Martens, P., R. S. Kovats, S. Nijhof, P. Vries, M. T. J. Livermore, and D. J. Bradley (1999), Climate change and future populations at risk of malaria, *Glob Env. Chang.*, *9*, 89–107, doi:10.1016/S0959-3780(99)00020-5.

Matsumoto, K., and N. Gruber (2005), How accurate is the estimation of anthropogenic carbon in the ocean? An evaluation of the delC* method, *Global Biogeochem. Cycles*, *19*(3), 1–17, doi:10.1029/2004GB002397.

Mazloff, M. R., P. Heimbach, and C. Wunsch (2010), An Eddy-Permitting Southern Ocean State Estimate, *J. Phys. Oceanogr.*, *40*(5), 880–899, doi:10.1175/2009JPO4236.1.

McIntyre, A., and A. W. H. Bé (1967), Modern coccolithophoridae of the atlantic ocean—I. Placoliths and cyrtoliths, *Deep Sea Res. Oceanogr. Abstr.*, *14*(5), 561–597, doi:10.1016/0011-7471(67)90065-4.

McNeil, B. I., R. J. Matear, R. M. Key, J. L. Bullister, and J. L. Sarmiento (2003), Anthropogenic CO2 uptake by the ocean based on the global chlorofluorocarbon data set., *Science*, *299*(5604), 235–9, doi:10.1126/science.1077429.

McNeil, B. I., N. Metzl, R. M. Key, R. J. Matear, and A. Corbiere (2007), An empirical estimate of the Southern Ocean air-sea CO2 flux, *Global Biogeochem. Cycles*, *21*, GB3011, doi:10.1029/2007GB002991.

Meehl, G. a, W. M. Washington, and W. D. Collins (2009), How Much More Global Warming and Sea Level How Much More Global Warming and Sea Level Rise ?, *Science*, *307*, 1769–1773, doi:10.1126/science.1106663.

Millero, F. J. et al. (1998a), Assessment of the quality of the shipboard measurements of total alkalinity on the WOCE Hydrographic Program Indian Ocean CO2 survey cruises 1994–1996, *Mar. Chem.*, *63*, 9–20, doi:10.1016/S0304-4203(98)00043-7.

Millero, F. J., K. Lee, and M. Roche (1998b), Distribution of alkalinity in the surface waters of the major oceans, *Mar. Chem.*, *60*, 111–130, doi:10.1016/S0304-4203(97)00084-4.

Milliman, J. D., and A. W. Droxler (1996), Neritic and pelagic carbonate sedimentation in the marine environment: ignorance is not bliss, *Geol. Rundschau, 85*, 496–504, doi:10.1007/BF02369004.

Milliman, J. D., P. J. Troy, W. M. Balch, A. K. Adams, Y.-H. Li, and F. T. Mackenzie (1999), Biologically mediated dissolution of calcium carbonate above the chemical lysocline?, *Deep Sea Res. Part I Oceanogr. Res. Pap.*, *46*, 1653–1669, doi:10.1016/S0967-0637(99)00034-5.

Min, S.-K., X. Zhang, F. W. Zwiers, and G. C. Hegerl (2011), Human contribution to more-intense precipitation extremes., *Nature*, *470*(7334), 378–381, doi:10.1038/nature09763.

Mohan, R., L. P. Mergulhao, M. V. S. Guptha, A. Rajakumar, M. Thamban, N. AnilKumar, M. Sudhakar, and R. Ravindra (2008), Ecology of coccolithophores in the Indian sector of the Southern Ocean, *Mar. Micropaleontol.*, *67*(1–2), 30–45, doi:10.1016/j.marmicro.2007.08.005.

Montenegro, A., V. Brovkin, M. Eby, D. Archer, and A. J. Weaver (2007), Long term fate of anthropogenic carbon, *Geophys. Res. Lett.*, *34*(19), L19707, doi:10.1029/2007GL030905.

Monterey, G., and S. Levitus (1997), *Seasonal Variability of Mixed Layer Depth for the World Ocean*, U.S. Government Printing Office, Washington D.C.

Moore, T. S., M. D. Dowell, and B. A. Franz (2012), Detection of coccolithophore blooms in ocean color satellite imagery: A generalized approach for use with multiple sensors, *Remote Sens. Environ.*, *117*, 249–263, doi:10.1016/j.rse.2011.10.001.

Mora, S. J. de (1983), The distribution of alkalinity and pH in the Fraser estuary, *Environ. Technol. Lett.*, *4*(1), 35–46, doi:10.1080/09593338309384169.

Moy, A. D., W. R. Howard, S. G. Bray, and T. W. Trull (2009), Reduced calcification in modern Southern Ocean planktonic foraminifera, *Nat. Geosci.*, *2*(4), 276–280, doi:10.1038/ngeo460.

Muller, F. L. L., and B. Bleie (2008), Estimating the organic acid contribution to coastal seawater alkalinity by potentiometric titrations in a closed cell, *Anal. Chim. Acta*, *619*(2), 183–191, doi:10.1016/j.aca.2008.05.018.

Neori, A., and O. Holm-Hansen (1982), Effect of temperature on rate of photosynthesis in Antarctic phytoplankton, *Polar Biol.*, *1*(1), 33–38, doi:10.1007/BF00568752.

Nomura, D., P. Assmy, G. Nehrke, M. A. Granskog, M. Fischer, G. S. Dieckmann, A. Fransson, Y. Hu, and B. Schnetger (2013), Characterization of ikaite (CaCO3 •6H2O) crystals in first-year Arctic sea ice north of Svalbard, *Ann. Glaciol.*, *54*(62), 125–131, doi:10.3189/2013AoG62A034.

Ohno, Y., N. Iwasaka, F. Kobashi, and Y. Sato (2008), Mixed layer depth climatology of the North Pacific based on Argo observations, *J. Oceanogr.*, *65*(1), 1–16, doi:10.1007/s10872-009-0001-4.

Olsen, A. et al. (2016), Global Ocean Data Analysis Project version 2 (GLODAPv2) - an internally consistent data product for the world ocean, *Earth Syst. Sci. Data, 8*, 297–323, doi:10.5194/essd-8-297-2016.

Olson, E. J., and C.-T. A. Chen (1982), Interference in the determination of calcium in seawater, *Limnol. Oceanogr.*, *27*(2), 375–380, doi:10.4319/lo.1982.27.2.0375.

Orr, J. C. et al. (2005), Anthropogenic ocean acidification over the twenty-first century and its impact on calcifying organisms., *Nature*, *437*, 681–6, doi:10.1038/nature04095.

Orsi, A. H., and U. Harris (2015), Locations of the various fronts in the Southern Ocean, *Aust. Antarct. Data Centre, - CAASM Metadata*. Available from: http://data.aad.gov.au/aadc/metadata/metadata_redirect.cfm?md=/AMD/AU/southern_ocean_fronts

Orsi, A. H., T. Whitworth, and W. D. Nowlin (1995), On the meridional extent and fronts of the Antarctic Circumpolar Current, *Deep Sea Res. Part I Oceanogr. Res. Pap.*, *42*(5), 641–673, doi:10.1016/0967-0637(95)00021-W.

Paquay, F. S., and R. E. Zeebe (2013), Assessing possible consequences of ocean liming on ocean pH, atmospheric CO2 concentration and associated costs, *Int. J. Greenh. Gas Control, 17*, 183–188, doi:10.1016/j.ijggc.2013.05.005.

Pardo, P. C., M. Vázquez-Rodríguez, F. F. Pérez, and A. F. Rios (2011), CO2 air–sea disequilibrium and preformed alkalinity in the Pacific and Indian oceans calculated from subsurface layer data, *J. Mar. Syst.*, *84*(3–4), 67–77, doi:10.1016/j.jmarsys.2010.08.006.

Park, P. K., G. R. Webster, and R. Yamamoto (1969), Alkalinity budget of the Columbia River, *Limnol. Oceanogr.*, *14*(4), 559–567.

Patz, J. A., D. Campbell-Lendrum, T. Holloway, and J. A. Foley (2005), Impact of regional climate change on human health, *Nature*, *438*(7066), 310–317, doi:10.1038/nature04188.

Pavlova, G. Y., P. Y. Tishchenko, and A. P. Nedashkovskii (2008), Distribution of alkalinity and dissolved calcium in the Sea of Okhotsk, *Oceanology*, *48*(1), 23–32, doi:10.1134/S0001437008010049.

Perkin, R. G., and L. Y. N. Lewis (1980), The Practical Salinity Scale 1978 : Fitting the Data, *IEEE J. Ocean. Eng.*, *OE-S*(1), 9–16, doi:10.1109/JOE.1980.1145441.

Pfeil, B. et al. (2013), A uniform, quality controlled Surface Ocean CO2 Atlas (SOCAT), *Earth Syst. Sci. Data*, *5*(1), 125–143, doi:10.5194/essd-5-125-2013.

Postma, H. (1964), The exchange of oxygen and carbon dioxide between the ocean and the atmosphere, *Netherlands J. Sea Res.*, *2*(2), 258–283.

Poulton, A. J., R. Sanders, P. M. Holligan, M. C. Stinchcombe, T. R. Adey, L. Brown, and K. Chamberlain (2006), Phytoplankton mineralization in the tropical and subtropical Atlantic Ocean, *Global Biogeochem. Cycles*, *20*, GB4002, doi:10.1029/2006GB002712.

Poulton, A. J., A. Charalampopoulou, J. R. Young, G. A. Tarran, M. I. Lucas, and G. D. Quartly (2010), Coccolithophore dynamics in non-bloom conditions during late summer in the central Iceland Basin (July-August 2007), *Limnol. Oceanogr., 55*(4), 1601–1613, doi:10.4319/lo.2010.55.4.1601.

Poulton, A. J., S. C. Painter, J. R. Young, N. R. Bates, B. Bowler, D. Drapeau, E. Lyczsckowski, and W. M. Balch (2013), The 2008 Emiliania huxleyi bloom along the Patagonian Shelf: Ecology, biogeochemistry, and cellular calcification, *Global Biogeochem. Cycles, 27*(4), 1023–1033, doi:10.1002/2013GB004641.

Prather, M. J., C. D. Holmes, and J. Hsu (2012), Reactive greenhouse gas scenarios: Systematic exploration of uncertainties and the role of atmospheric chemistry, *Geophys. Res. Lett.*, *39*(9), 6–10, doi:10.1029/2012GL051440.

Le Quéré, C. et al. (2005), Ecosystem dynamics based on plankton functional types for global ocean biogeochemistry models\rdoi:10.1111/j.1365-2486.2005.1004.x, *Glob. Chang. Biol.*, *11*(11), 2016–2040, doi:10.1111/j.1365-2486.2005.01004.x.

Le Quéré, C. et al. (2007), Saturation of the southern ocean CO2 sink due to recent climate change., *Science*, *316*(5832), 1735–8, doi:10.1126/science.1136188.

Le Quéré, C. et al. (2009), Trends in the sources and sinks of carbon dioxide, *Nat. Geosci.*, *2*, 831–836, doi:10.1038/ngeo689.

Rahmstorf, S. (2007), Projecting Future Sea-Level Rise, *Science*, *315*, 368–370.

Ridgwell, A., and R. E. Zeebe (2005), The role of the global carbonate cycle in the regulation and evolution of the Earth system, *Earth Planet. Sci. Lett., 234*(3–4), 299–315, doi:10.1016/j.epsl.2005.03.006.

Ridgwell, A. J., M. J. Kennedy, and K. Caldeira (2003), Carbonate deposition, climate stability, and Neoproterozoic ice ages., *Science, 302*(5646), 859–862, doi:10.1126/science.1088342.

Riebesell, U., I. Zondervan, B. Rost, P. D. Tortell, R. E. Zeebe, and F. M. M. Morel (2000), Reduced calcication of marine plankton in response to increased atmospheric CO2, *Nature*, *407*, 364–367.

Rubin, S. I., and R. M. Key (2002), Separating natural and bomb-produced radiocarbon in the ocean: The potential alkalinity method, *Global Biogeochem. Cycles*, *16*(4), doi:10.1029/2001GB001432.

Rysgaard, S., J. Mortensen, T. Juul-Pedersen, L. L. Sørensen, K. Lennert, D. H. Søgaard, K. E. Arendt, M. E. Blicher, M. K. Sejr, and J. Bendtsen (2012a), High air–sea CO2 uptake rates in nearshore and shelf areas of Southern Greenland: Temporal and spatial variability, *Mar. Chem.*, *128–129*, 26–33, doi:10.1016/j.marchem.2011.11.002.

Rysgaard, S., R. N. Glud, K. Lennert, M. Cooper, N. Halden, R. J. G. Leakey, F. C. Hawthorne, and D. Barber (2012b), Ikaite crystals in melting sea ice – implications for pCO2 and pH levels in Arctic surface waters, *Cryosph.*, *6*, 1–8, doi:10.5194/tc-6-1-2012.

Rysgaard, S. et al. (2013), Ikaite crystal distribution in winter sea ice and implications for CO2 system dynamics, *Cryosph.*, *7*, 707–718, doi:10.5194/tc-7-707-2013.

Sabine, C. L., R. M. Key, K. M. Johnson, F. J. Millero, A. Poisson, J. L. Sarmiento, D. W. R. Wallace, and C. D. Winn (1999), Anthropogenic CO2 inventory of the Indian Ocean, *Global Biogeochem. Cycles*, *13*(1), 179–198.

Sabine, C. L., R. M. Key, R. A. Feely, and D. Greeley (2002), Inorganic carbon in the Indian Ocean: Distribution and dissolution processes, *Global Biogeochem. Cycles*, *16*(4), 1067, doi:10.1029/2002GB001869.

Sabine, C. L., R. M. Key, A. Kozyr, R. A. Feely, R. Wanninkhof, F. J. Millero, T. Peng, J. L. Bullister, and K. Lee (2005), *Global Ocean Data Analysis Project: Results and Data. ORNL/CDIAC-145, NDP-083*, Oak Ridge, Tennessee.

Salter, I., R. S. Lampitt, R. Sanders, A. Poulton, A. E. S. Kemp, B. Boorman, K. Saw, and R. Pearce (2007), Estimating carbon, silica and diatom export from a naturally fertilised phytoplankton bloom in the Southern Ocean using PELAGRA: A novel drifting sediment trap, *Deep. Res. Part II Top. Stud. Oceanogr.*, *54*(18–20), 2233–2259, doi:10.1016/j.dsr2.2007.06.008.

Salter, I., R. Schiebel, P. Ziveri, A. Movellan, R. Lampitt, and G. A. Wol (2014), Carbonate counter pump stimulated by natural iron fertilization in the Polar Frontal Zone, *Nat. Geosci., 7*, 885–889, doi:10.1038/NGEO2285.

Sarmiento, J. L., and N. Gruber (2006), *Ocean Biogeochemical Dynamics*, Princeton University Press, Princeton.

Sarmiento, J. L., and C. Le Quéré (1996), Oceanic Carbon Dioxide Uptake in a Model of Century-Scale Global Warming, *Science*, *274*(5291), 1346–1350, doi:10.1126/science.274.5291.1346.

Sarmiento, J. L., J. Dunne, A. Gnanadesikan, R. M. Key, K. Matsumoto, and R. Slater (2002), A new estimate of the CaCO3 to organic carbon export ratio, *Global Biogeochem. Cycles*, *16*(4), 1107, doi:10.1029/2002GB001919.

Sarmiento, J. L., N. Gruber, M. A. Brzezinski, and J. P. Dunne (2004), High-latitude controls of thermocline nutrients and low latitude biological productivity, *Nature*, *427*, 56–60, doi:10.1038/nature02204.1.

Sasse, T. P., B. I. McNeil, and G. Abramowitz (2013), A novel method for diagnosing seasonal to inter-annual surface ocean carbon dynamics from bottle data using neural networks, *Biogeosciences*, *10*(6), 4319–4340, doi:10.5194/bg-10-4319-2013.

Schiebel, R. (2002), Planktic foraminiferal sedimentation and the marine calcite budget, *Glob. Biogeochem. Cycles*, *16*(4), 1065, doi:10.1029/2001gb001459.

Schlitzer, R. (2000), Applying the Adjoint Method for Biogeochemical Modeling: Export of Particulate Organic Matter in the World Ocean, in *Inverse Methods in Global Biogeochemical Cycles*, edited by P. Kasibhatla, M. Heimann, P. Rayner, N. Mahowald, R. G. Prinn, and D. E. Hartley, pp. 107–124, American Geophysical Union, Washington D.C.

Schloesing, T. (1880), Sur la constance de la proportion d'acide carbonique dans l'air, *CR Acad. Sci.*

Serreze, M. C., M. M. Holland, and J. Stroeve (2007), Perspectives on the Arctic's shrinking sea-ice cover, *Science*, *315*(5818), 1533–1536, doi:10.1126/science.1139426.

Shimada, K., T. Kamoshida, M. Itoh, S. Nishino, E. Carmack, F. McLaughlin, S. Zimmermann, and A. Proshutinsky (2006), Pacific Ocean inflow: Influence on catastrophic reduction of sea ice cover in the Arctic Ocean, *Geophys. Res. Lett.*, *33*(8), 3–6, doi:10.1029/2005GL025624.

Simpson, S. D., P. L. Munday, M. L. Wittenrich, R. Manassa, D. L. Dixson, M. Gagliano, and H. Y. Yan (2011), Ocean acidification erodes crucial auditory behaviour in a marine fish, *Biol. Lett.*, *7*(6), 917–920, doi:10.1098/rsbl.2011.0293.

Soden, B., and I. Held (2006), An Assessment of Climate Feedbacks in Coupled Ocean – Atmosphere Models, *J. Clim.*, *19*(2003), 3354–3360, doi:10.1175/JCLI9028.1.

Sommer, U., and K. Lengfellner (2008), Climate change and the timing, magnitude, and composition of the phytoplankton spring bloom, *Glob. Chang. Biol.*, *14*(6), 1199–1208, doi:10.1111/j.1365-2486.2008.01571.x.

Sommer, U., and A. Lewandowska (2011), Climate change and the phytoplankton spring bloom: Warming and overwintering zooplankton have similar effects on phytoplankton, *Glob. Chang. Biol.*, *17*(1), 154–162, doi:10.1111/j.1365-2486.2010.02182.x.

Steinacher, M., F. Joos, T. L. Frolicher, G.-K. Plattner, and S. C. Doney (2009), Imminent ocean acidification in the Arctic projected with the NCAR global coupled carbon cycle-climate model, *Biogeosciences*, *6*, 515–533.

Stern, N. H. et al. (2006), *Stern Review: The economics of climate change*, Cambridge University Press, Cambridge.

Sun, X., and A. V. Turchyn (2014), Significant contribution of authigenic carbonate to marine carbon burial, *Nat. Geosci., 8*(1), 201–204, doi:10.1038/ngeo2070.

Suzuki, T. et al. (2013), PACIFICA Data Synthesis Project. ORNL/CDIAC-159, NDP-092, Oak Ridge, Tennessee.

Sydeman, W. J., M. García-Reyes, D. S. Schoeman, R. R. Rykaczewski, S. A. Thompson, B. A. Black, and S. J. Bograd (2014), Climate change and wind intensification in coastal upwelling ecosystems., *Science*, *345*, 77–80, doi:10.1126/science.1251635.

Takahashi, T., and S. C. Sutherland (2009), Global ocean surface water partial pressure of CO2 database: Measurements performed during 1968-2008 (Version 2008), Oak Ridge, Tennessee, Tennessee.

Takatani, Y., K. Enyo, Y. Iida, A. Kojima, T. Nakano, D. Sasano, N. Kosugi, T. Midorikawa, T. Suzuki, and M. Ishii (2014), Relationship between total alkalinity in surface water and sea surface dynamic height in the Pacific Ocean, *J. Geophys. Res. Ocean.*, *199*, doi:10.1002/2013JC009739.

Talley, L. D. (1985), Ventilation of the Subtropical North Pacific: The Shallow Salinity Minimum, *J. Phys. Oceanogr.*, *15*, 633–649, doi:10.1175/1520-0485(1985)015<0633:VOTSNP>2.0.CO;2.

Talley, L. D. (1988), Potential Vorticity Distribution in the North Pacific, *J. Phys. Oceanogr.*, *18*, 89–106, doi:10.1175/1520-0485(1988)018<0089:PVDITN>2.0.CO;2.

Talley, L. D., J. L. Reid, and P. E. Robbins (2003), Data-Based Meridional Overturning Streamfunctions for the Global Ocean, *J. Clim.*, *16*, 3213–3226.

Tanhua, T., S. van Heuven, R. M. Key, A. Velo, A. Olsen, and C. Schirnick (2010), Quality control procedures and methods of the CARINA database, *Earth Syst. Sci. Data*, *2*, 35–49, doi:10.3334/CDIAC/otg.CARINA.SO.V1.0.

Tans, P., and C. D. Keeling (2015), No Title, Available from: ftp://aftp.cmdl.noaa.gov/products/trends/co2/co2_annmean_mlo.txt

Tanser, F. C., B. L. Sharp, and D. le Sueur (2003), Potential effect of climate change on malaria transmission in Africa, *Lancet*, *362*(9398), 1792–1798, doi:10.1016/S0140-6736(03)14898-2.

Taylor, J. R. (1982), An introduction to error analysis: The study of uncertainties in physical measurements, University Science Books, Mill Valley, C.A.

Thomas, H., L.-S. Schiettecatte, K. Suykens, Y. J. M. Koné, E. H. Shadwick, A. E. F. Prowe, Y. Bozec, H. J. W. de Baar, and A. V. Borges (2008), Enhanced ocean carbon storage from anaerobic alkalinity generation in coastal sediments, *Biogeosciences Discuss.*, *5*(4), 3575–3591, doi:10.5194/bgd-5-3575-2008.

Timmermann, A., J. Oberhuber, A. Bacher, M. Esch, M. Latif, and E. Roeckner (1999), Increased El Nino frequency in a climate model forced by future greenhouse warming, *Nature*, *398*(6729), 694–697, doi:10.1038/19505.

Toggweiler, J. R., and B. Samuels (1995), Effect of drake passage on the global thermohaline circulation, *Deep Sea Res. Part I Oceanogr. Res. Pap.*, *42*(4), 477–500, doi:10.1016/0967-0637(95)00012-U.

Touratier, F., and C. Goyet (2011), Impact of the Eastern Mediterranean Transient on the distribution of anthropogenic CO2 and first estimate of acidification for the Mediterranean Sea, *Deep. Res. Part I Oceanogr. Res. Pap.*, *58*(1), 1–15, doi:10.1016/j.dsr.2010.10.002.

Touratier, F., L. Azouzi, and C. Goyet (2007), CFC-11, 14C and 3H tracers as a means to assess anthropogenic CO2 concentrations in the ocean, *Tellus, Ser. B Chem. Phys. Meteorol.*, *59*(2), 318–325, doi:10.1111/j.1600-0889.2006.00247.x.

Trenberth, K. E. (1998), Atmospheric moisture residence times and cycling: Implications for rainfall rates and climate change, *Clim. Change*, *39*(4), 667–694, doi:10.1023/A:1005319109110.

Trull, T. W., S. G. Bray, S. J. Manganini, S. Honjo, and R. François (2001), Moored sediment trap measurements of carbon export in the Subantarctic and Polar Frontal Zones of the Southern Ocean, south of Australia, *J. Geophys. Res.*, *106*(C12), 31489–31509.

Tsunogai, S., H. Yamahata, S. Kudo, and O. Saito (1973), Calcium in the Pacific Ocean, *Deep Sea Res. Oceanogr. Abstr.*, *20*(8), 717–726, doi:10.1016/0011-7471(73)90087-9.

Tsunogai, S., S. Watanabe, J. Nakamura, T. Ono, and T. Sato (1997), A Preliminary Study of Carbon System in the East, *J. Oceanogr.*, *53*, 9–17.

Tyrrell, T., and A. Merico (2004), Emiliania huxleyi: bloom observations and the conditions that induce them, in *Coccolithophores*, edited by H. R. Thierstein and J. R. Young, pp. 75–97, Springer, Berlin.

Tyrrell, T., J. G. Shepherd, and S. Castle (2007), The long-term legacy of fossil fuels, *Tellus, Ser. B Chem. Phys. Meteorol.*, *59*(4), 664–672, doi:10.1111/j.1600-0889.2007.00290.x.

Vázquez-Rodríguez, M., X. A. Padin, P. C. Pardo, A. F. Ríos, and F. F. Pérez (2012), The subsurface layer reference to calculate preformed alkalinity and air–sea CO2 disequilibrium in the Atlantic Ocean, *J. Mar. Syst.*, *94*, 52–63, doi:10.1016/j.jmarsys.2011.10.008.

Velo, A., F. F. Perez, P. Brown, T. Tanhua, U. Schuster, and R. M. Key (2009), Science Data CARINA alkalinity data in the Atlantic Ocean, *Earth Syst. Sci. Data*, *1*, 45–61, doi:10.3334/CDIAC/otg.CARINA.ATL.V1.0.

Velo, A., F. F. Pérez, T. Tanhua, M. Gilcoto, A. F. Ríos, and R. M. Key (2013), Total alkalinity estimation using MLR and neural network techniques, *J. Mar. Syst.*, *111–112*, 11–18, doi:10.1016/j.jmarsys.2012.09.002.

de Villiers, S. (1998), Excess dissolved Ca in the deep ocean: a hydrothermal hypothesis, *Earth Planet. Sci. Lett.*, *164*(3–4), 627–641, doi:10.1016/S0012-821X(98)00232-5.

de Villiers, S., and D. M. Nelson (1999), Detection of Low-Temperature Hydrothermal Fluxes by Seawater Mg and Ca Anomalies, *Science*, *285*(5428), 721–723, doi:10.1126/science.285.5428.721.

Visinelli, L., S. Masina, M. Vichi, A. Storto, and T. Lovato (2016), Impacts of data assimilation on the global ocean carbonate system, *J. Mar. Syst.*, *158*, 106–119, doi:10.1016/j.jmarsys.2016.02.01.

Ware, J. R., S. V. Smith, and M. L. Reaka-Kudla (1992), Coral reefs: sources or sinks of atmospheric CO2?, *Coral Reefs, 11*(3), 127–130, doi:10.1007/bf00255465.

Waugh, D. W., T. W. N. Haine, and T. M. Hall (2004), Transport times and anthropogenic carbon in the subpolar North Atlantic Ocean, *Deep. Res. Part I Oceanogr. Res. Pap.*, *51*(11), 1475–1491, doi:10.1016/j.dsr.2004.06.011.

Wefer, G., and G. Fischer (1991), Annual primary production and export flux in the Southern Ocean from sediment trap data, *Mar. Chem.*, *35*(1–4), 597–613, doi:10.1016/S0304-4203(09)90045-7.

Wigley, T. M. L., and S. C. B. Raper (1987), Thermal expansion of sea water associated with global warming, *Nature*, *330*(6144), 127–131, doi:10.1038/330127a0.

Wild, M., D. Folini, C. Schär, N. Loeb, E. G. Dutton, and G. König-Langlo (2013), The global energy balance from a surface perspective, *Clim. Dyn.*, *40*(11–12), 3107–3134, doi:10.1007/s00382-012-1569-8.

Williamson, P., and C. Turley (2012), Ocean acidification in a geoengineering context, *Philos. Trans. A. Math. Phys. Eng. Sci., 370*(1974), 4317–42, doi:10.1098/rsta.2012.0167.

Wolf-Gladrow, D. A., R. E. Zeebe, C. Klaas, A. Körtzinger, and A. G. Dickson (2007), Total alkalinity: The explicit conservative expression and its application to biogeochemical processes, *Mar. Chem.*, *106*(1–2), 287–300, doi:10.1016/j.marchem.2007.01.006.

Wong, C. S., N. A. D. Waser, Y. Nojiri, F. A. Whitney, J. S. Page, and J. Zeng (2002), Seasonal cycles of nutrients and dissolved inorganic carbon at high and mid latitudes in the North Pacific Ocean during the Skaugran cruises: determination of new production and nutrient uptake ratios, *Deep Sea Res. Part II Top. Stud. Oceanogr.*, *49*(24–25), 5317–5338, doi:10.1016/S0967-0645(02)00193-5.

Wong, G. T. F. (1979), Alkalinity and pH in the southern Chesapeake Bay and the James River estuary, *Limnol. Oceanogr.*, *24*(5), 970–977.

Wootton, J. T., C. A. Pfister, and J. D. Forester (2008), Dynamic patterns and ecological impacts of declining ocean pH in a high-resolution multi-year dataset., *Proc. Natl. Acad. Sci. U. S. A.*, *105*(48), 18848–18853, doi:10.1073/pnas.0810079105.

Xie, S.-P., and S. G. H. Philander (1994), A coupled ocean-atmosphere model of relevance to the ITCZ in the eastern Pacific, *Tellus A*, *46*, 340–350, doi:10.3402/tellusa.v46i4.15484.

Yang, B., R. H. Byrne, and M. Lindemuth (2015), Contributions of organic alkalinity to total alkalinity in coastal waters: A spectrophotometric approach, *Mar. Chem.*, *176*, 199–207, doi:10.1016/j.marchem.2015.09.008.

Yara, Y., M. Vogt, M. Fujii, H. Yamano, C. Hauri, M. Steinacher, N. Gruber, and Y. Yamanaka (2012), Ocean acidification limits temperature-induced poleward expansion of coral habitats around Japan, *Biogeosciences*, *9*, 4955–4968, doi:10.5194/bg-9-4955-2012.

Yeh, S.-W., J.-S. Kug, B. Dewitte, M.-H. Kwon, B. P. Kirtman, and F.-F. Jin (2009), El Niño in a changing climate, *Nature*, *461*, 511–514, doi:10.1038/nature08316.

Zeebe, R. E., and D. A. Wolf-Gladrow (2001), CO2 in Seawater: Equilibrium, Kinetics, Isotopes, in *Elsevier Oceanography Series, 65*, Elsevier, Amsterdam.